

**Development and field testing of a stationary net-frame bedload
sampler for measuring entrainment of
pebble and cobble particles**

Kristin Bunte

Engineering Research Center, Colorado State University, Fort Collins, CO 80523
Phone: (970) 491-3980; email: kbunte@engr.colostate.edu

Report

Prepared for the

Stream Systems Technology Center

**U.S.D.A. Forest Service
Rocky Mountain Forest and Range Experiment Station, Fort Collins, CO**

November 1998

Abstract

Critical flow for entrainment of gravel particles in mountain streams is difficult to predict from equations. The availability of portable bedload sampler that can measure low transport rates of infrequently moving particles, as well as transport rates of large particles such as large gravels and cobbles would help to overcome this problem. A handheld 3 inch Helley-Smith sampler is not suited to either of those tasks.

A portable bedload sampler was designed with a 12 by 8 inch opening and a sturdy 3 feet trailing fishing net as a bag. An array of 5 samplers was installed across the stream, a task that can be done in a few hours. Although one person could operate the samplers, a team of two persons is recommended when wading in a mountain stream during high flows.

Stationary net-frame samplers were field tested at a mountain cobble-bed river 6.5 m wide, and a gradient of 0.018 during flows up to 70% of bankfull. At low flows about 40% of bankfull, transport rates measured with the stationary net-frame samplers for 4-16 mm gravel were about 3 orders of magnitude smaller than those measured with a Helley-Smith sampler at a site a few hundred yards upstream over a previous 5-year period. For flows 70% of bankfull, this difference reduced to 1 order of magnitude. Equity between both rating curves might occur for flows above bankfull. It is believed that much of this difference between the two samplers is attributable to their different sampling schemes.

Having an array of 5 net-frame samplers stationary in the stream for about 1 hour at a time resulted in sampling intensities that exceeded those from a typical Helley-Smith sampling scheme (in this case 13 verticals, 2 min. each) by a factor of almost 50, or 1.5 orders of magnitude. This high sampling intensity and its ability to sample infrequently moving particles permits the computation of actual low transport rates instead of "zero" values which are both uninformative as well as useless for power function rating curve computations. Thus, rating curves produced by high sampling intensity start out at much smaller transport rates and increase more steeply over medium flows than rating curves from less intensive sampling schemes. For high transport rates around bankfull flow, rating curves from both samplers are probably similar, though long sampling periods that average over highly fluctuating transport rates reduce rating curve scatter and increase sampling accuracy. The steepness of rating curves from intensive sampling schemes with exponents several times larger than those obtained from non-intensive sampling schemes needs to be considered when comparing bedload rating curves obtained from different samplers.

Other factors might have contributed to the discrepancy in transport rates. These include a somewhat reduced sediment supply at the sampling site for the stationary net-frame samplers attributed to a beaver dam and two previous years of above average high flows. Finally, it remains to be tested whether the ground plate under the stationary net-frame samplers was too high off the ground and prevented gravel particles from getting into the sampler, or whether the Helley-Smith sampler oversampled by scooping gravel particles which were not part of bedload transport.

The ability to sample infrequently moving particles makes the stationary net-frame sampler well suited for computing critical flow for initial motion. When critical transport rates are expressed in terms of a low (e.g., 2-5) number of particles per size class per time and width, critical flow increases with particle size, whereas initial motion expressed as a low weight-based rate results in roughly the same critical flow for all particle sizes. For coarse gravel particles the concept of higher flow required for moving larger particles seems to be more intuitively understandable than the concept that all particle sizes move at roughly the same flow because the critical transport rate is based on a preset weight per width and time.

Table of contents

1. Introduction.....	5
2. Current sampling techniques for coarse bedload	5
2.1 Helley-Smith samplers.....	5
2.2 Other samplers for instantaneous transport rates of pebbles and cobbles.....	6
3. The stationary net-frame sampler.....	7
3.1 Sampler design	7
3.1.1 Sampling frame, ground plate, and stakes	7
3.1.2 Webbing loops	9
3.1.3 Sampling net.....	10
3.2 Installation of the sampler in the stream.....	12
3.3 Sampler locations in the stream bed	14
3.4 Operation of the sampler	15
3.4.1 Emptying the samplers	15
3.4.2 Field examination of the samples.....	15
4. Field testing the stationary net-frame sampler.....	18
4.1 The field site: St. Louis Creek.....	18
4.2 Field measurements	22
4.2.1 Measurement of flow	22
4.2.2 Bedload transport measurements with the stationary net-frame sampler	24
4.2.3 Bedload transport measurements with a 3-by-3 inch Helley-Smith sampler	24
4.2.4 Site surveys and stream morphology	24
4.2.5 Bed material.....	27
5. Results	29
5.1 Analysis of flow	29
5.1.1 Stage-discharge rating curve and hydrograph.....	29
5.1.2 Percent bankfull flow.....	29
5.2 Computation of bedload transport rates	33
5.2.1 Particle transport rates.....	34
5.2.2 Total and fractional weight-based bedload transport rates.....	34
5.3 Variability of bedload transport.....	38
5.3.1 Temporal variability of bedload transport rates	38
5.3.2 Spatial variability of bedload transport rates.....	41
6. Comparison between the stationary net-frame sampler and Helley- Smith sampler	42
6.1 Sampling intensity	42
6.2 Comparison of transport rates	43

6.2.1 Helley-Smith transport rates: 1998 versus 1992-1997	43
6.2.2 Transport rates from the stationary net-frame sampler and Helley-Smith samples at Site 4a	44
6.2.3 Steepness of bedload transport rating curves	46
6.3 Comparison of sampled particle sizes	47
7. Initial motion considerations	49
7.1 Computation of critical discharge	50
7.1.1 Preset low fractional transport rate	50
7.1.2 Flow competence curve	52
7.1.3 Graphical-visual approach	52
7.1.4 x-axis intercept	54
7.1.5 Reference transport rate $W_{t}^{*} = 0.002$	58
7.2 Comparison of critical discharge	59
7.2.1 Bedload samples from the net-frame sampler	59
7.2.2 Ryan's bedload samples from the Helley-Smith sampler	61
7.2.3 Critical discharge for gravel beds at about 2/3 of bankfull flow?	61
7.3 Critical dimensionless shear stress τ_{c}^{*} for net-frame samples	63
7.4 Initial motion criteria for channel maintenance flows	64
8. Evaluation of the stationary net-frame sampler and summary	67
9. References	70
10. Appendix	73
10.1 Recommendations for using the stationary net-frame sampler	73
10.2 Field equipment for bedload sampling with stationary net-frame samplers and supporting field measurements	74

1. Introduction

The knowledge of critical flows conditions at which pebble and cobble particles are entrained is important for bedload transport computations including the determination of channel maintenance flows. Knowing the critical flow would also improve the prediction of coarse bedload transport rates from measured parameters of flow and bed-material size distributions.

The prediction of critical flow and particle entrainment of particles from mixtures of different sizes is difficult for several reasons: (1) There is no conceptual agreement about the processes responsible for entrainment of particles mixture. The equal mobility concept, for example, assumes that effects of particle hiding and exposure cause a near equal mobility of all bed-material particle sizes, while the selective transport concept argues that it takes progressively higher flows to mobilize progressively larger particle sizes. (2) There is no agreement on a minimum transport rate, or minimum number of particles that need to be in motion per time to qualify as initial motion. (3) The site-specific conditions of particle shape and stream-bed packing, both of which largely control the resistance of particles to motion, are complex and difficult to quantify. (4) Critical dimensionless shear stress, i.e., the Shields parameter τ^*_c which takes a constant value around 0.05 for unsorted beds, varies over a wide range between 0.03 and 0.2 for gravel-bed rivers with poorly sorted beds and features of structural stability such as clustering, imbrication, or bed steps. A systematic allotment of critical dimensionless shear stress values to stream types (Rosgen 1994, 1996) and various conditions of bed-material structure and particle packing (Kirchner et al. 1990; Buffington et al. 1992) is only beginning to be investigated.

Some of the inconsistencies and inadequacies of the current approaches for predicting initial motion can be overcome if critical flow conditions are determined from direct measurements of bedload transport (assuming a critical transport rate can be determined and point (2) above is of no concern). Measuring the onset of pebble and cobble motion in remote¹ mountain streams requires a simple and portable sampler that accurately determines fractional gravel transport rates. The only portable sampler currently available is the Helley-Smith with its known set of deficiencies.

2. Current sampling techniques for coarse bedload

2.1 Helley-Smith samplers

Although the 3 by 3 inch Helley-Smith sampler is not the optimal device for bedload sampling in gravel-bed mountain stream, its practicality and portability make it the device that is most often used. Sampling results from Helley-Smith samplers lack representativeness in mountain gravel-bed rivers for several reasons:

- The opening (7.5 by 7.5 cm) is too small to representatively collect large gravels and cobbles;
- Relatively short sampling times which commonly range between 30-120 seconds per vertical make representative sampling of pebbles and cobbles unlikely because such particles move infrequently, especially during low transport rates;

¹ "remote" in this context means an unequipped measuring site without nearby vehicle access and implies the necessity of portability of all equipment used.

- The repeated relocation of the sampler when picking it up and setting it down at the sampling locations across the stream may scoop pebbles off the stream bed and thus includes pebbles in the sample which would not have been sampled had they not been dislodged by the sampler;
- Fine gravel can pass under the sampler if the contact between the sampler and a cobble bed is poor.
- The relatively small sampling bag leads to reduced sampling efficiency² when the sampler is filled to more than 1/3 of its holding capacity, or when sand clogs the mesh bag.

The 6-by-6 inch Helley-Smith sampler allows pebbles and cobbles to pass through the sampler opening, and has a larger bag than the 3-inch Helley-Smith sampler, but the bulkiness makes the 6-inch sampler difficult to maneuver, place, and hold on the bed, especially during high flows. This struggling with the sampler increases the potential for scooping particles off the stream bed. Besides, the standard 6-by-6 inch sampler with its entrance-to-exit ratio of 3.22 pronouncedly oversamples transport rates. For pea-sized gravel, Hubbell (1987) determined a sampling efficiency of almost 4, which is 2.5 times more than the sampling efficiency of the standard 3-by-3 inch Helley-Smith sampler.

2.2 Other samplers for instantaneous transport rates of pebbles and cobbles

Current techniques for representative measurements of instantaneous transport rates of pebble and cobble bedload transport in mountain streams require either substantial construction in the stream bed, such as vortex samplers (Milhous 1973, Hayward and Sutherland 1974, Tacconi and Billi 1987), and continuously weighable pit samplers (Powell et al. 1995; Reid and Laronne 1995; Reid and Frostick 1986; Reid et al. 1980, 1985). Small non-recording trap samplers (Church et al. 1991, Bunte 1997) require less construction and can be installed in a stream by a small field crew with shovels and buckets. But trap operation is limited to flow conditions during which an operator can reach down to the stream bottom to empty the traps. Another problem with traps installed in the bottom of a mountain stream is that sampling efficiency for a given particle size varies with flow and thus with location within the reach. Highly energetic flows over steep riffles can cause sand and pebbles to go into suspension, thereby greatly diminishing the local trap efficiency and underpredicting transport rates.

Stationary bedload samplers with large, vertical openings of several square feet have been used to collect sampled gravels in fishing nets. These net-frame samplers have been successfully used to sample pebble and cobble bedload in gravel-bed mountain streams (Bunte 1996, Whitaker and Potts 1996). But large net-frame samplers require a bridge with sturdy vertical bars for support, a sill on the stream bottom for good ground contact, and the strength of several people to operate.

None of the samplers described above is suitable for measuring incipient motion of pebbles and cobbles in remote mountain streams by a small, mobile field team.

² Sampling efficiency is the ratio of the amount of sediment collected in the sampler per time versus the amount of sediment that would have passed the sampler location had the sampler not been there. Sampling efficiencies larger 1 express oversampling.

3. The stationary net-frame sampler

The aim of this study is to develop and field test a portable sampler to *measure the onset of gravel and cobble bedload transport* in remote mountain streams. For this objective it is important that the sampler representatively collects all mobile gravel particle sizes, whereas the computation of cross-sectional transport rates is of lesser concern. The sampler should not require substantial construction in the stream bed, should cause only minimal stream bed disturbance, and should be relatively easy to operate as long as the stream remains wadable. To achieve this, a sampler needs to have the following characteristics:

- have a large enough sampler entrance to allow cobbles to easily enter into the sampler,
- be stationary in order to allow long sampling times (up to several hours) to increase the probability of sampling infrequently moving particle sizes,
- have a large sampler bag to accommodate large sample volumes without reducing sampling efficiency,
- have a comparatively large mesh width to keep flow resistance at a minimum,
- be light-weight for portability,
- be operable in flow depths and velocity up to bankfull discharge, and
- require no more than two field persons to operate.

3.1 Sampler design

Given the criteria above, a sampler was designed consisting of the following parts (Fig. 3.1):

- sturdy aluminum sampler frame,
- webbing loops with buckles,
- sampling bag made of fishing net,
- aluminum ground plate, and
- two smooth iron holding stakes.

3.1.1 Sampling frame, ground plate, and stakes

The sampler frame is made from a strip of flat aluminum 0.25 inch thick and 4 inches wide. The strip is cut and welded to a frame 12 inch wide, 8 inch high, and 4 inch deep. The bottom piece of the sampler is beveled at an angle of ca. 30°, so that particles do not have to pass over an edge when entering the sampler. The sampler rests on a ground plate 16 by 10 inches in size (Fig. 3.2) to ensure a good contact with the stream bottom. The ground plate can be made of 0.25 inch aluminum or 1/8 inch steel, weighting portability against an a slightly increased probability of entrainment by flow. The ground plate is slightly bent (10°) along the front edge to provide a smooth transition between the stream bed and the sampler entrance (Fig. 3.3). Two holes of 5/8 or 3/4 inch \varnothing are drilled on the sides of the ground plate, with about 1 inch space between the center of the hole and the frame. This space is necessary because the stakes pounded into the cobbly stream bed will usually not be perfectly vertical but oblique, pointing into different directions.

The stakes are 0.5 inch in \varnothing , about 3 feet long and have a sharpened tip. The stakes should be smooth on the outside (no rebar stakes). This makes them easier to pound into the stream bed, and makes it easier to fasten the webbing loops onto the stakes. A stake driver helps keeping the stakes straight as they are pounded into the stream bed. A stake driver is a miniature version of a fence post driver and can be made by welding a 6 inch piece of solid rod with a 1 inch outside \varnothing end to end of a 10 inch piece of pipe with a 3/4 inch inside \varnothing .

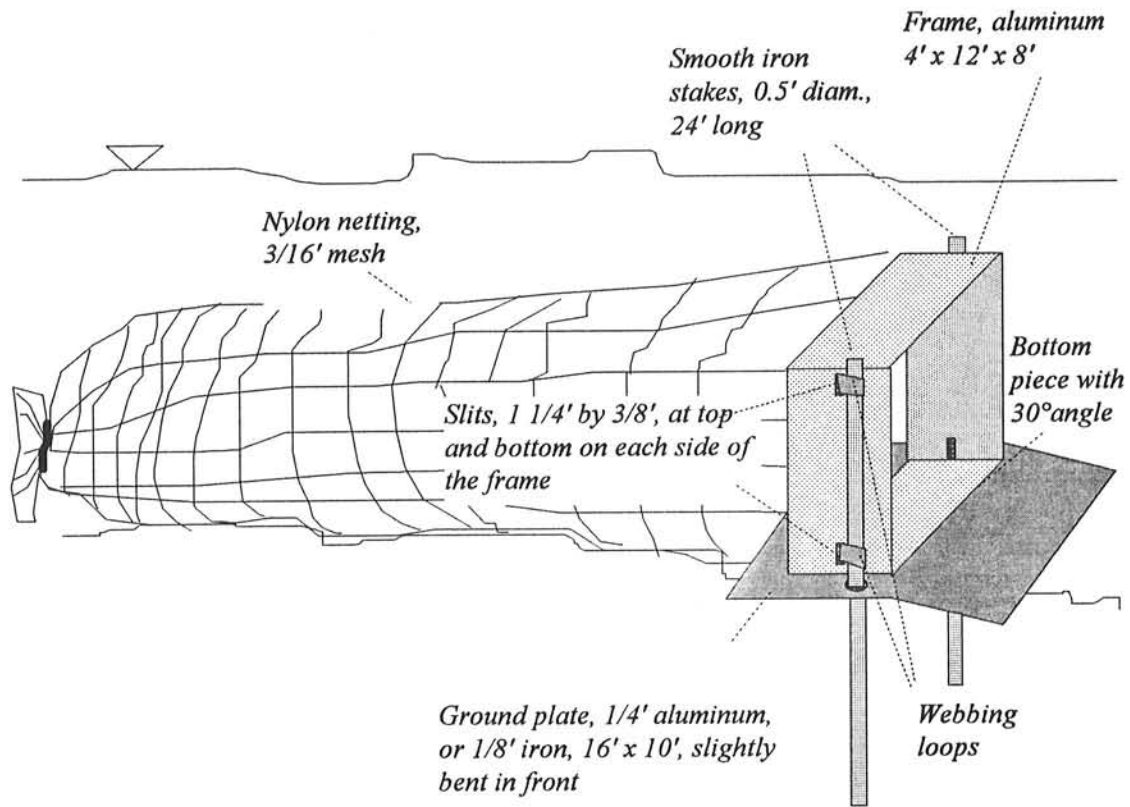


Fig. 3.1 Schematic diagram of the stationary net-frame sampler. All measurements in inches.

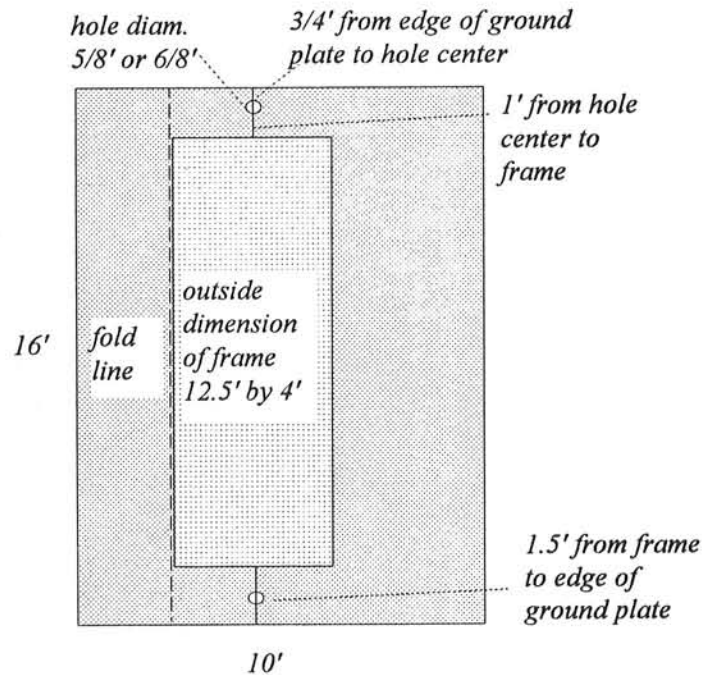


Fig. 3.2: Dimensions of ground plate and holes. All measurements in inches.

Two slits are cut into the top and bottom of the aluminum pieces that make up the sides of the sampler frame (Fig. 3.3). The slits are 1.25 inch long, 3/8 inch wide and are used to hold the webbing loops with which the sampler is fastened to the stakes. To prevent damage to the webbing, all edges of the slits should be well rounded and smoothed.

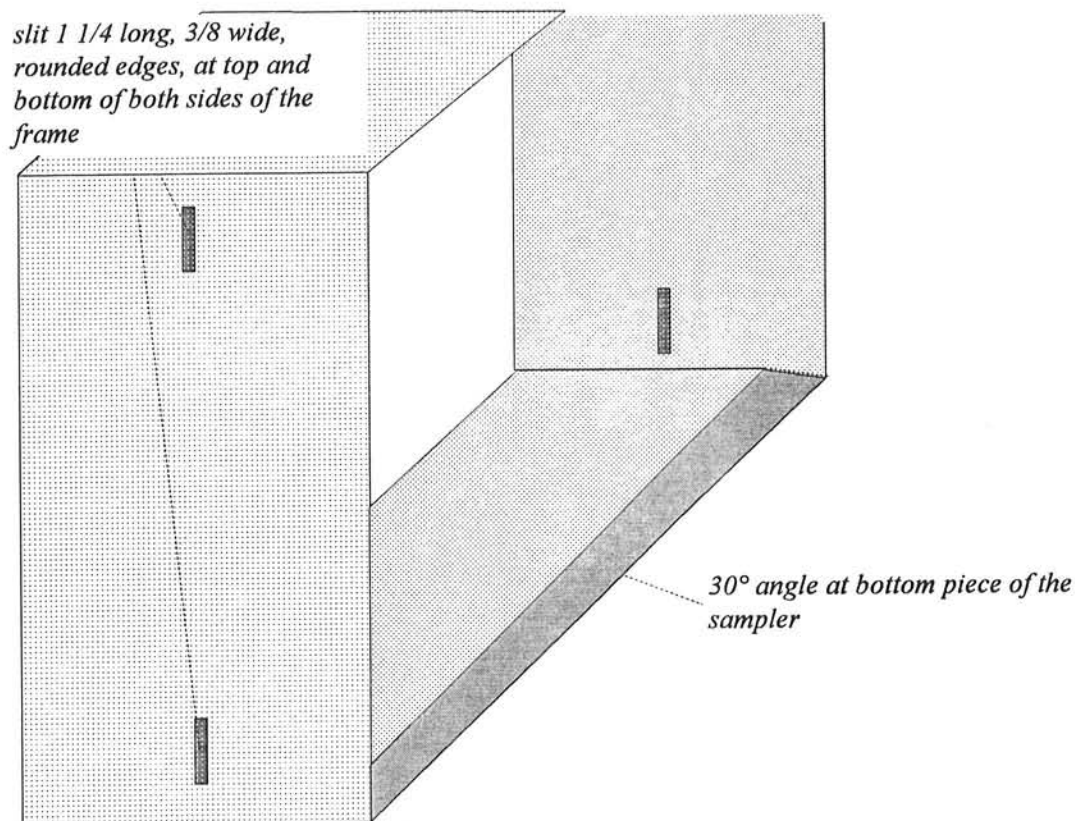


Fig. 3.3: Detail of the sampling frame with beveled front edge and slits.

3.1.2 Webbing loops

Pieces of tubular strap webbing³ 14 inch long by one inch wide are used for the loops. Tubular webbing is not only strong, but also thick enough not to slide involuntarily through standard-sized 1-inch buckles. A slip lock buckle holds the webbing at the inside of the sampling frame, while a 1-inch tension lock buckle with four slots connects both ends of the webbing in an adjustable way (see buckle at the lower end of a backpack shoulder strap). Fig. 3.4 shows how the webbing connects sampler frame and stakes and the path of the webbing through the buckles⁴.

³ Tubular webbing can be bought from a roll in sporting goods and hardware stores. All cut ends should be seared.

⁴ Both kinds of buckles can be found in sporting goods stores and in some hardware stores.

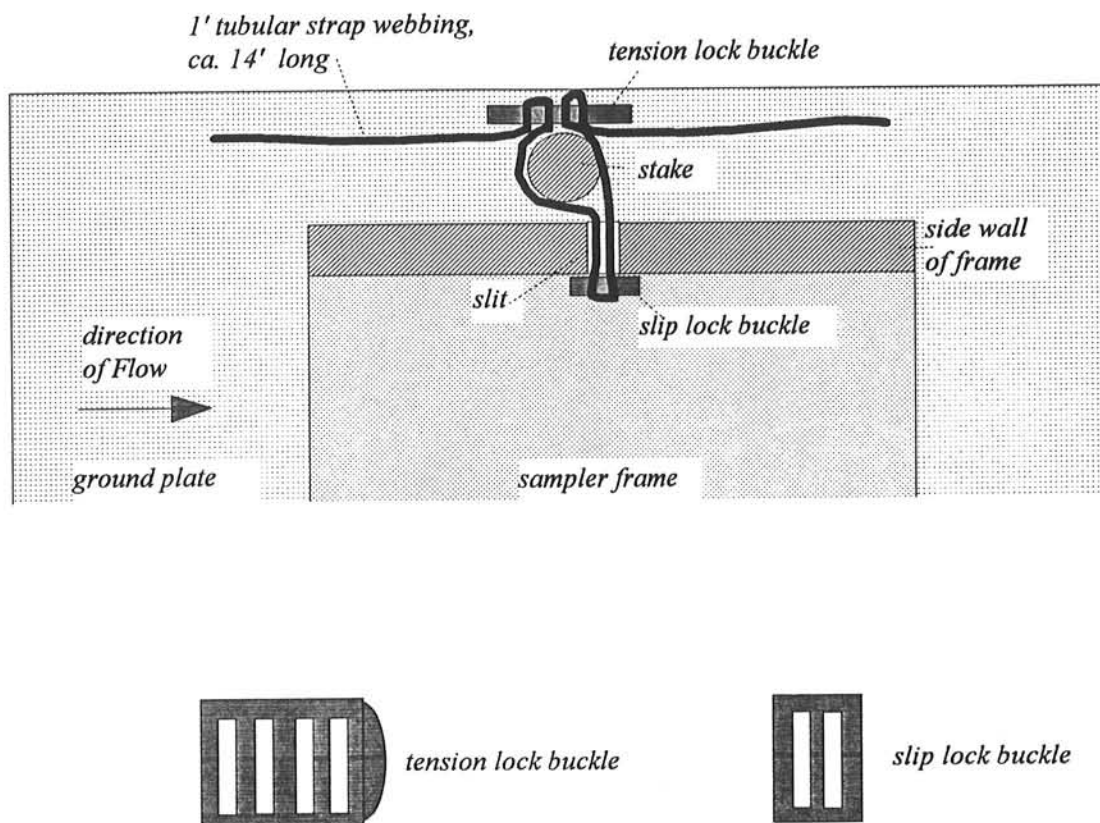


Fig. 3.4: Webbing loops, schematics of buckles, and the way webbing loops connect sampler to stakes.

3.1.3 Sampling net

Sediment entering the sampler is collected in a trailing (fishing) net three feet long. A mesh width of 3/16 (4.7mm) was chosen as a compromise between unobstructed conveyance of water flow and small trapable particle size (Fig. 3.5). Netting with such mesh width is knottless and crocheted in thin nylon yarn (Raschel)⁵. Raschel netting is quite sturdy and abrasion resistant. Other mesh sizes, net strengths, and fabrications are available and can be chosen depending on expected transport rates and particle sizes. Common mesh widths are 0.25, 0.5, 1, 1.5 and 2 inches.

The Raschel 3/16 inch netting is sold from a roll 8 feet wide. To make the net, the netting is cut along the middle line into pieces 4 by 4 feet when stretched so that meshes are open. It is important to lay out the netting for each sampler in such a way that a pull of the net in streamwise direction does not close the meshes, but opens them. Each piece of netting is hand-sewn to form a net, using non-stretchable nylon yarn about 1 mm thick and a blunt slightly curved upholstery needle. The seam is made by applying two parallel rows of a weaving stockinette stitch⁶ (Fig. 3.6) through the mesh holes (not through the thread).

⁵ A sturdy type of netting (Raschel) can be purchased from Delta Net and Twine Company, Inc. in Greenville, Mississippi, 1-800-255-5917.

⁶ Unless a helper holds the netting ready for sewing, this seam is easiest using a weaving stockinette stitch: the two parts of the net are held apart, the needle goes through the appropriate mesh holes in each piece of the netting. The appropriate mesh holes can easily be identified when the nets are apart, and once a couple a stitches are completed the yarn is pulled tight.

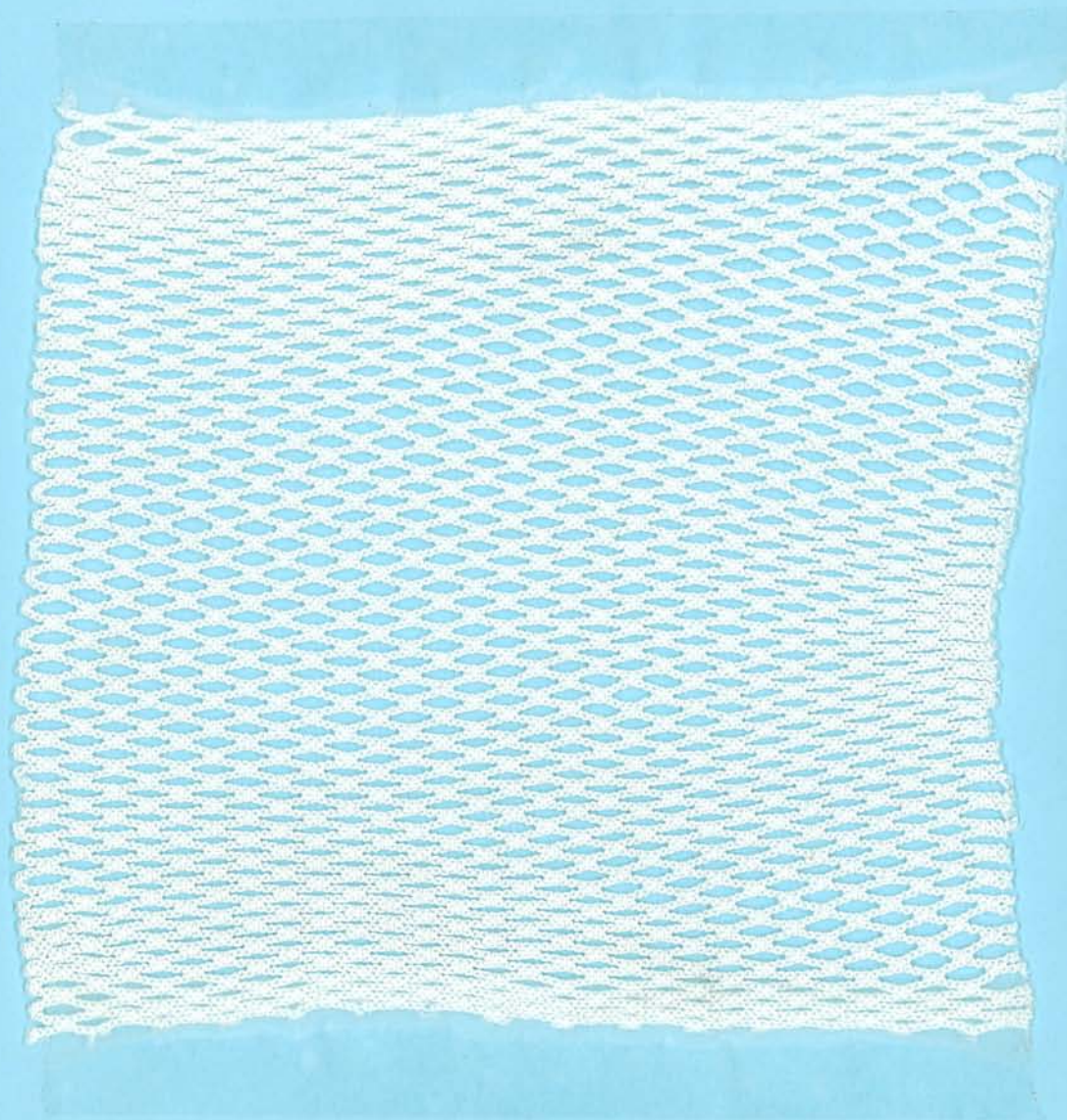


Fig. 3.5: Sample of the netting used for the sampler nets

piece of the netting. The appropriate mesh holes can easily be identified when the nets are apart, and once a couple a stitches are completed the yarn is pulled tight.

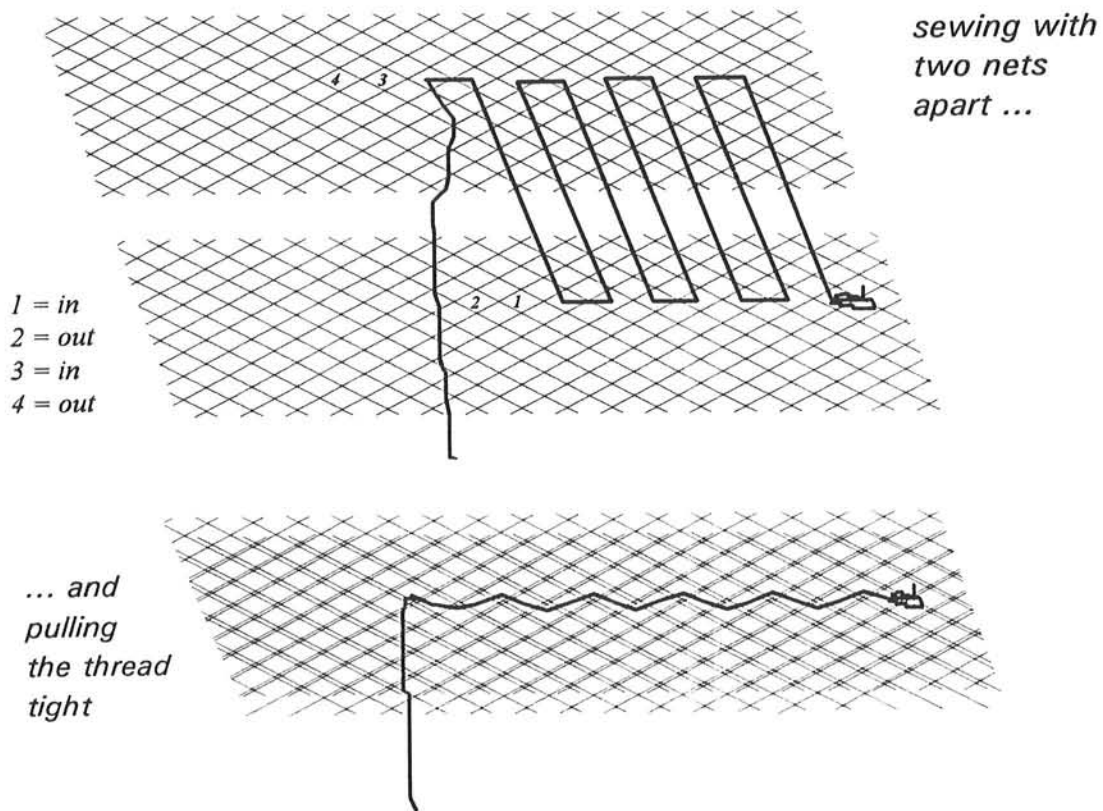


Fig. 3.6: Sewing seams on the net using a weaving stockinette stitch: The first step pulls the thread through the appropriate mesh holes. This step is repeated a couple of times before the thread is pulled tight in the second step.

The seam needs to be stretched while sewing. Once the nets are completed, one end of the net is folded around the sampler frame and sewn back onto itself with two parallel rows of weaving stockinette stitches.

Small holes are cut into the net where it covers the slits and the webbing loops are threaded through them. All cuts in the netting should be seared to protect against unraveling.

The downstream end of the net is tied shut with a piece of cotton covered rope (clothline). A couple of tight turns, finished with a simple knot and bow (like tying shoe laces) has never come undone during sampling. A more complicated knot would be difficult to open with wet, cold, or gloved fingers, and there is enough friction on the cotton covered rope to hold the knot securely. The clothline could be replaced by a velcro strap or other device.

The Raschel nylon netting proved to be very sturdy. However, when sample mass exceeds a bucket full per sampling duration, the fine-meshed Raschel netting may need to be supported by an outer stronger, wide-meshed net (e.g., 1-inch knotted nylon net).

3.2 Installation of the sampler in the stream

The ground plate is placed onto a level location on the stream bed from which surface layer particles have been removed. The beveled front edge of the plate is then slightly pushed into the bottom sediment. If the ground plate fails to rest firmly on the bottom, additional

protruding rocks may need to be removed. The objective is to build a smooth transition between stream bed and ground plate. The edge of a heavy rock can be placed on the ground plate to help hold it down during fast flow.

Once the ground plate is satisfactorily placed on the stream bed, both stakes are pounded through the holes of the ground plate 1 to 2 feet deep into the stream bed. Stakes should be driven almost flush with the top of the sampling frame. This is for safety purposes, and to reduce the risk of catching floating debris. When driving in the stakes, the actual hammering (short-handled, heavy drill hammer) is onto the stake driver positioned over the stake. The stake driver enlarges the surface to be hit and aids in holding the stake in place during pounding. If the tip of a stake hits the side of a rock the stake begins to move away from the vertical direction. Pulling and pushing the stake with the stake driver while pounding can help to regain a somewhat vertical position. If a stake hits the middle of an unpenetrable rock the ground plate may have to be moved to a new location. Several tries may be necessary to find a location at which both stakes can be placed in a semi-vertical position. Once installed, the ground plate remains in place for the entire sampling season.

Installation of the ground plates is easiest during low, but it can be installed during high flows as long as it is possible for a person to reach down to the stream bed to position the plate. In fast flow, it is easier to first pound in one of the stakes, then slide the ground plate over the stake and properly position it on the stream bed. Then, the second stake is pounded in. While low flows are easiest for sampler installation, care must be taken to anticipate high flow conditions, and to select a cross-section in which all locations remain wadable during high flow.

The sampler frame is held in place between the stakes on the ground plate by four adjustable loops of 1 inch webbing straps fastened to the sides of the sampler frame. The webbing loops are slid over the stakes and the sampler is pressed down onto the ground plate. The webbing loops are pulled tight and the sampler frame is checked for good contact with the ground plate. Once the sampler is satisfactorily positioned, the webbing loops are prevented from sliding up by fastening a shaft collar⁷ (Fig. 3.7) onto each stake. For easy operability, the small hex-wrench screw that comes with the shaft collar is replaced by a thumb screw. The sampler is now ready for sampling. If sampling does not start immediately the net can be left in the stream without the end being tied shut.

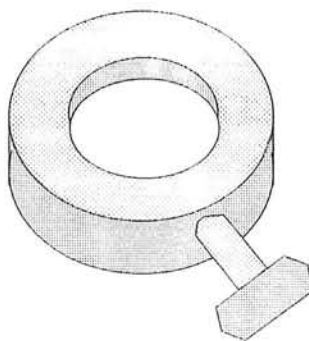


Fig. 3.7: Shaft collar with thumb screw.

⁷ Shaft collars can be found in the specialty hardware section of hardware stores. Some thumb screws have to be screwed in and out a couple of times in order to go smoothly.

Stream flow in mountain streams is cold during the beginning of snowmelt high flow. Neoprene gloves (diving gloves) work well for cold protection while maintaining relative good operability, but those gloves do not withstand vigorous use.

3.3 Sampler locations in the stream bed

Bedload transport is highly variable across the stream, especially at low transport rates when bedload is confined to narrow “streets”. Those bedload streets are often associated with the location of flow cells and locally upwelling flow. Upwelling flow and high local transport rates are not associated with the deepest and fastest flow in the thalweg. In this study, (Section 5.3.2) most of the bedload traveled over the toe of the bar, while next to none of the fine gravel bedload came through the thalweg. Since it is difficult to identify the exact location of highest transport rates, and since these locations may not be wadable during high flow, samplers should be installed in a relatively even-shaped cross-section (riffle or run) so that all samplers can be reached by wading during high flow.

Although the computation of a cross-sectionally mean transport rate is not the main objective when sampling to detect the onset of gravel motion, several samplers should be installed across the stream to increase the probability of collecting gravels moving somewhere through the stream cross-section. The number of samplers needed to measure a representative transport rate for the entire stream width depends on the width of the streams. A sampler spacing of about 1 m seems to be suitable in mountain streams about 5-15 m wide.

Samplers in this study were positioned along an imaginary diagonal line across the stream. The intent of this arrangement was to help to prevent debris (branches and sticks) from getting caught behind the stakes (Fig. 3.8).

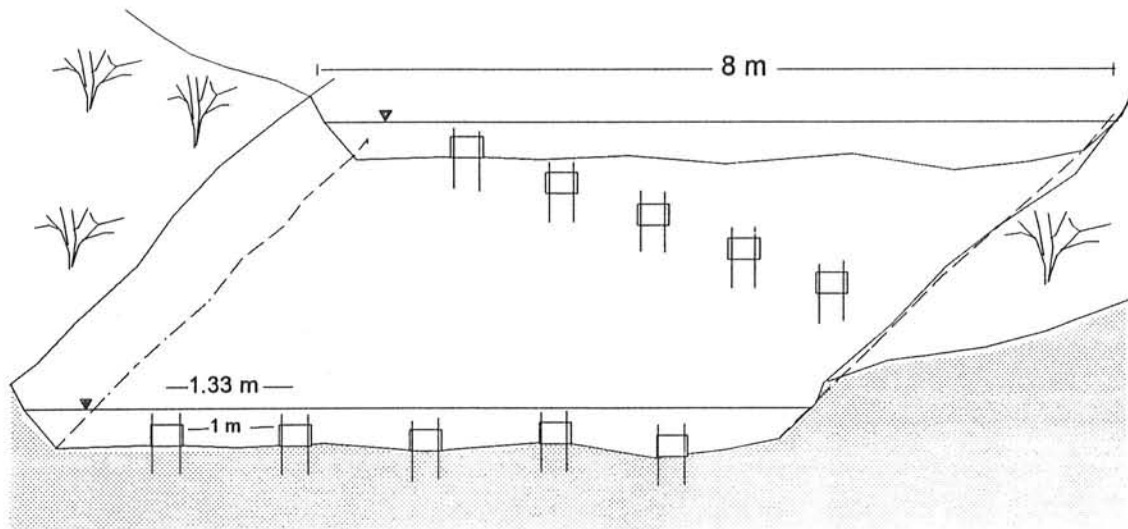


Fig. 3.8: Diagonal arrangement of the samplers in an example stream 8 m wide.

3.4 Operation of the sampler

3.4.1 Emptying the samplers

After the sampling period is completed, the operator wades to the sampler and lifts the end of the net out of the flow, leaving the sampler frame in place on the stream bottom (Photo 1). Bedload and organic debris that accumulated in the net is shaken towards the downstream end of the net which is tied shut (Photo 2). The clothline is untied and the contents of the net is emptied into a large prelabelled ziplock bag (Photo 3). The net is tied shut again and dropped into the current for another sampling period (Photo 4). Restrict wading around the samplers to the downstream side, so that gravel kicked lose is not sampled as bedload. A single operator can empty the samplers, but operation is easier and safer when a second person assists the operation, especially when wading start to become more difficult as flow increases.

3.4.2 Field examination of the samples

Even in seemingly clear flow, much of the contents of the net can be organic debris, especially during early parts of high flow. The majority of the debris consists of sticks, branches, herbaceous riparian vegetation, benthic invertebrates (esp. nymphs of stonefly and mayfly, and caddis fly larvae cases), ants, bugs and earthworms. Thus, stationary net-frame samplers may provide a useful sampling tool for fisheries biologists, and stream ecologists as well.

The sampled organic debris can easily conceal bedload particles in the net, especially if the sample contains only a few small pebbles. Thus, no sample should be discarded before careful inspection for bedload particles. Organic debris is best removed from the sample in the field. This reduces the sample mass to be hauled back to the lab, and provides immediate information about the number and size of transported particles. To separate organic debris and bedload particles, pour the sample mixture into a metal bowl⁸, cover with water and gently stir and wash the mixture. The heavier bedload particles accumulate at the bottom of the bowl. The organic material (most of which is so water-logged that it doesn't float) is carefully picked up, a good pinch at a time, inspected for adhering small pebbles, and discarded back to the stream. Bedload particles in the bottom of the bowl are bagged for sieve analysis or counted and sieved (using a gravelometer) directly in the field.

⁸ Light-weight 10-12 inch Ø metal bowl are sold in houseware sections of discount stores or large food stores.



Photo 1: For emptying the sampler, the end of the net is lifted out of the flow. All debris and bedload collected in the sampler are shaken to the end of the net before untying the clothline.

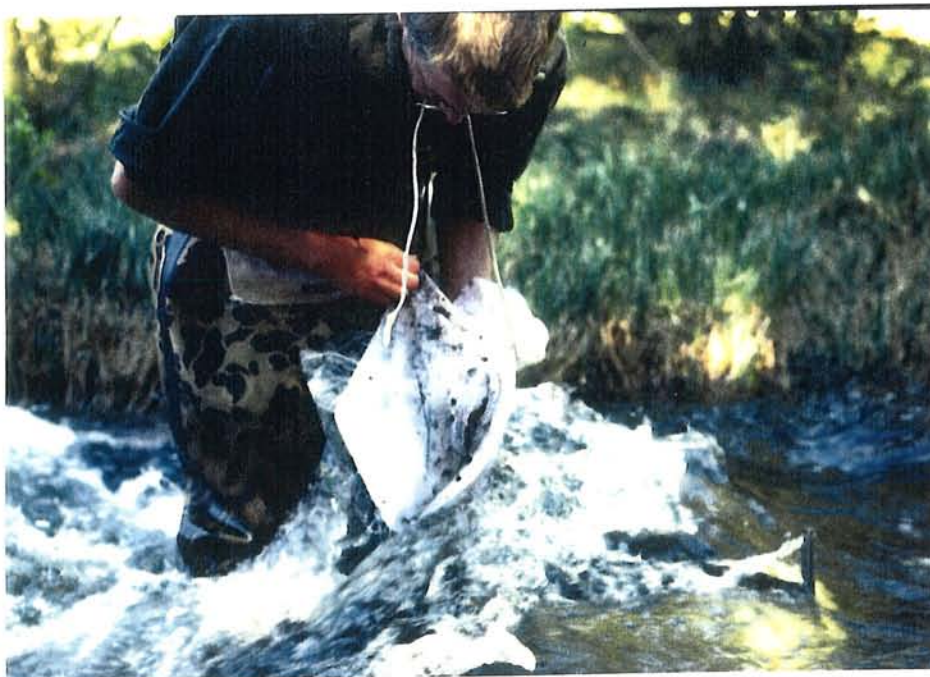


Photo 2: The net is untied...



Photo 3: ...and all debris and bedload is shaken into a large ziplock bag



Photo 4: The net is tied shut and put back into the flow for another sampling period.

4. Field testing the stationary net-frame sampler

Bedload sampling for initial motion studies in mountain gravel-bed streams is often aimed at flows between half bankfull and bankfull flow since gravel and cobble particle sizes are typically entrained during those flows.

4.1 The field site: St. Louis Creek

St. Louis Creek near Fraser, CO. is a cobble-bed mountain stream in north-central Colorado, about 75 miles NW of Denver. Most of the catchment is mountainous, reaching from 9,000 feet at the lower end to 12,500 feet at the highest peaks. The main direction of the stream is south to north. Some water from St. Louis Creek and its tributaries is diverted for use in Denver. Several measuring sites have been established by Ryan (1994) along St. Louis Creek, with Sites 2 and 3 (elevation of 9,300 feet) below, and Sites 4 and 4a (9,500 feet) above the diversion (Fig. 4.1).

The stream was selected as a field site for several reasons: (1) The stream is of moderate size. Stream width ranges from 8.5 m at the lower sites to 6.5 m above the diversion dam. The stream morphology can be generally classified as a Rosgen B-type stream with only a slight riffle-pool pattern. Thus, much of the stream bed comprises riffles and runs which remain wadable during bankfull flow. (2) The stream is accessible from a gravel road at several locations. (3) Field facilities of the Fraser Experimental Station allows measurements to be made over the entire range of daily flows which, being a snowmelt regime, includes the falling limb of flow in the morning, low flow around noon, rising limb in the afternoon with peak flow around 6 p.m., and the early falling limb after 8 p.m. (4) Bedload and stream morphology data have been collected by the Rocky Mountain Research Station and were available for comparison.

A field site was set up between the established sites 2 and 3 because this was a convenient location, with a suitable stream type, and prior bedload sampling locations nearby. The study was not concerned with effects of water diversion on sediment transport.

Timing of high flows and field work

A 40-year post-diversion record of daily flows from St. Louis Creek (station ID 09026500) from 1956 to 1996 indicated that peakflow (mean daily flows more than twice the average annual mean daily flow) can occur between mid May and mid July. Moderate high flows less than twice the average annual flow most likely peak during the second and third week of June. Small high flows that barely exceed mean annual flow tend to peak in mid June (Fig. 4.2). Since snowpack was below average this year, it was assumed that high flow would be moderate at best, and that timing of field work would be critical.

Unfortunately, current flow conditions for St. Louis Creek cannot be monitored via the internet. The nearest gaging station with on-line internet access is Williams Fork near Leal, CO (station ID 09036000). Williams Fork is the next large drainage southwest of the St. Louis Creek drainage. The Williams Fork drainage has an area of about 200 km², while the St. Louis Creek drainage has an area of 54 km² at Sites 2 and 3 below the diversion, and 34 km² at Site 4 upstream of the diversion. Slope aspect is different for the two drainages as well: main slope aspect in the Williams Fork drainage is SW, while many slopes face into a northerly direction (between East, North, and West) in the St. Louis Creek drainage. Consequently, only the highest flows are approximately proportional between Williams Fork and St. Louis Creek (Fig. 4.3). In years with moderate high flows, high flow tends to peak earlier at Williams Fork.

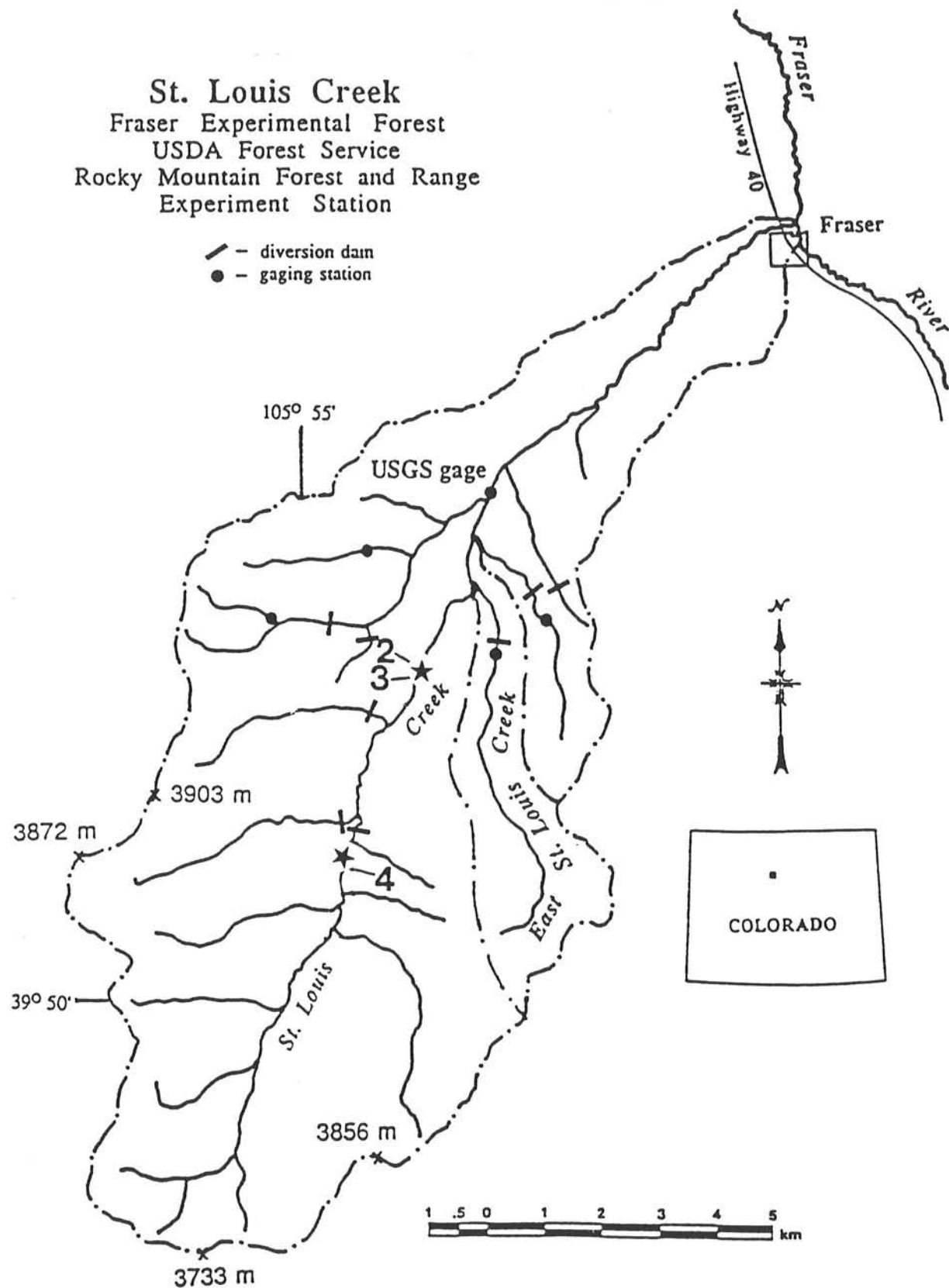


Fig. 4.1: Map of St. Louis Creek drainage. The lower and upper site are marked with a star (slightly altered, from: Ryan 1994).

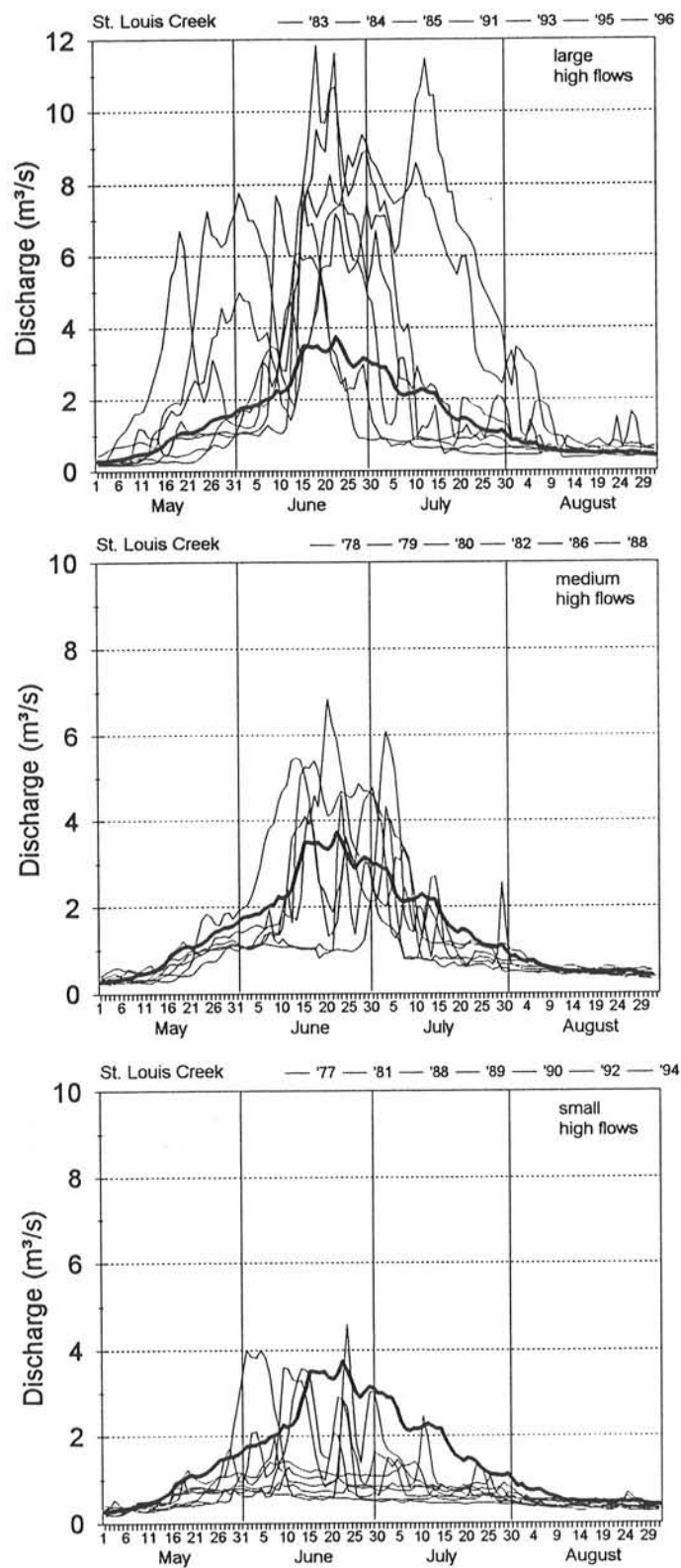


Fig. 4.2: High flow patterns for large (top), moderate (center), and small (bottom) high flows at St. Louis Creek near Fraser, Station ID 09026500. (Replotted from data obtained from the USGS).

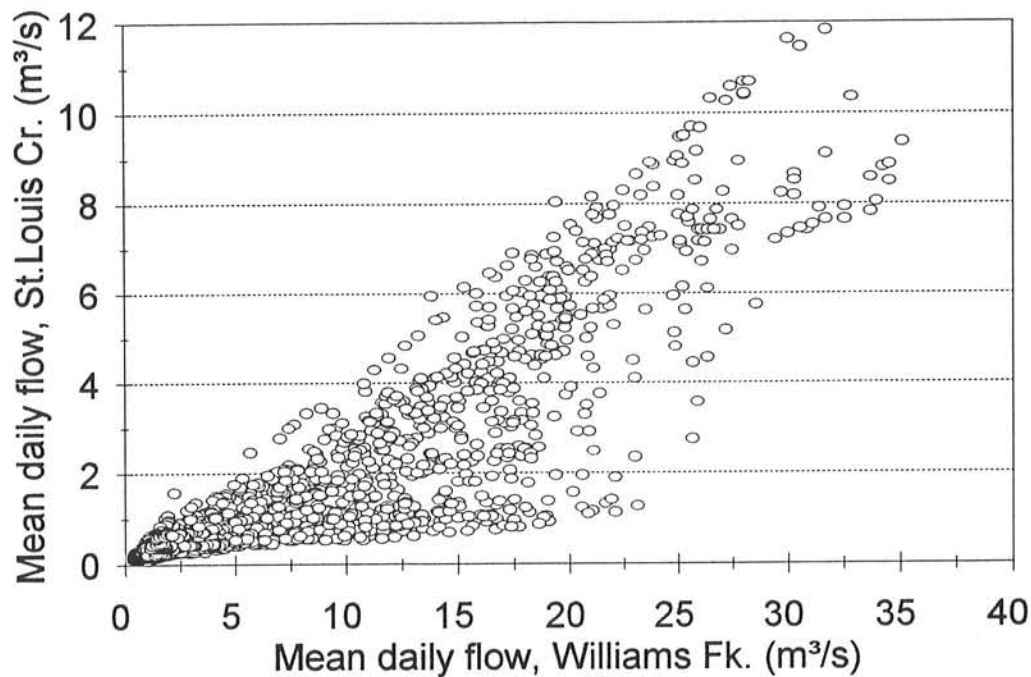


Fig. 4.3: Annual hystereses loops of mean daily flow at Williams Fork versus St. Louis Creek

Mean daily flow at Williams Fork remained below the longterm average for almost the entire 1998 snowmelt high flow season, except for a 10-day period when unseasonably hot weather lead to an early snowmelt peak between June 1-3 (Fig. 4.4). A cold front with snowfall to below 8,000 feet dropped flow drastically. On June 6, flows at the lower field site at St. Louis Creek (between the established sites 2 and 3) were about 50% of bankfull, assuming a bankfull flow of $5.2 \text{ m}^3/\text{s}$ (Ryan and Troendle 1994). The high flow water line was about 10 cm above the current flow and extrapolation of a later constructed stage-discharge curve indicated that peak flow had reached 60-65% of bankfull. Flow continued to drop for another two weeks.

A second snowmelt runoff period started on June 19. Since it was obvious by that time that the snowpack would not sustain a large second peak flow, a new field site had to be found at which peak flow would be as close to bankfull as possible. Staying within the St. Louis Creek drainage, this meant that the site should:

- be above all potential water diversions,
- be above low-elevation tributaries that had already peaked,
- be close to where alpine tributaries join the mainstem,
- be low enough within the watershed to feature a plane-bed (B-type) stream morphology as opposed to a step-pool morphology, and
- have bed-material particle sizes within the gravel-cobble range, as opposed to the cobble-boulder range, in order to obtain particle mobility during high flows.

Williams Fork near Leal, Co, 1998

station ID: 09036000

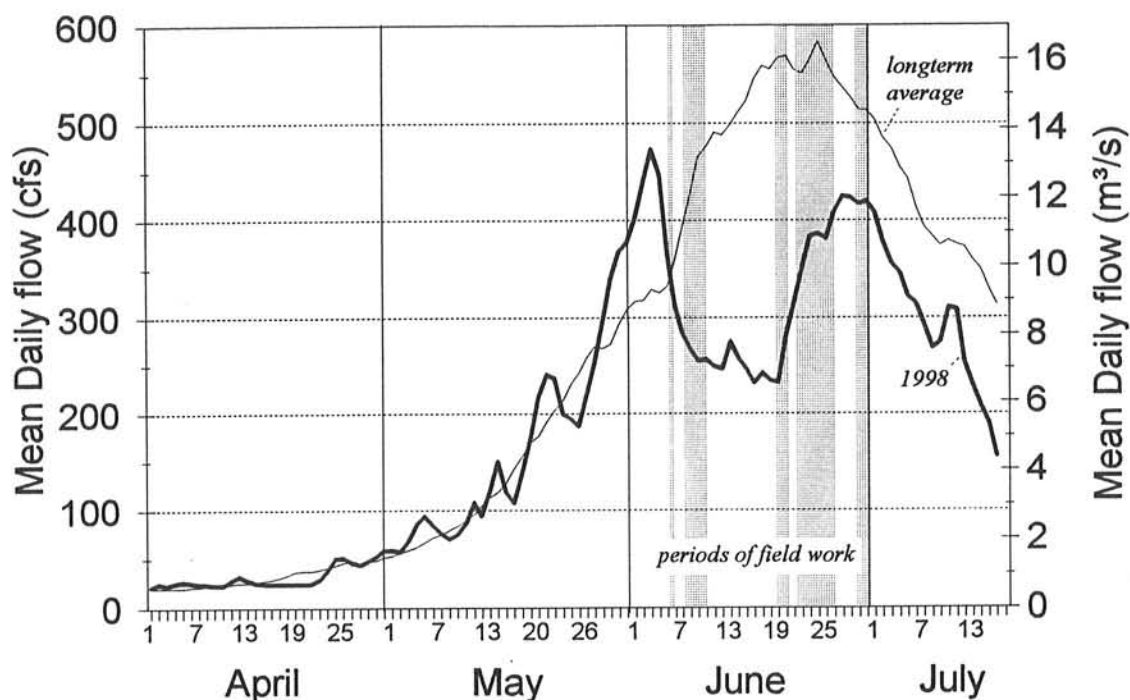


Fig. 4.4: Mean daily flows during the 1998 snowmelt season for Williams Fork (replotted from data obtained from the USGS web site "http://nwis-colo.cr.usgs.gov/rt-cgi/gen_stn_pg?station=09036000").

After inspecting several kilometers of stream above the mainstem diversion, an "upper" site was selected (Photo 5 and 6) a few 100 m upstream from the diversion pond and about 150 m below the established site 4 (see Fig. 4.1). That site had no immediate road access and thus put the portability of the samplers to a test.

4.2 Field measurements

Field measurements included measurements of discharge and bedload transport using both the newly designed stationary net-frame samplers and the Helley-Smith sampler. Site surveys and surface and subsurface bed material sampling was done at both sampling locations. Most measurements of flow and bedload transport were taken on the upper site where flows reached a higher percent of bankfull than at the lower site.

4.2.1 Measurement of flow

Flow velocity was measured with an electromagnetic Marsh McBirney current meter several times per day at the upper site, and periodically at the lower site, totalling 23 measurements at the upper site, and 9 at the lower site. Flow velocity at each vertical was measured at 0.6 of the total depth (40% above ground), and verticals were spaced 0.5 m apart.

At the lower site, water stage was read off an established staff gage. At the upper site, a ruler fastened to a stake at the left stream bank served as a provisional staff gage. Water stage was read at hourly intervals or whenever possible.



Photo 5: View downstream at the upper site at St. Louis Creek.



Photo 6: View downstream at the upper site at St. Louis Creek.

4.2.2 Bedload transport measurements with the stationary net-frame sampler

Five ground plates for stationary net-frame samplers were installed at the upper site. The ground plates were spaced at about equal distances from each other along an imaginary line diagonally across the stream. The diagonal arrangement was thought to help prevent branches from getting caught behind the samplers. For similar reasons, samplers were removed from their ground plates when unattended at night and reinstalled in the morning. To prevent the ground plates from moving up the stakes and getting lost, they were held down by collar shafts after the samplers were removed.

Between June 19-30, 41 measurements of bedload transport were made at each of the 5 samplers at the upper site at various times during the day. Sampling periods lasted about one hour. The lower site had four ground plates installed in the central part of the stream at 2.8, 3.8, 5.3, and 7 m from the left bank. Only 8 samples were taken at the lower site because we had only five samplers, and flow was not expected to reach bankfull at the lower site.

Most of the hour-long bedload samples obtained with the stationary net-frame samplers were small, ranging from one pebble per hour to about one cup full of small gravels. Small samples with just a few particles were "sieved" in the field using a gravelometer, and the number of particles per size class was counted. Larger samples, and all Helley-Smith samples, were bagged for lab analysis which included removal of organic debris, air drying, sieving in 0.5- ϕ increments, weighing, and counting the number of particles for all size classes > 4 mm.

4.2.3 Bedload transport measurements with a 3-by-3 inch Helley-Smith sampler

Bedload transport was also measured with a 3-by-3 inch, thin-walled Helley-Smith sampler with an orifice ratio of 3.22 (as manufactured by GBC, Denver). Sampling locations across the stream were spaced at 0.5 m intervals, and sampling duration was 2 minutes per vertical. One traverse yielded 12-13 verticals at the upper site, and 18 verticals at the lower site. Since transport rates were small and amounted to less than a cup full per traverse, sediment sampled at each vertical was not individually bagged but accumulated in the sampler over all locations. A total of 18 Helley-Smith samples was taken at the upper site, and 8 at the lower site.

4.2.4 Site surveys and stream morphology

The stream at the upper site is 6.5 m wide with a mean flow depth of 0.34 m at 70% of bankfull (Fig. 4.5). Stream gradient is 0.018 (Fig. 4.6). The stream is incised into a floodplain covered by grass and a willow thicket. The floodplain is about 2-3 foot above the channel bottom. Thus, flow needs to increase by about 1 foot over the level of half bankfull to reach the flood plain. The right bank is almost vertical and stabilized by roots mats of grass, willows, and trees. The left bank is 0.5 - 1 foot lower, also vertical, and vegetated with mature conifer forest. Stream morphology varies between plane bed and riffle-pool with pools irregularly spaced and often affected by LWD.

Stream width at the lower site is 8.4 m, mean depth is similar to the upper site (Fig. 4.5). The stream is incised by 2-3 feet as well, and banks are stable and near vertical. The stream has a gradient of 0.012 (Fig. 4.6) and a riffle-pool morphology.

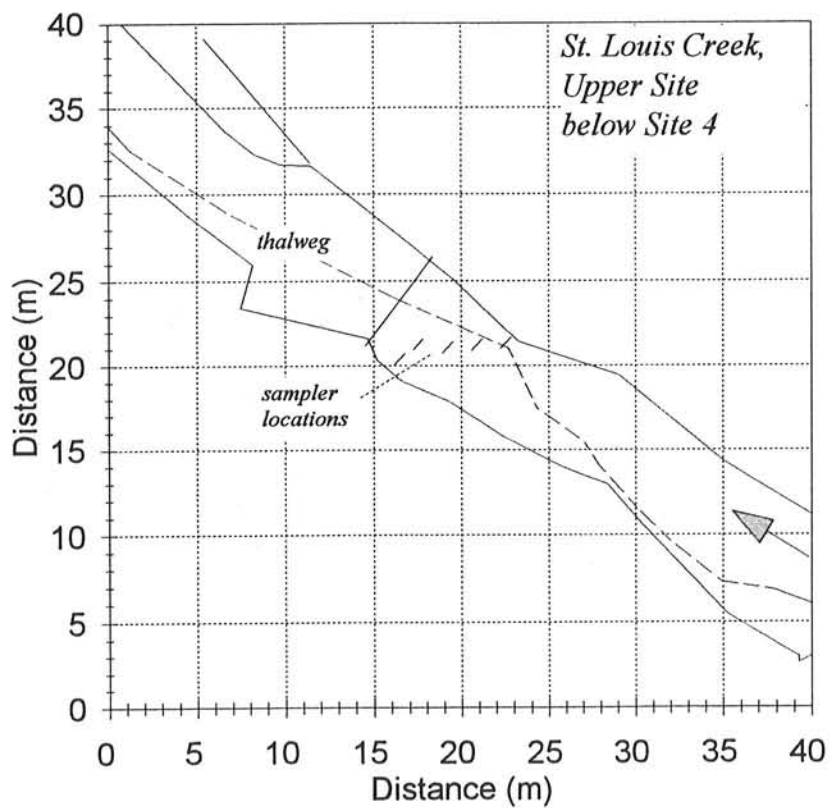
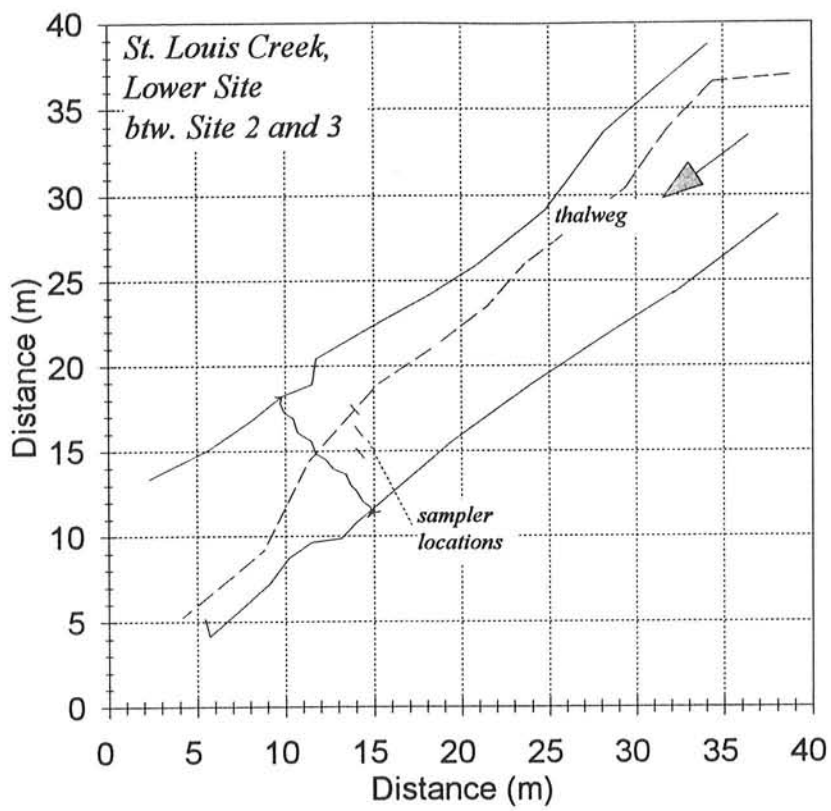


Fig. 4.5: Survey of the lower (top) and the upper (bottom) site.

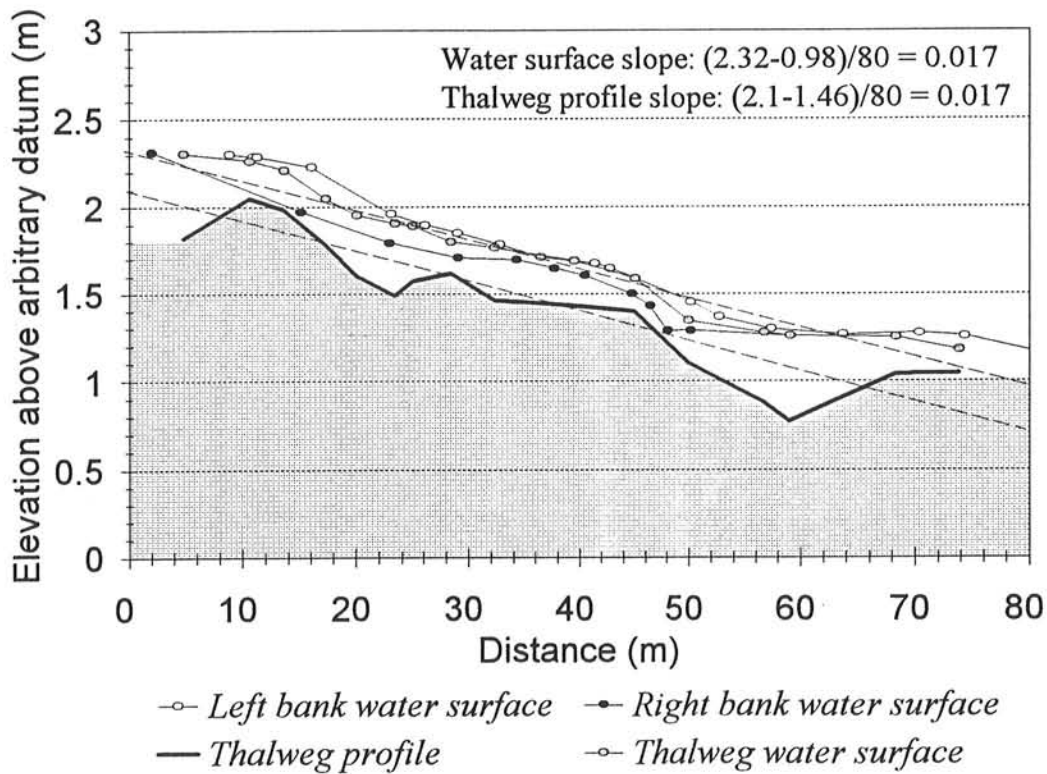
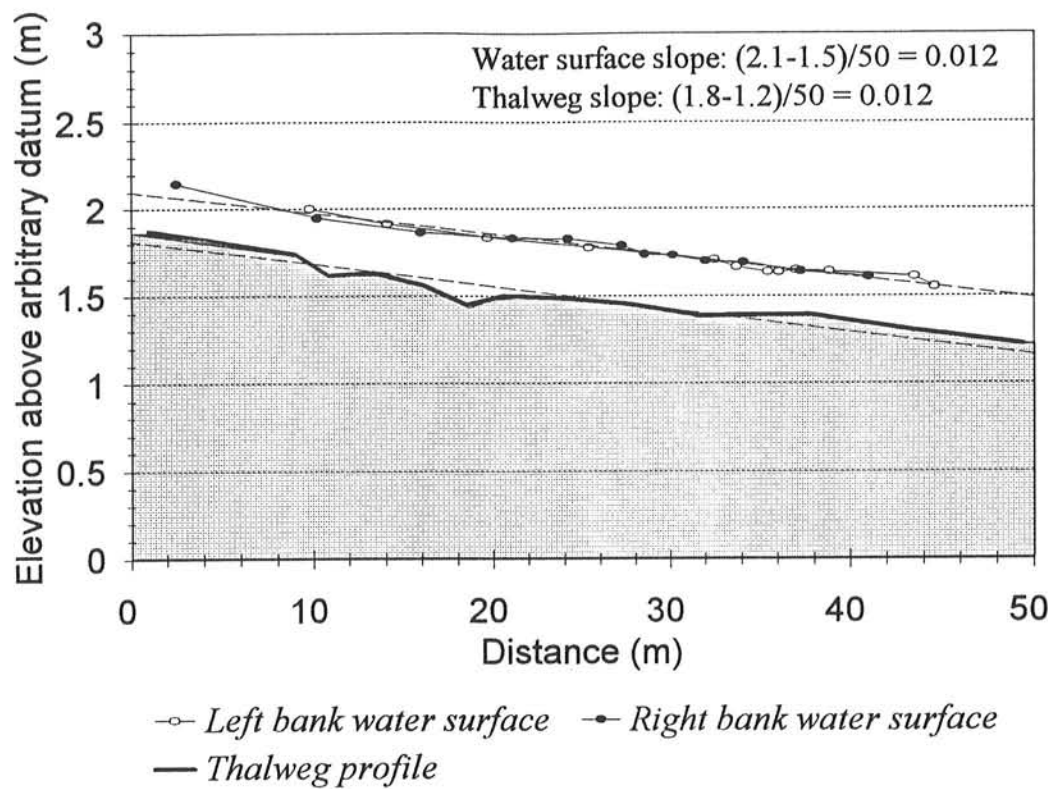


Fig. 4.6: Longitudinal profile along the thalweg channel bottom (—), and water surface profiles along the left and right bank, and computed gradient (---) at the lower site (top), and the upper site (bottom).

4.2.5 Bed material

Surface pebble counts of more than 400 particles were performed at both sites in 10-11 traverses, covering a riffle or run stream segment of 10-15 m near the bedload sampling locations. At the lower site, the surface D_{50} was 53 mm, with a D_{16} and D_{84} of 17, and 120 mm, respectively (Fig. 4.7). This classifies the bed as a poorly sorted gravel-bed stream. The upper site was slightly coarser with a surface D_{50} of 76 mm, a D_{16} and D_{84} of 22, and 160 mm, respectively, which classifies as a poorly sorted cobble-bed stream.

(Milhous et al. 1995)

Two subsurface samples were taken next to each other with a barrel sampler at the lower and upper site a few meters downstream from the stationary net samplers near the center of the stream. At the lower site, each of the sample weighed 80 kg, and the D_{16} , D_{50} , and D_{84} of the two combined samples were 7 mm, 37 mm, and 100 mm, respectively (Fig. 4.7). At the upper site, each sample weighed about 65 kg. The D_{16} , D_{50} , and D_{84} of the combined samples were 4 mm, 41 mm, and 207 mm, respectively (Fig. 4.7). Both samples were bimodal with a mode in large gravels (45 - 64 mm), and in cobbles (180 - 256 mm). The "kinked" gradation curve of the combined sample is probably not a sample error, but indicates a deposition of large gravels in between cobbles under a reworked surface. The particle size separating matrix from framework gravels is 26 mm at both sites (Fig. 4.8).

I'd assume now that the kinked distribution is a sampling error, and that a more representative value for the D_{84} is 125 mm (instead of 207 mm).

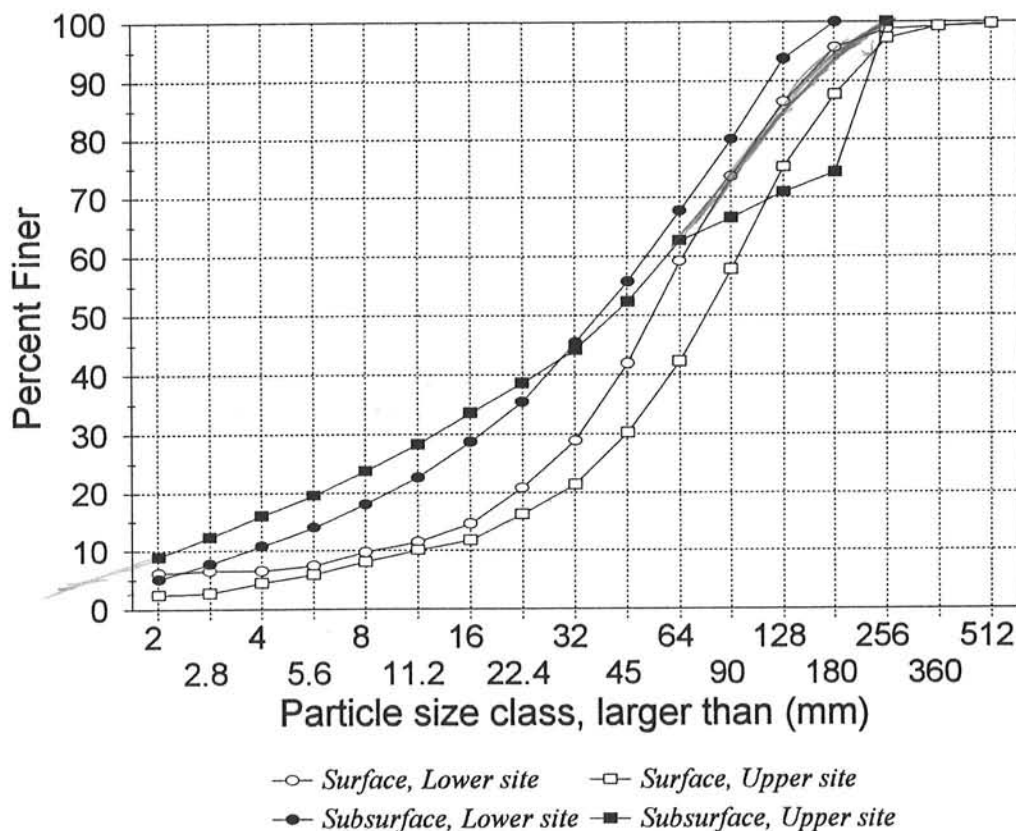


Fig. 4.7: Cumulative frequency distributions of a surface pebble count (> 400 particles) and two neighboring combined subsurface samples with a combined weight of ca. 160 kg at the lower site and a combined weight of 130 kg at the upper site.

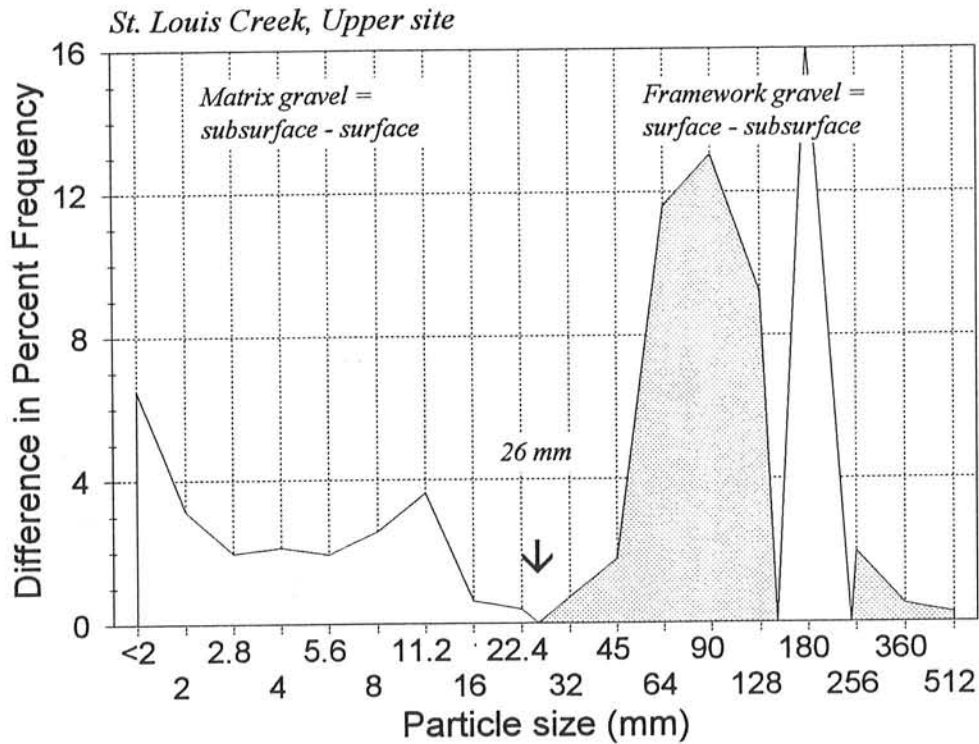
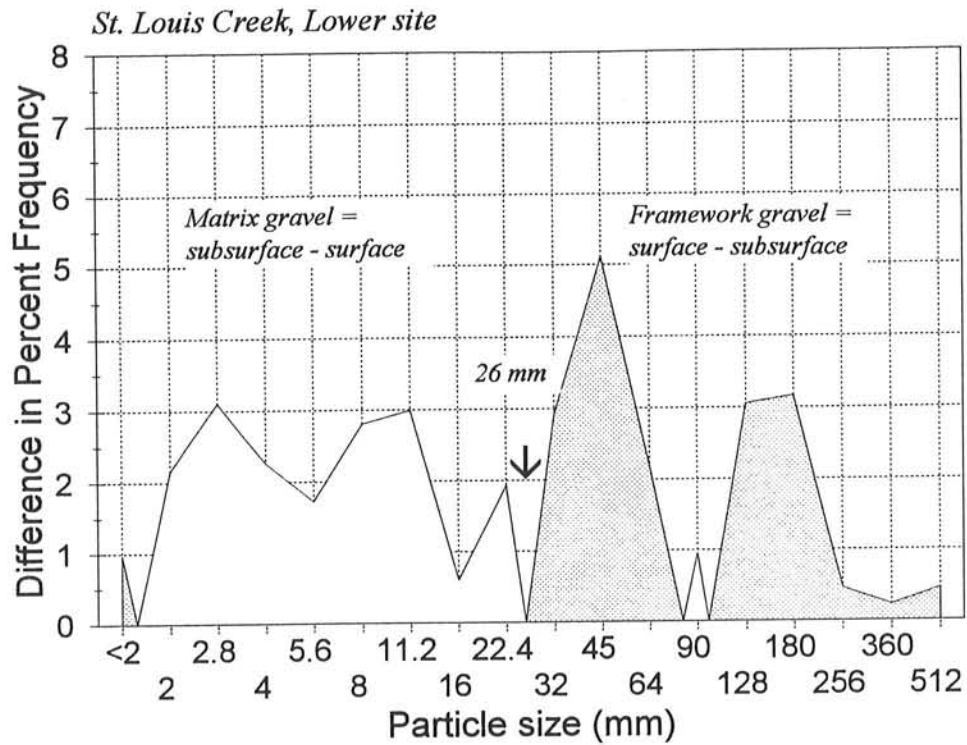


Fig. 4.8: Distribution of matrix and framework gravels computed from the difference in percent frequency between the frequency distribution of subsurface - surface (= matrix) and surface - subsurface (= framework). Cutoff point between matrix and framework gravels is 26 mm at both the lower site (top) and at the upper site (bottom).

5. Results

5.1 Analysis of flow

Discharge was computed by multiplying mean flow velocity per vertical by depth of flow at the vertical and the width increment to which the flow measurement was allotted. These discharge increments were summed over the width of the stream to obtain total stream flow Q . Mean flow velocity v_m is computed by dividing Q by the cross-sectional area of flow which is summed from local depth times incremental width. Mean depth of flow d_m is v_m divided by total width of flow w .

5.1.1 Stage-discharge rating curve and hydrograph

Stage-discharge relationships were developed for both sites (Fig. 5.1) so that a discharge value could be related to stage readings. The variability of flow around the rating curve regression function is about $\pm 12\%$, and attributable to several factors which include that verticals for flow measurements were not always in the same location along the cross-section, the unevenness of the cobble-covered stream bottom, the fluctuating display of the Marsh-McBirney current meter, and laterally shifting flow. On several occasions, flow velocity and depth increased recognizably at the far right side of the stream, while the staff gage at the left side remained unaffected by this increase. Fig. 5.2 shows examples of the lateral variation of unit discharge and the resulting differences in discharge for a given stage height.

Based on stage readings and a stage-discharge relationship, a hydrograph that spanned a time period of about 2 week around peak flow was constructed for the upper site (Fig. 5.3). The hydrographs clearly shows the daily fluctuations of flow induced by snowmelt runoff. Peak flow occurred during the last week of June. Peak flow reached $2.6 \text{ m}^3/\text{s}$ according to the stage-discharge relationship (Fig. 5.3), but $2.9 \text{ m}^3/\text{s}$ according to the actual discharge measurement. The computed percent bankfull varies accordingly (see below).

Since bedload transport and stage were measured almost hourly, but discharge only a few times per day, each bedload transport measurement was assigned a corresponding value of discharge from the stage-discharge rating curve. The variability in the stage-discharge relation consequently introduced some error into the bedload - discharge relationship. An alternative would have been to measure discharge at the beginning and end of daily rising flow, to assume a linear increase of flow over time, and to interpolate a discharge value for the time period of each bedload measurement.

5.1.2 Percent bankfull flow

Bankfull discharge is difficult to estimate at the upper field site because the stream is incised into a flood plain and most banks are vertical. Locations with depositional features are sparse, and often pertain to stoss and wake deposits and local hydraulics. A minimum estimate of bankfull was set at a stage of 20 cm, which in the stage-discharge rating curve corresponds to a discharge of $3.3\text{-}3.5 \text{ m}^3/\text{s}$. Ryan and Troendle (1996) estimated bankfull flow for site 4 at $4 \text{ m}^3/\text{s}$, based on direct measurement when flow was considered to have reached bankfull. This flow corresponds to a stage of 26 cm at the current stage-discharge rating curve. Although this value for stage appears to be a bit on the high side, values extrapolated for bankfull mean flow velocity of 1.5 m/s and bankfull mean flow depth of 0.39 m do not seem unrealistic (Fig. 5.4). Applying hydraulic geometry relations, mean flow velocity and depth are 1.43 m/s and 0.35 m for the low estimate of $Q_{bkf} = 3.4 \text{ m}^3/\text{s}$,

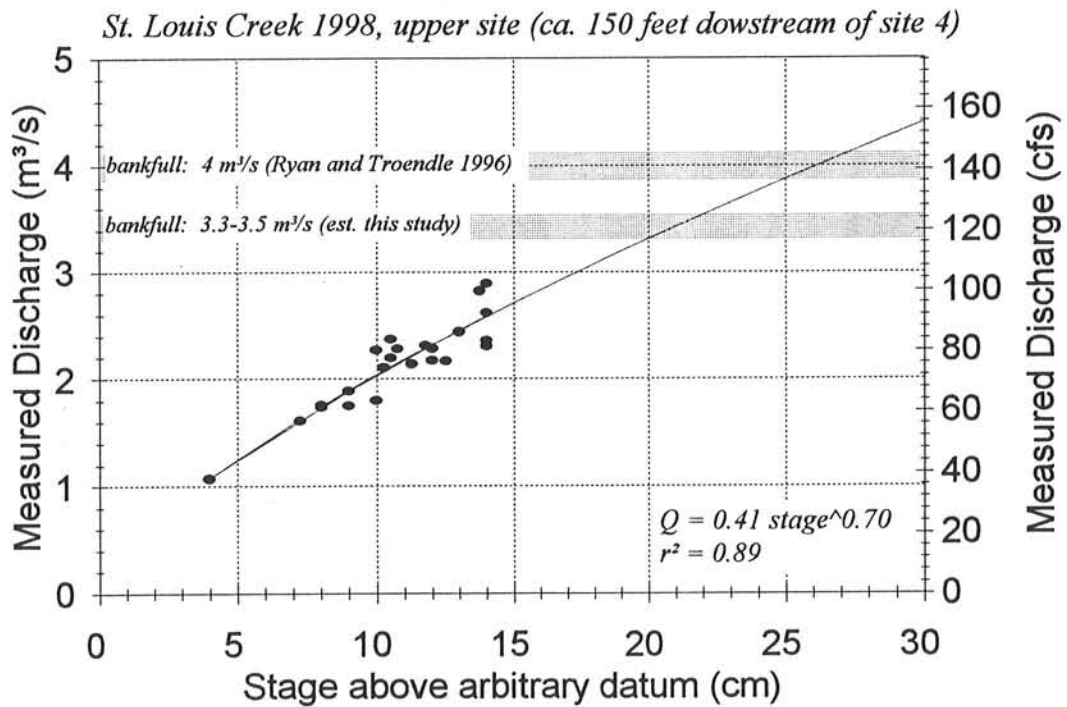
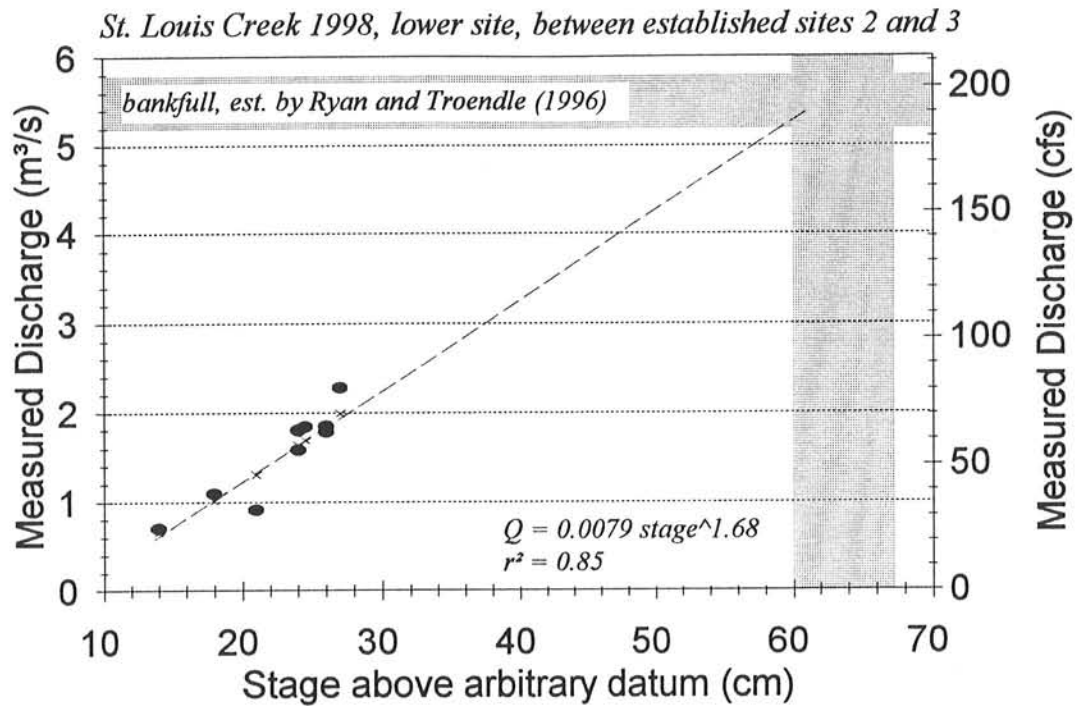


Fig. 5.1: Stage-discharge relationship for the upper site (top) and the lower site (bottom).

or 1.6 m/s and 0.37 m for the high estimate of $Q_{bkr} = 4 \text{ m}^3/\text{s}$ (Fig. 5.5), confirming that both estimates of bankfull are within a range of reasonable values.

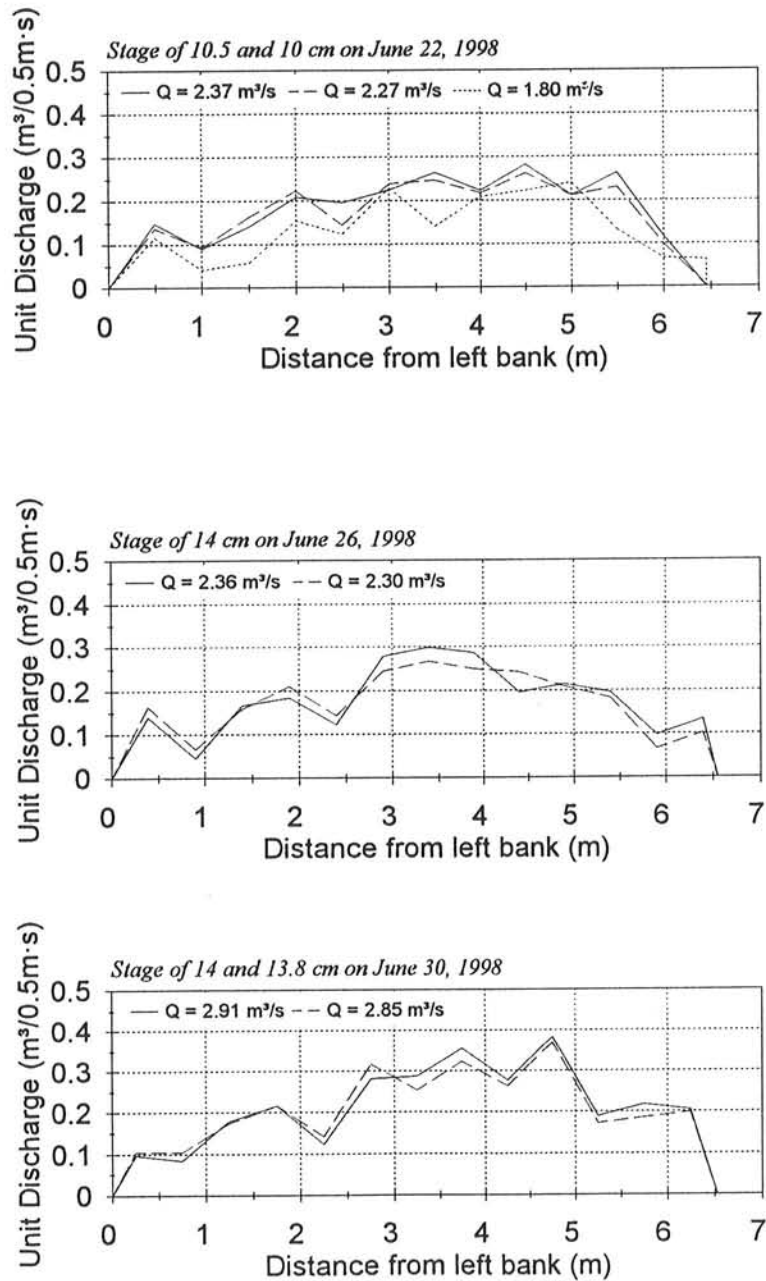


Fig. 5.2: Examples of lateral variation of unit discharge and the resulting differences in discharge for a given stage height.

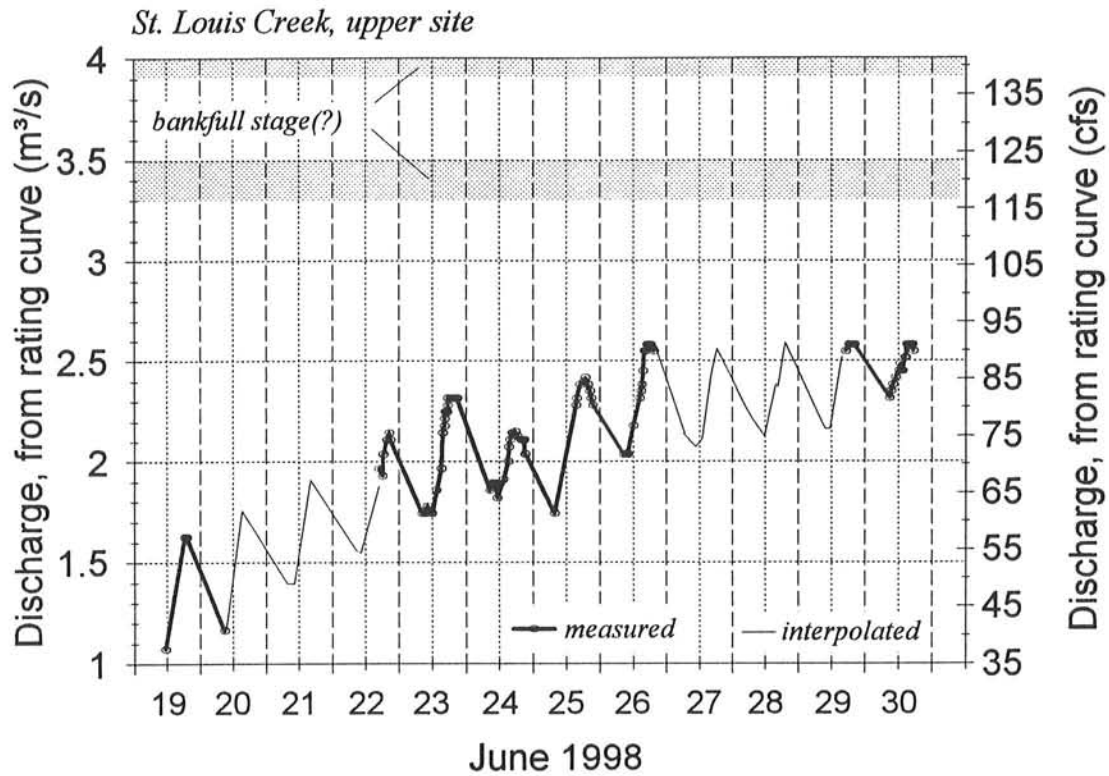


Fig. 5.3: Hydrograph constructed for the upper site for the high flow period June 19-30. The hydrograph is based on stage readings and a stage-discharge relationship.

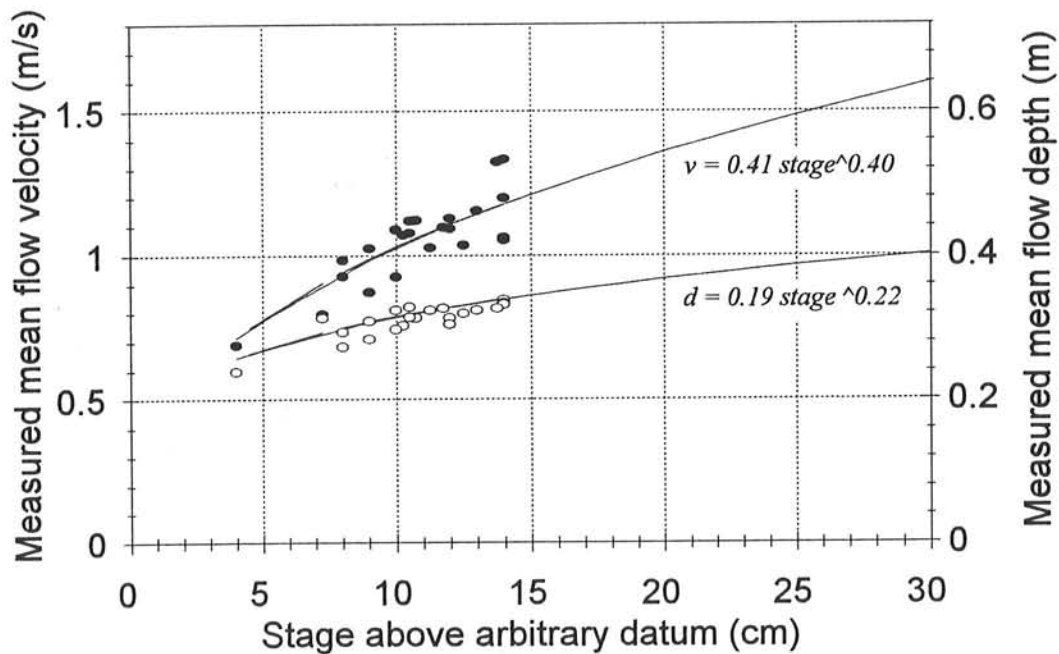


Fig. 5.4: Measured mean flow velocity and mean flow depth versus stage at the upper site at St. Louis Creek.

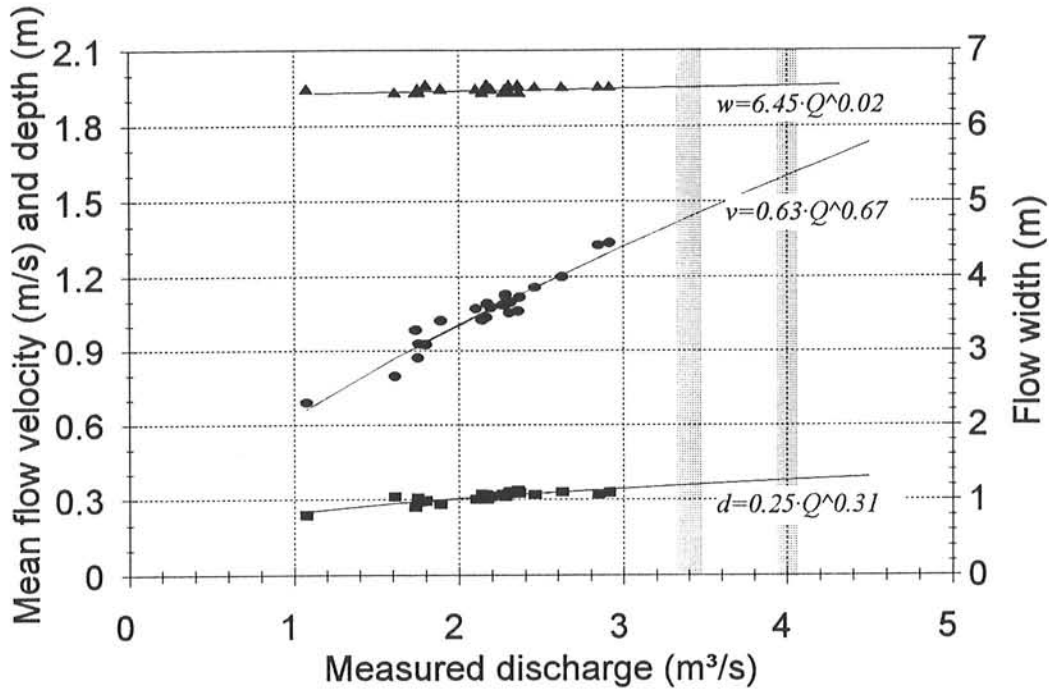


Fig. 5.5: Hydraulic geometry relations: mean flow velocity, mean flow depth, and width versus measured discharge at the upper site at St. Louis Creek.

Depending on the value chosen for bankfull, the highest measured instantaneous flow of 2.9 m³/s reached 85% of bankfull if $Q_{bkf} = 3.4$ m³/s, or 73% of bankfull if $Q_{bkf} = 4$ m³/s. A flow of 2.6 m³/s that corresponds to the highest measured stage then reached either 78% of bankfull for the low estimate, or 66% of bankfull for the high estimate. Considering these uncertainties, flow most likely reached 70-75% of bankfull during the second peak in annual flow this year at the upper site of St. Louis Creek. This findings are in agreement with flows at Williams Fork near Leal where mean daily flows of 12 m³/s during the last days of June reached 75% of the longterm average peak daily flow of 16 m³/s.

The highest measured discharge at the lower site between the established sites 2 and 3 was 2.4 m³/s (see Fig. 5.1). Estimates for bankfull discharge based on morphological evidence are 5.2 and 5.8 m³/s for sites 3 and 2, while the 1.5-year return flow is 4.6 and 5.2 m³/s at sites 3 and 2 (Ryan and Troendle 1996). Assuming $Q_{bkf} = 5.2$ m³/s, the highest measured flow reached less than 50% of bankfull during the second peak flow at the lower site.

5.2 Computation of bedload transport rates

If a few particles only are collected per size class, the quickest way of bedload transport analysis is simply counting the number of particles per size class. Particle transport rates can be computed and compared directly in the field provided that sampling time is about the same for all samples. The computation of bedload transport rates in terms of weight is more labor intensive and requires sample bagging, drying and weighing.

5.2.1 Particle transport rates

To compute cross-sectional, hourly fractional particle transport rates from samples of the stationary net-frame samplers, the number of particles per size class n_{pi} , sampler width w_s , number of sampling locations x_s , and sampling time t_s are summed for all 5 concurrently used samplers n_s .

$$\text{Fractional particle transport rate} = \sum_{n_s=1}^5 \frac{n_{pi}}{x_s \cdot n_s \cdot w_s \cdot t_s} \quad (1)$$

96i

This study used units of number of particles per combined sampler width of 1.52 m and one hour. For units of particle numbers/m · hr, Eq. 1 multiplied by 1/1.52 = 0.66.

actual opening
The mesh width of the stationary net-frame sampler is *3.5 mm* $3/16$ inch ($= 4.76$ mm $= 2.25 \phi$). Samples from the stationary net-frame sampler contain grains $< 4 \phi$ mm, and even sand particles, especially when organic debris blocks the back part of the net. It is obvious, though, that the collected amount of coarse sand and fine gravel particles is not < 4 mm representative of the amount of this size class in transport. Some of the particles of the size class of 4 - 5.6 mm also passed through the net and were lost. If the size of transported particles had reached well into the cobble range, the study could have afforded to discard the incompletely sampled size-class 4 - 5.6 mm. However, transport comprised particles from 5 size classes only, and since the size class 4 - 5.6 mm contained the majority of sampled particles, this size class was not excluded from the analysis.

The sampled number of particles in the size class 4 - 5.6 mm, however, ought to be adjusted upward to compensate for the loss of particles passing through the net, but finding the exact adjustment factor is difficult. The mesh width of 4.76 mm corresponds to the logarithmic mean of 4 and 5.6 mm ($10^{(\log 4 + \log 5.6)/2} = 4.76$). If particles of all incrementally small size fractions within the size class 4 - 5.6 mm were transported at the same rate in terms of number of particles per width and time, but *all* particles within the range 4 - 4.76 mm had escaped through the net, and consequently only half of all transported particles in the size class 4 - 5.6 mm had been sampled, then the sampled particle transport rate for 4 - 5.6 mm should be doubled. But some particles of the size class 2.8 - 4 mm, and even sand was captured in the sampler, so some particles within the size range 4 - 4.76 mm must have been collected as well. Presumably, the net even retains a large proportion of the particles in the size range 4 - 4.76 after the back part of the net is blocked by organic debris. Based on these considerations, an adjustment factor around 1.5 to 1.3 seems reasonable. But since there is uncertainty about the appropriate adjustment factor, particle transport rates of 4-5.5 mm particles are shown as measured (Fig. 5.6) and are used that way for all further computations.

5.2.2 Total and fractional weight-based bedload transport rates

Computations for Helley-Smith sampler

For measurements made with the Helley-Smith sampler, unit bedload transport rates q_b in kg/m·s are computed from the ratio of total sample weight m_s accumulated over all locations within the stream and sampling intensity I_s

$$q_b = \frac{m_s}{I_s} = \frac{m_s}{w_s \cdot x_s \cdot n_s \cdot t_s} \quad (2)$$

0.076 m · 16 · 2 min
0.3 · 5 · 60 min

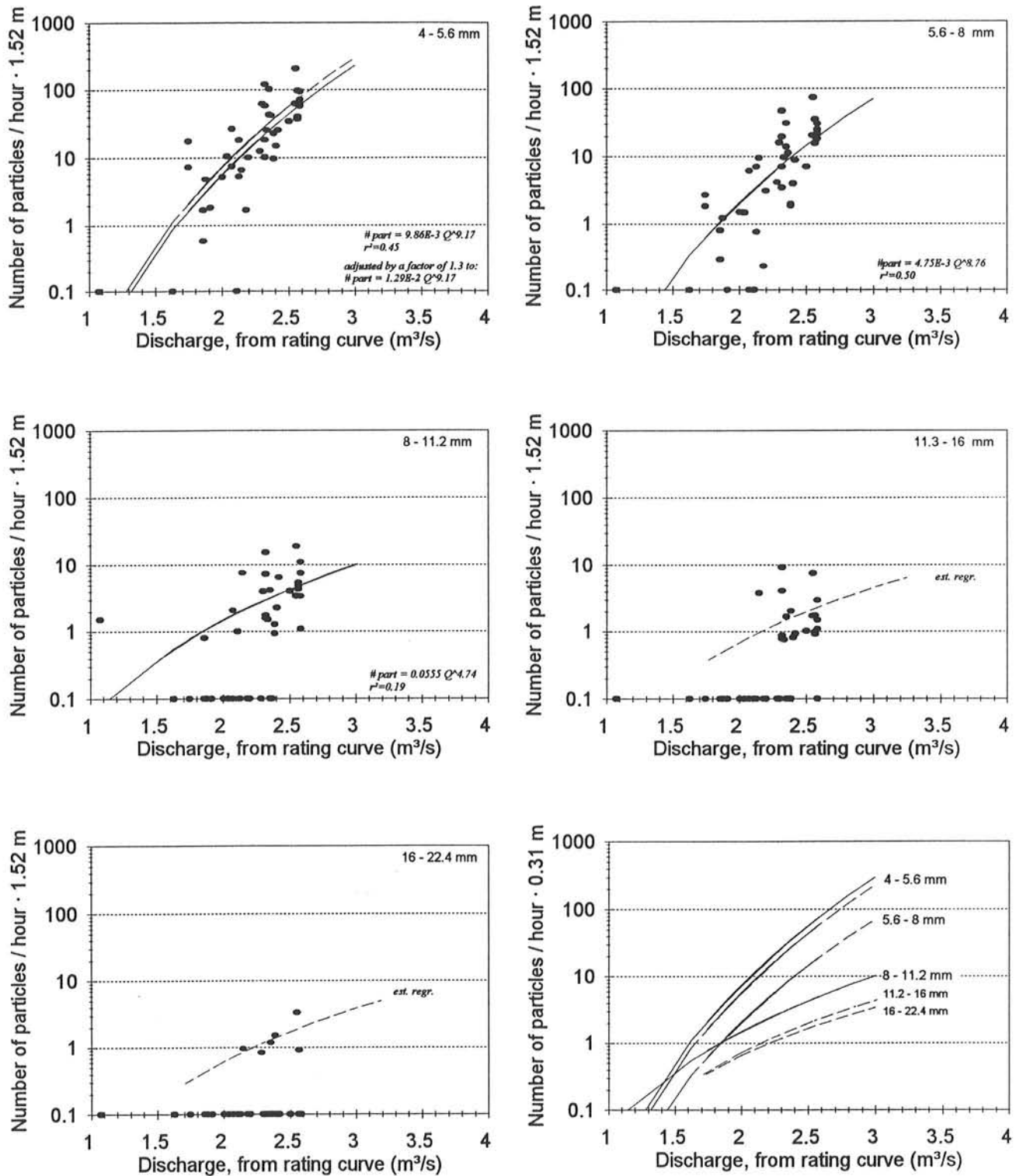


Fig. 5.6: Particle number transport rates combined for all five net-frame samplers for each of the sampled particle size fractions. Zero-transport rates are plotted as a rate of 0.1 particles/hour · 1.52 m, and not included in the power function regression analysis. Regression functions for all size classes are combined in the plot on the bottom right corner.

where w_s is the sampler width, x_s is the number of sampling locations across the stream, n_s is the number of samplers used concurrently, and t_s is the sampling duration. For the computation of fractional transport rates, sample weight is restricted to the measured weight of particles per individual size class.

Computation for stationary net-frame sampler

Since many samples from the stationary net-frame samplers consisted of only a few particles which were counted in the field and discarded with no further weighing, weight-based fractional transport rates qb_i in $\text{g/m} \cdot \text{s}$ are obtained from multiplying the number of particles per size class n_{pi} (Eq. 1) by the average particle weight per size class m_{pi} . For fractional transport rates qb_i of a size class, sample mass m_i is divided by sampler width w_s , number of concurrently used samplers n_s , number of sampling verticals x_s , and by sampling time t_s , which is 3,600 to obtain units of meter and second in the denominator.

$$qb_i = \sum_{n_s=1}^5 \frac{n_{pi} \cdot m_{pi}}{w_s \cdot x_s \cdot n_s \cdot 3600} \quad \left(\frac{\text{g}}{\text{m} \cdot \text{s}} \right) \quad (3)$$

0.3 \cdot 5 \cdot 3600

Fractional transport rates are summed for all size classes to obtain weight-based transport rates per unit width.

$$Qb_i = \sum_{D_i=D_{min}}^{D_{max}} \sum_{n_s=1}^5 \frac{n_{pi} \cdot m_{pi}}{w_s \cdot x_s \cdot n_s \cdot 3600} \quad \left(\frac{\text{g}}{\text{m} \cdot \text{s}} \right) \quad (4)$$

The average particle weight per size class was obtained from a regression function relating average weight of an individual particle per size class m_i (g) to the sieve diameter D_i of that size class (mm). For the upper site at St. Louis Creek, the regression function is

the lower sieve boundary

$$m_{pi} = 0.00363 D_i^{2.920} \quad (5)$$

Exponents and coefficients of such regression functions vary with site specific conditions of particle density and particle shape, but exponent were found to take values close to 3 and coefficients close to 0.003 for several mountain gravel-bed streams with mainly granitic or andesite lithology.

Fractional weight-based gravel transport rates were computed for all size classes (Fig. 5.7). Gravel transport rates measured with the stationary net-frame sampler are below 0.1 g/ms, with the majority of transport rates between 0.001 and 0.01 g/ms. Those rates are very small both in absolute terms and in comparison to gravel bedload samples taken with the Helley-Smith sampler during previous years (see Section 6.2). The results presented above are discussed in the framework of initial motion considerations in Section 7.

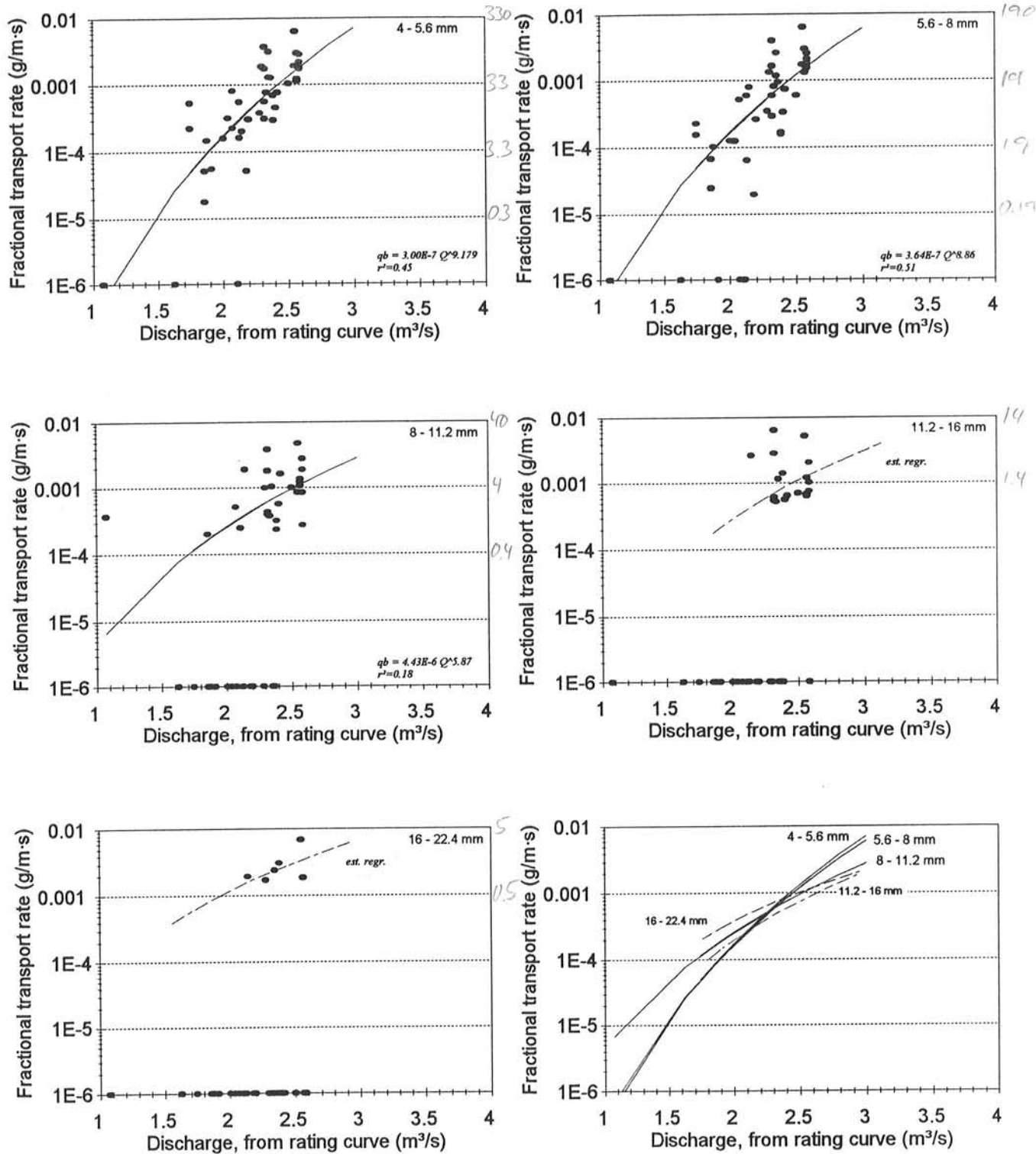


Fig. 5.7 Fractional bedload transport rates combined for all five net-frame samplers for each particle size class. Zero-transport rates are plotted as fractional transport rates of $1E-6 g/m \cdot s$ and were not included in the power function regression analysis. Regression functions for all size classes are combined in the plot on the bottom right corner.

5.3 Variability of bedload transport

Bedload transport measurements made with the stationary net-frame sampler and the Helley-Smith sampler reflect a high degree of temporal and spatial variability.

5.3.1 Temporal variability of bedload transport rates

Transport rates from the stationary net-frame sampler vary by two orders of magnitude around the regression function (Fig. 5.8). Some of this scatter results from one order of magnitude difference between consecutive samples collected at 1-hour intervals (Fig. 5.9).

Rating curve scatter is also attributable to hysteresis effects over time scales of days and weeks. Highest daily transport rates occurred during the first few hours after peak flow, while daily transport rates were not lowest during daily low flow which had rather high transport rates, but during the early hours of the rising stage. Consequently, daily hysteresis forms wide counterclockwise loops indicative of a lag response of bedload transport to flow. The shape of the daily hysteresis changes over time. During the first high flow days with generally increasing flow, loops span up to 3 orders of magnitude and spiral upward (Fig. 5.10). On later days with only slightly higher flows loops become smaller and lose their upward trend, suggesting exhaustion of sediment supply. Bedload transport measured with the Helley-Smith sampler clearly shows depletion of sediment supply over time (Fig. 5.11). Each daily transport-discharge relationship is lower than the one from the previous day.

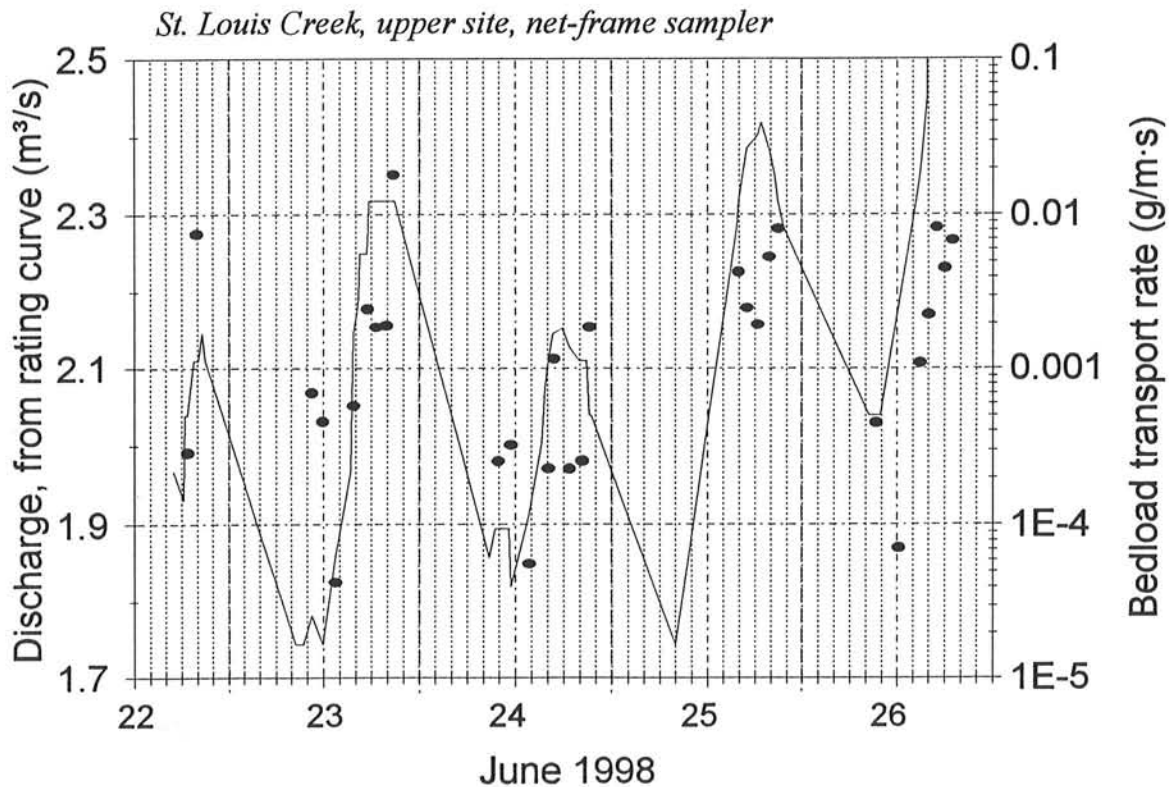


Fig. 5.9: Hydrograph (based on stage-discharge relationship) and the temporal variation of bedload transport rates computed from the stationary net-frame samplers.

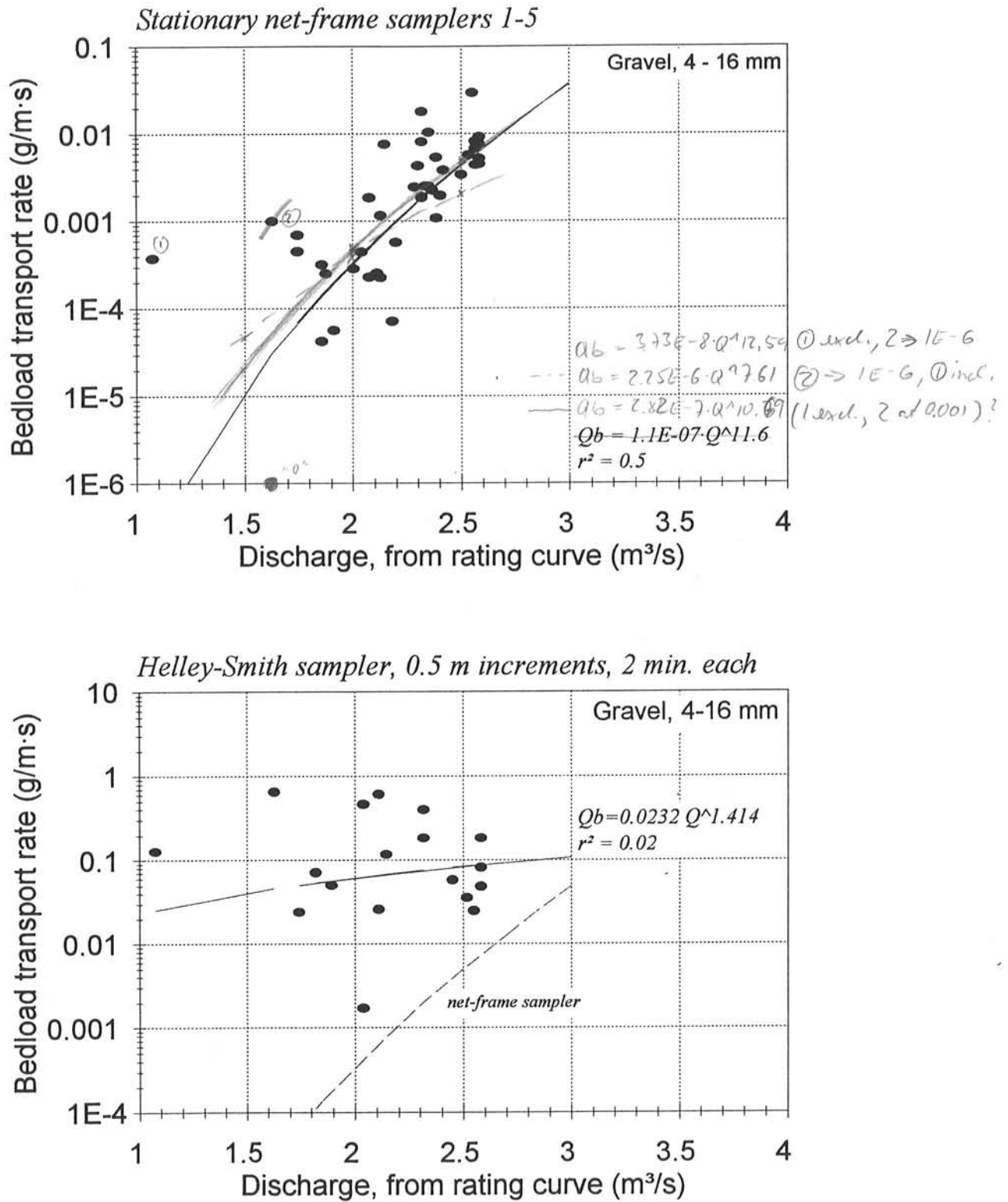


Fig. 5.8: Transport rates for gravel of 4-16 mm sampled with the stationary net-frame sampler (top) and the Helley-Smith sampler (bottom) at the upper site at St. Louis Creek in 1998.

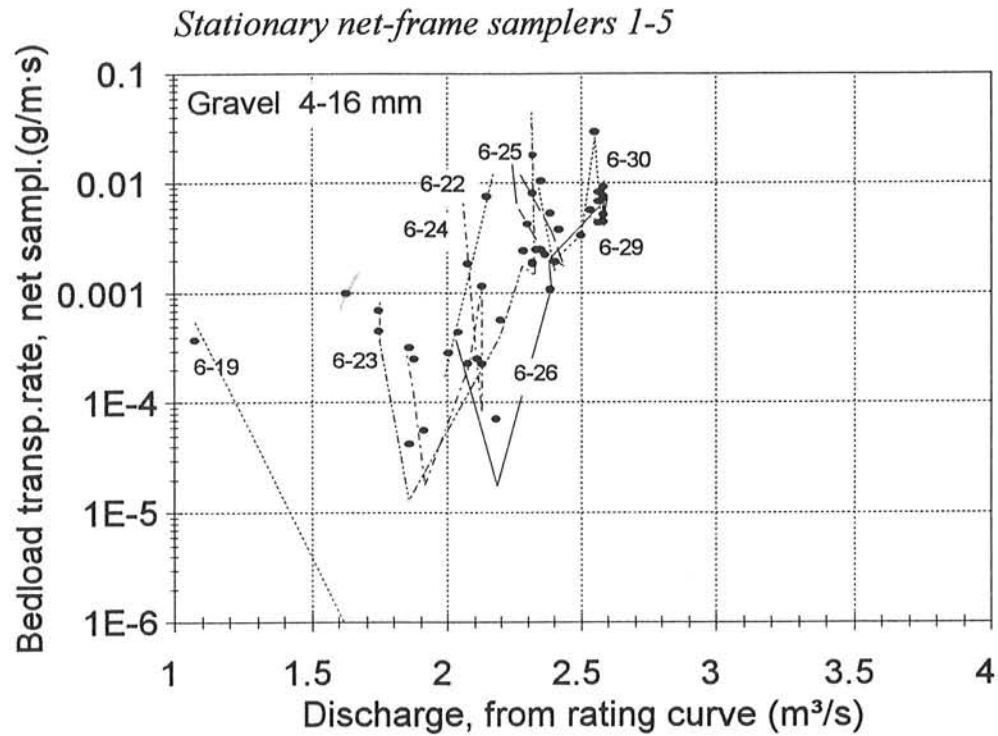


Fig. 5.10: Daily hysteresis effects of transport rates computed from the stationary net-frame sampler.

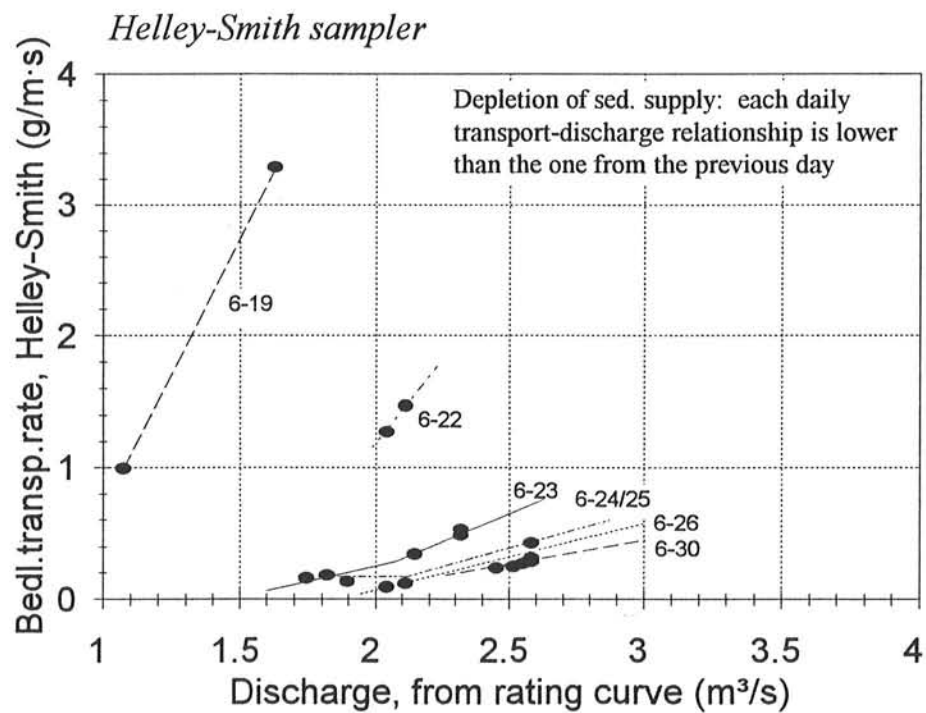


Fig. 5.11: Daily change in bedload transport rating curves measured with the Helley-Smith sampler

5.3.2 Spatial variability of bedload transport rates

Five stationary net-frame samplers were installed across the stream along a diagonal line. Sampler 5 close to the right bank is in a thalweg position where flow is deepest and fastest, while sampler 1 close to the left bank is at a location where flow fans out laterally. Measured transport rates were highest at sampler 4 which was located at the lower, permanently submerged part of a bar. Upwelling flow, recognizable by a boiling appearance of the water surface and a small longitudinal low mound, lead to the formation of a "pebble street" that transported the majority (81%) of the gravels. Almost no transport was measured at the thalweg location 5 with the deepest and fastest flow. The concentration of bedload transport at a single location was most pronounced for the largest particles (Fig. 5.12). Location 4 had 90% of all particles in the size class 11.2 - 16 mm, 95 % of the class 8 - 11.2 mm, 80% of the class 5.6 - 8, and 70% of the class 4 - 5.6 mm. Extrapolating this trend suggests that sand transport is more evenly distributed across the stream.

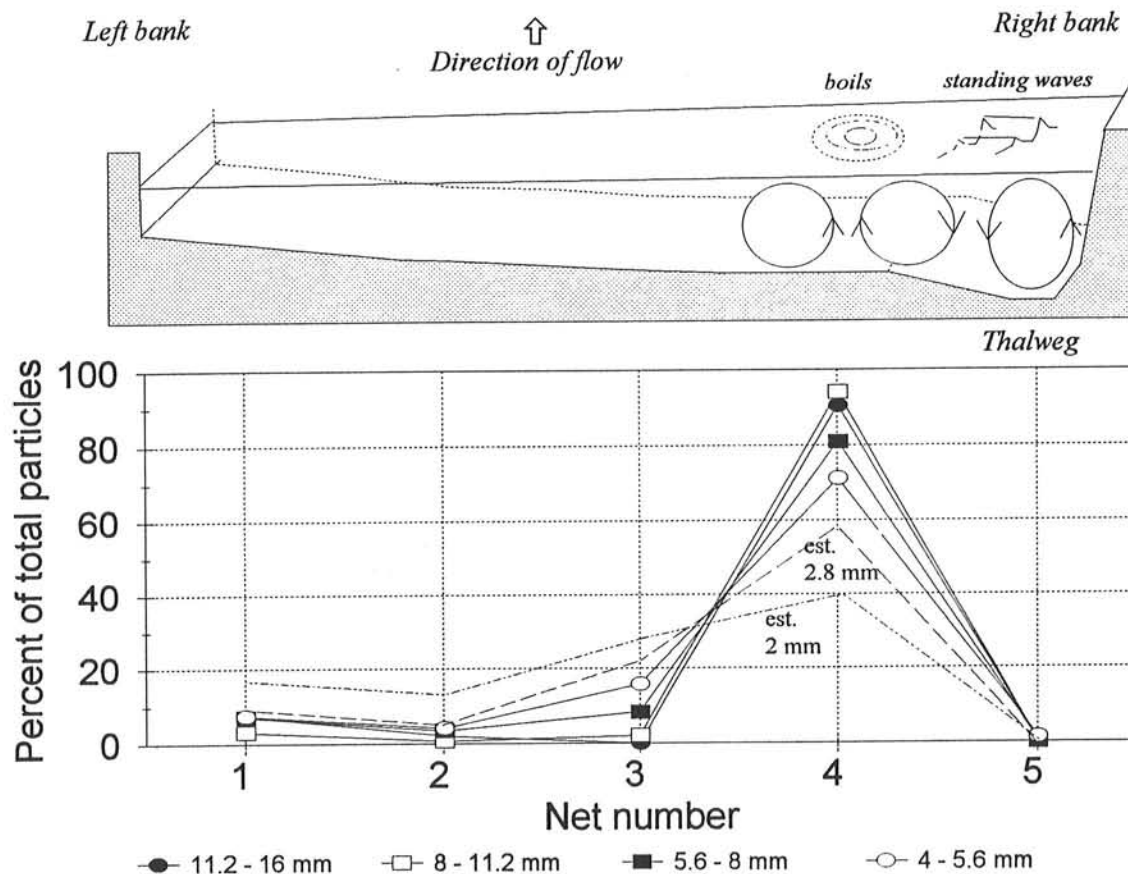


Fig. 5.12: Concentration of gravel particle-transport rates at a pebble street (bottom) at the upper site. The diagram on top schematically indicates the cross-sectional location of flow cells with upwelling and downwelling flow.

6. Comparison between the stationary net-frame sampler and Helley-Smith sampler

In order to evaluate the sampling performance of the newly designed stationary net-frame sampler, sampling intensity, transport rates, and sampled particle-size distributions are compared to samples obtained from a Helley Smith sampler.

6.1 Sampling intensity

Sampling intensity affects sampled transport rates and thus leads to differences in sampling results between the stationary net-frame and the Helley-Smith sampler. Sampling intensity I_s can be defined as

$$I_s = w_s \cdot x_s \cdot n_s \cdot t_s \quad (6)$$

where w_s is the width of the sampler, x_s is the number of sampling verticals across the stream, n_s is the number of samplers used concurrently in the stream, and t_s is the sampling period of each sampler in the stream. A typical sampling scheme employed for the Helley-Smith sampler in relatively low transport rates in mountain gravel-bed streams collects 10 - 20 samples at 0.5 m increments across the stream for 2 minutes per vertical. A stream 6.5 m wide, yields 13 sampling verticals spaced 0.5 m apart, and the resulting sampling intensity is

$$I_s = \frac{w_s \cdot x_s \cdot n_s \cdot t_s}{l_{tot}} = \frac{0.075 \cdot 13 \cdot 1 \cdot 2 \text{ min}}{6.5 \text{ m} \cdot 60 \text{ min}} = 0.0051 = 0.5\%$$

$$I_s = 0.075 \text{ m} \cdot 13 \cdot 1 \cdot 120 \text{ s} = 117 \text{ m} \cdot \text{s} \quad (6a)$$

For the stationary net-frame sampler, a practical sampling duration is about one hour. The sampling intensity of a set of 5 stationary net-frame samplers installed in the same stream is

$$I_s = 0.305 \text{ m} \cdot 5 \cdot 1 \cdot 3600 \text{ s} = 5486 \text{ m} \cdot \text{s} \quad \frac{0.305 \cdot 5 \cdot 60 \text{ min}}{6.5 \cdot 60 \text{ min}} = 23\% \quad (6b)$$

which exceeds the sampling intensity of a typical Helley-Smith sampling scheme by almost a factor of 50, or 1.5 orders of magnitude. If one bedload sample was taken each hour in a stream 6.5 m wide ($6.5 \text{ m} \cdot 3600 \text{ s} = 23,400 \text{ m} \cdot \text{s} = 100\%$), the Helley-Smith sampler samples 0.5 % of bedload passing over the total time and space, while the stationary net-frame samplers sample bedload 23% of the total time and space. It is theoretically possible to increase the typical Helley-Smith sampling intensity by using several samplers that are made stationary, such as by clamping them to stakes pounded in the river bed, but this approach can only be employed when transport rates and loading of organic debris are small. Otherwise, bedload and debris accumulating over an hour overflow the bad, and clog its small mesh width, both of which strongly reduces sampling efficiency.

Bedload transport rates in mountain gravel-bed rivers fluctuate considerably over time within minutes and hours even when flow remains constant (see Sect. 5.3 and Figs. 5.9, 5.10, and 5.11. Sampling intensity increases sampling accuracy, since high sampling intensity with long sampling durations averages over highly fluctuating transport rates and reduces rating curve scatter.

6.2 Comparison of transport rates

Ideally, for comparison of sampling performance, transport rates should be constant over space and time, so that both samplers can be used one at a time. Sampler comparison when transport rates are highly variable over space and time (see Section 5.3) demand that both samplers be used at the same time in the same locations, an impossible task. The stationarity of the net-frame samplers suggested using both the net-frame and the Helley-Smith samplers over the same time period, but at different locations. Close proximity between the two samplers to be compared was desirable to account for the spatial variability of transport, but wading and operating the Helley-Smith sampler next to the entrance of the stationary net-frame samplers might locally destabilize the bed, and eventually destabilize the samplers themselves. A further concern was that the presence of the Helley-Smith sampler next to the stationary net-frame samplers might alter the flow field and thus the sampling efficiency of the stationary samplers as well.

Since field testing the stationary net-frame sampler was the primary study objective, comparative Helley-Smith samples were made a few meters downstream from the stationary net-frame samplers. Consequently, the presence of the stationary samplers may have influenced transport rates and particle size-distributions sampled with the Helley-Smith sampler, but this had to be accepted. There was a concern that transport rates sampled with the Helley-Smith could be reduced because bedload caught in the upstream stationary net-frame samplers was no longer available for the downstream Helley-Smith sampler. On the other hand, wading around the stationary net-frame samplers to collect these samples a few meters upstream from the location of Helley-Smith sampling may have supplied extra sediment to the Helley-Smith sampler from particles as a result of.

A comparison of 4-16 mm gravel transport rates sampled with the stationarity net-frame sampler and with the Helley-Smith sampler showed that transport rates from the Helley-Smith sampler were about two orders of magnitude higher than those from the stationary net-frame samplers. However, the lack of a strong relation between transport and flow for the Helley-Smith samples (Fig. 5.8), raised disturbing questions about data validity.

6.2.1 Helley-Smith transport rates: 1998 versus 1992-1997

A comparison of the 1998 Helley-Smith data with transport rates obtained from a Helley-Smith sampler at nearby Site 4a over the period of 1992-1997 by Ryan (1998) showed that 1998's gravel transport rates are approximately the same, perhaps slightly lower, but still within the expectable range of data gathered at Site 4a (Fig. 6.1). Reasons for the slightly lower transport rates of the Helley-Smith this year could be:

- Development of a beaver dam below Site 4a after 1997 may have trapped sediment so that less sediment was available for transport below the beaver dam at the upper site in 1998 than at Site 4a above the beaver dam in previous years;
- 1998 was the first year of below average high flow after two consecutive years of above average flows which may have produced a dearth of transportable small gravel;
- Some of the sediment which otherwise could have been collected in the Helley-Smith sampler might have retained in the upstream stationary net-frame samplers;
- Different operators and using measurement techniques might have contributed to differences in sampled transport rates as well. Sampling during the period of 1992 - 1997 was done from a footbridge, while sampling in 1998 was done by wading.

Sandra's H-S 1992-1997, all sizes

$$Qb(g/s) = 3.88 E-5 \cdot Q^{2.84}, \quad r^2 = 0.69, \quad n = 709$$

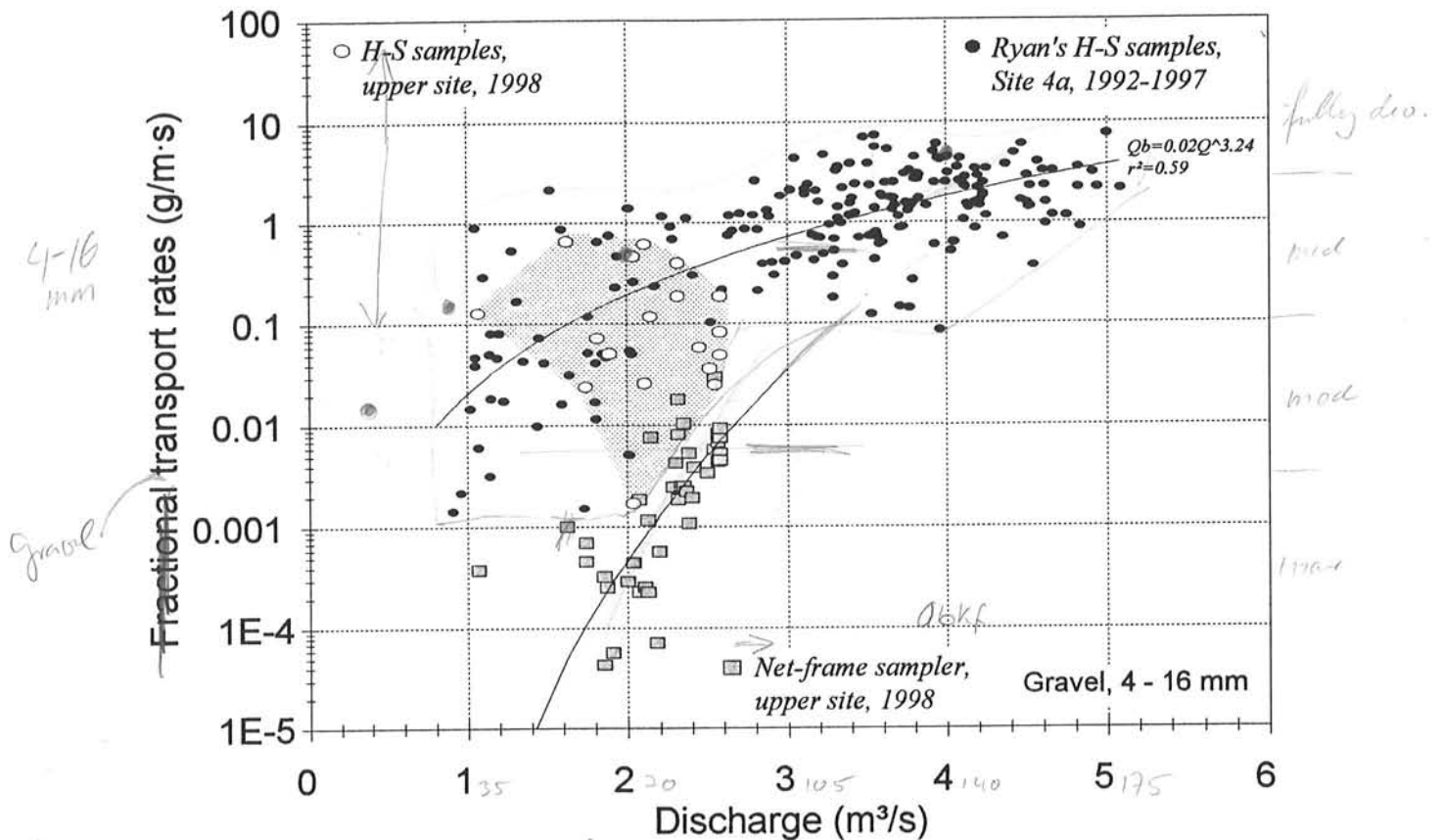


Fig. 6.1: Comparison of gravel transport rates (4-16 mm) measured with the Helley-Smith sampler in 1998 by Bunte at the upper site (shaded area) with gravel transport rates measured with a Helley-Smith sampler at site 4a about 400 m upstream in 1992-1997 by Ryan (1998). *4-16 mm*

Since transport rates measured with the Helley-Smith in 1998 generally correspond to those measured during 1992-1997, stationary net-frame gravel transport rates will be compared to the data from 1992-1997 because that data set contains about 200 bedload transport measurements and has a well defined rating curve, which is absent for the 18 concurrent Helley-Smith samples collected in 1998.

6.2.2 Transport rates from the stationary net-frame sampler and Helley-Smith samples at Site 4a

For flows around 40% of bankfull, the 4-16 mm gravel transport rating curve (Fig. 6.1) from the stationary net-frame sampler is about 3 orders of magnitude smaller than the gravel transport rating curve from the Helley-Smith sampler at Site 4a. The difference decreases to one order of magnitude for flows at 70% of bankfull, and both rating curves approach each other near bankfull flow. This discrepancy between samplers is similarly observable with particle number transport rates (Fig. 6.2). Much of this discrepancy is attributable to the temporal and spatial difference in sampling schemes. Other factors might include:

- Changes in site condition:
Transport rates may have been lower in 1998 at the site of the stationary net-frame samplers due to the upstream beaver dam and two previous above average high flow seasons;
- Flaw in the sampler design:
The ground plates intended to prevent particles from moving under the sampler might have positioned the net-frame samplers too high off the ground and allowed particles to pass under the sampler. Flume experiments, and observation of particle paths with a snoop-scope⁹ during a transport event, may clarify this point.
- Operation of the Helley-Smith sampler
The Helley-Smith sampler may scoop particles when being placed onto the stream bed and thus oversample coarse gravel particles. Again, observations of comparative sampler behavior in a flume, or in the field with a snoop-scope, may bring insights.

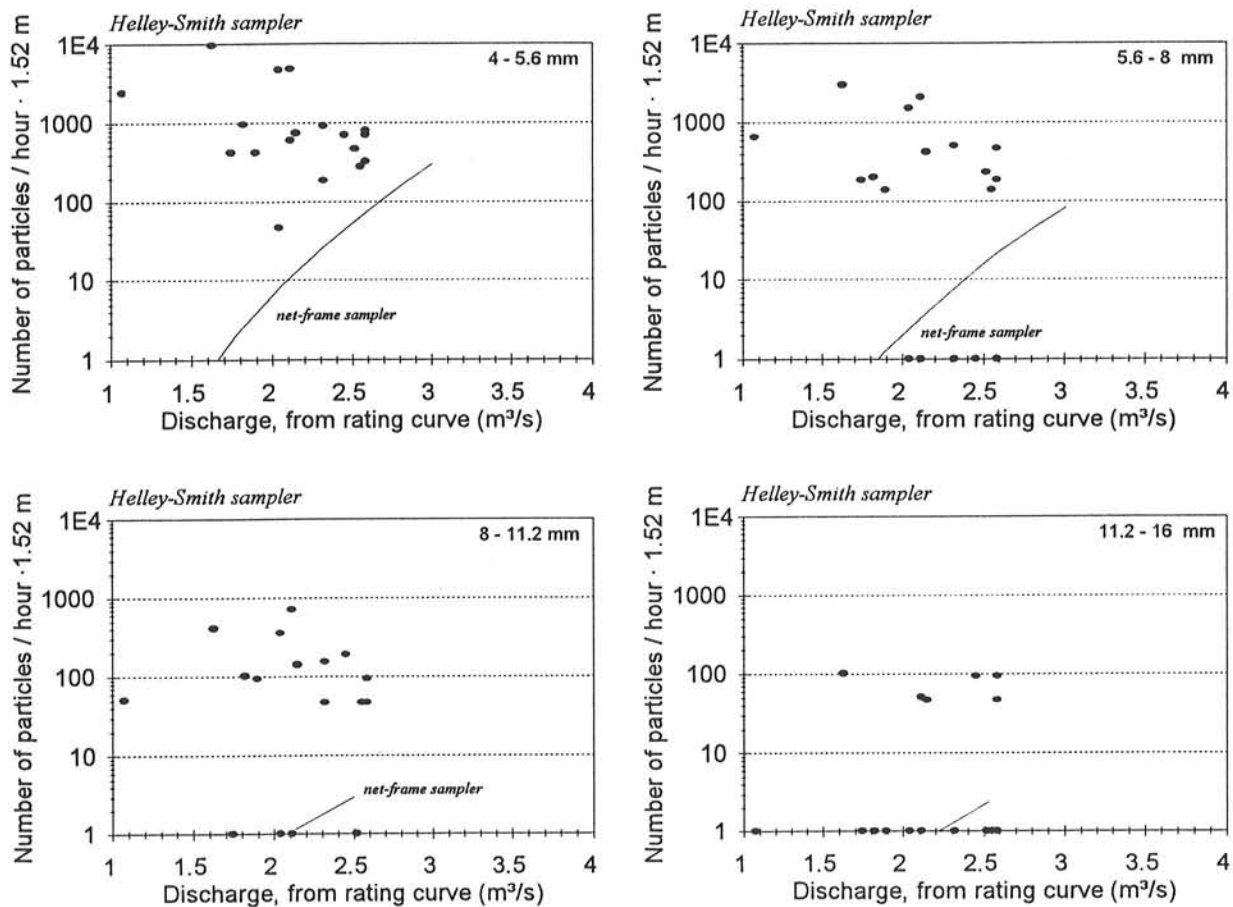


Fig. 6.2: Comparison of particle transport rates (number of particles /1.52 m·hr) computed for Helley-Smith samples with the rating curve of particle transport rates from the stationary net-frame sampler.

⁹ A snoop-scope allows to clearly see the stream bottom inundated by flow. The device consists of a 6-inch Ø PVC pipe, about 3 feet long, with a clear plastic lens mounted water proof at the submerged end of the pipe.

6.2.3 Steepness of bedload transport rating curves

The steepness of the rating curve is an important parameter in bedload transport studies. It affects the computation of effective discharge in a magnitude-frequency analysis, and can be assumed to vary systematically with stream type. Steep rating curves with large exponents $b \approx 10$ ($Q_b = a Q^b$) have been measured in mobile stream beds with unlimited sediment supply where increasing flow scours channel bed and banks. Rating curve exponents around 10 were obtained for example for large braided rivers (Knott et al. 1987), and during flash floods in ephemeral desert streams (Reid and Laronne 1995). Rating curve exponents around 10 were also obtained for gravel transport when samplers with large openings and large sampling capacity were used to sample cobble transport (Whitaker and Potts 1996, Bunte 1996).

Theoretical considerations suggest that the rating curve steepness is also affected by the sampling scheme employed. A high sampling intensity (Eq. 6) permits to sample very low transport rates when transport is marginal. Less intensive sampling schemes produce either "zero" transport rates if infrequently moving particles are not sampled, or a relative high transport rate if an infrequently moving particle happens to be sampled during a short sampling interval. Consequently, when measured at the same stream, intensive sampling schemes produce bedload transport rating curves that are low at the lower end, increase at a fast rate for medium flows, until the steep increase tapers off and merges with transport rates from a less intensive sampling scheme for higher flows probably around bankfull. The low start of the rating curve with the steep increase for medium flows produces a higher exponent than rating curves obtained from non-intensive sampling schemes which cannot accurately sample low transport rates (Fig. 6.3). Intensive sampling schemes also increase sampling accuracy during high transport rates when averaging over highly fluctuating transport rates reduces scatter in the transport relationship.

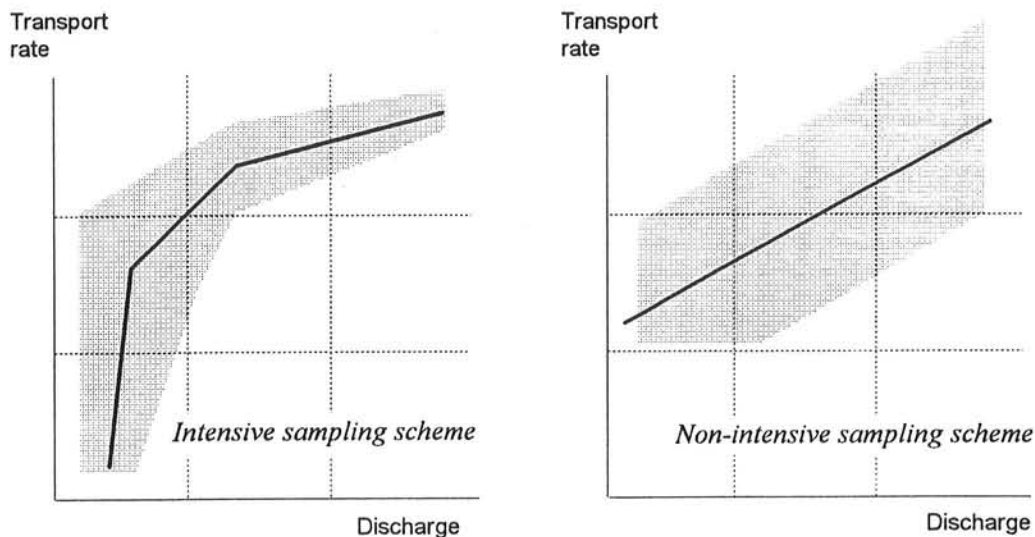


Fig. 6.3: Schematic difference in data fields (shaded area) and gravel transport rating curves (heavy lines) for intensive (left) and a non-intensive (right) sampling schemes. Intensive sampling extends over long periods (hours) and covers a large proportion of the stream width, while non-intensive sampling lasts for minutes only while covering small sections of the total stream width.

A comparison of gravel bedload rating curves from the two samplers at St. Louis Creek clearly shows the difference in steepness. The hand-fitted rating curve for gravel samples from Ryan's (1998) Helley-Smith samples has an exponent of 3.3, while the gravel rating curve for the stationary net-frame sampler has an exponent 11.6 (Fig. 6.1).

6.3 Comparison of sampled particle sizes

Although gravel transport rates differ by orders of magnitude, both samplers generally collected similar gravel particle sizes. The average D_{50} particle size for all samples collected during the high flow was 7.8 mm for both samplers. Cumulative particle-size frequency distributions of individual samples were too irregular to compare concurrent samples of both samplers. Even in grouped samples particles of the largest size class comprised 10-20% or more of the total weight, and caused the D_{50} to vary between of the two samplers (Fig. 6.4).

The disproportionately high weight of particles in the largest size class was especially pronounced in samples from the Helley-Smith sampler. Even grouped samples were "kinked" at the upper part, while gradation curves for the stationary net-frame sampler are generally s-shaped (Fig. 6.4). A few large particles in a small bedload sample could be due to low sampling intensity, when an infrequently moving large particle got sampled during small transport rates, or when a bedmaterial particle was involuntarily scooped into the sampler. A more detailed analysis of particle sizes between the two samplers requires more samples with higher transport rates and larger particle sizes.

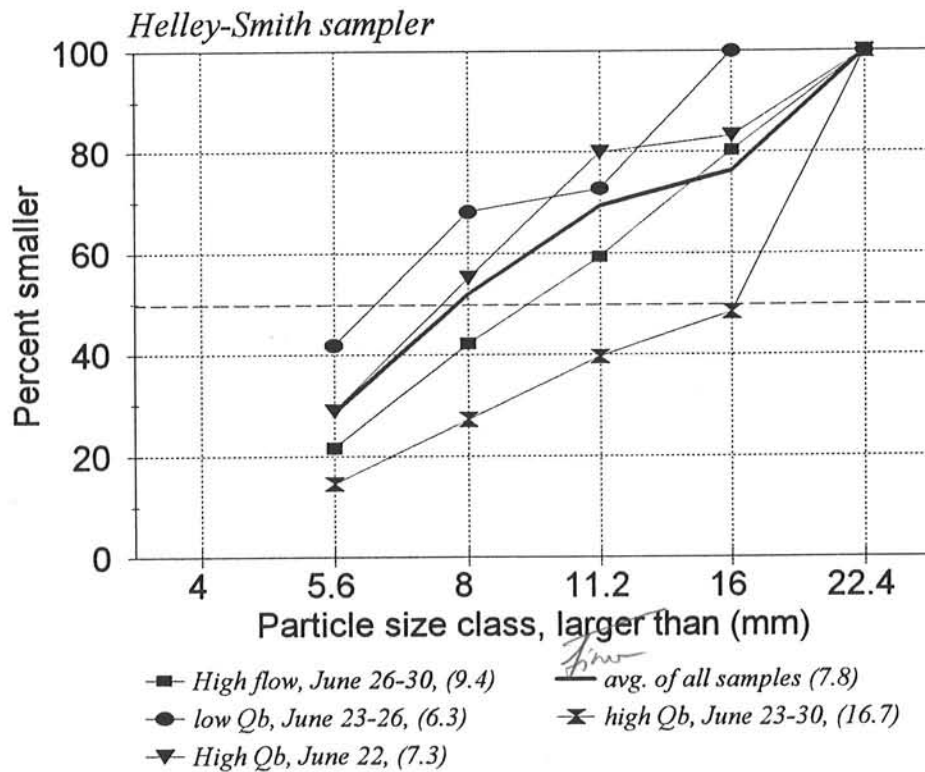
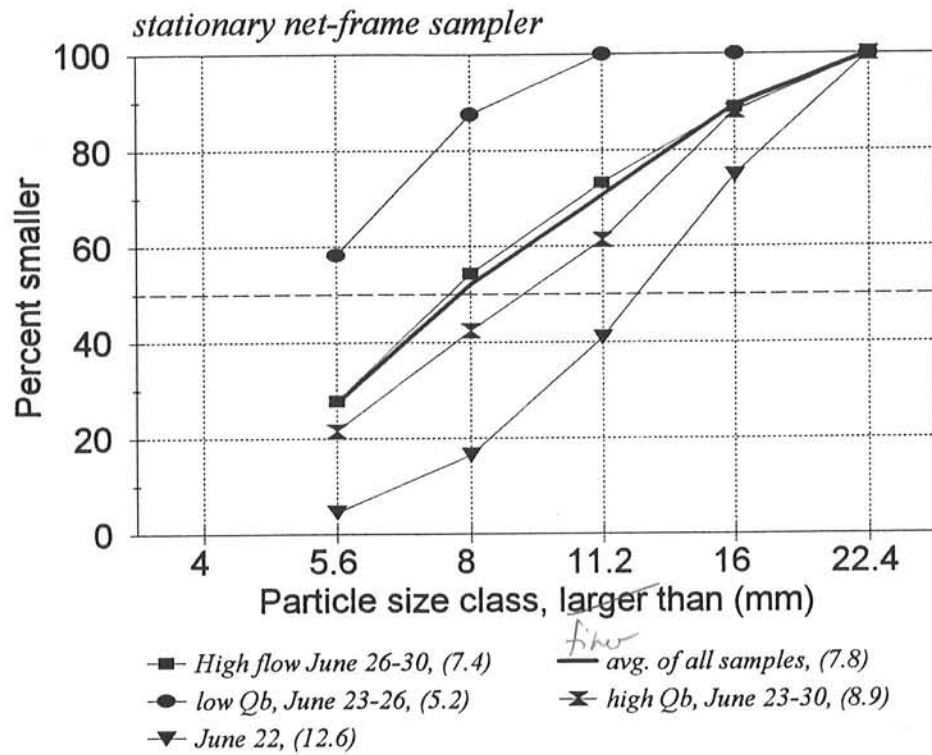


Fig. 6.4: Cumulative particle size-distribution curves for grouped samples from the stationary net-frame sampler (top) and the Helley-Smith sampler (bottom). Numbers in brackets indicate D_{50} particle sizes in mm.

7. Initial motion considerations

Critical flow at which particles of a given size class begin to move are predicted in two major ways: (1) based on actually measured fractional bedload transport rates, or by (2) the exceedance of a reference transport rate, a critical shear stress, or critical dimensionless shear stress. This studies explores several possibilities, focussing on the measurement approach:

1. **Exceedance of a particle number threshold transport rate.** A low observed particle transport rate can be used as the threshold particle transport rate for initial motion. Visualization of particle transport rates per width and time permits selecting a particle transport rate that fits the study aim. Possibilities include:
 - ♦ 10 particles/hour · m, or
 - ♦ 1 particles/hour · m;
2. **Exceedance of a weight-based threshold transport rate.** A low observed weight of transported particles can be used as the threshold transport rate for initial motion. The absolute value of the selected low transport rate depends on the range of transport rates observed at a particular stream, and that range can vary by several orders of magnitude between streams. The absolute value of a low transport rate for a given stream is also affected by the sampling scheme. Threshold transport rates are likely to be especially small if an intensive sampling scheme (sampling over much of the stream width and over long durations) is used. Possibilities include:
 - ♦ $q_b > 0.001$ g/m·s, and
 - ♦ $q_b > 0.0001$ g/m·s;
3. **Flow competence analysis.** Initial motion for a particular size class has occurred if one (or two, or three) particles of a size class are contained in the sample. The flow competence curve is the regression function fitted through individual measured data of D_{max} versus discharge. Flow competence can be based on:
 - ♦ largest transported particle size, or the
 - ♦ particle size of D_{84} or any other percentile of interest.
4. **Graphical-visual approach.** Transport rates are plotted for each size class. Initial motion occurs at the flow at which particles of a size class of concern start to have transport rates larger than zero or a preset low transport rate. This approach can be applied to plots of either particle number transport rates, or weight-based fractional transport rates versus discharge.
5. **Computation of rating curve x-axis intercept.** Rating curves for fractional transport rates are plotted with both axes in a linear scale. Critical discharge for initial motion is defined as the discharge for which the rating curve regression function intercepts the x-axis of the graph. This approach can be applied to rating curves of either particle number transport rates, or weight-based fractional transport rates.
6. **Reference transport rate.** The dimensionless reference transport rate for the i th size fraction W_i^* is basically the ratio of volumetric fractional transport rates to the product of flow depth, stream gradient, and percentage availability of the i th size class in the subsurface sediment (Parker and Klingeman 1982). The volumetric fractional transport rate for which W_i^* reaches the value of 0.002 is used as an indication of the transport rate at initial motion.

7.1 Computation of critical discharge

Critical flow for initial motion was computed for transport rates obtained from the stationary net-frame sampler using the approaches outlined above. Transport rates measured with the Helley-Smith sampler at the upper site were too few and too scattered to yield a regression function and thus unsuitable for initial motion computation (see Fig. 5.8, bottom).

Therefore, the set of about 200 Helley-Smith samples gathered by Ryan (1998) at Site 4a was used for comparison (Fig. 6.2).

7.1.1 Preset low fractional transport rate

For samples from the stationary net-frame sampler, particle transport rates (Fig. 5.6) and fractional weight-based transport rates (Fig. 5.7) were plotted versus discharge for the five 0.5 phi size-classes between 4 - 5.6 and 11.2 - 16 mm. Rating curve regression functions were fitted for data set of small particle sizes, since those data sets covered a sufficiently large data and value range. The range of flows and transport rates for data sets of large particle sizes were too small for a meaningful regression analysis, and rating curves were fitted by eye following the general trend of rating curves for smaller particles. Rating curves were extrapolated to extend about 0.5 m³/s beyond the lower and upper measured discharge range. The intercepts of the rating curves with discharge values for preset fractional particle transport rates of 1, and 10 particles/1.52 m³/hour, and preset fractional transport rates of 0.001, and 0.0001 g/m³s were read off the graphs and listed in Table 7.1.

Table 7.1: Critical discharge (m³/s) for 0.5 phi-unit particle size classes and various criteria for initial motion based on samples from the stationary net-frame sampler at the upper site (St. Louis Creek, 1998).

Size class (mm)	Fractional transport rates			Part. transp. rates		Flow comp. (D_{max})	Visual	x-axis intercept (weight or number)	Ref. transp. rate $W_i^*=0.002$
	0.0001	0.001	0.01	1	10				
	(g/m ³ s)			(part./1.52m ³ ·hr)					
4.0 - 5.6	1.95	2.45	3.10	1.62	2.07	1.62	1.72	1.74	1.72
5.6 - 8.0	1.95	2.48	3.20	1.84	2.38	1.86	1.72	1.77	1.74
8.0 - 11.2	1.72	2.51	3.50	1.84	2.90	2.17	2.10	1.72	1.69
11.2 - 16.0	1.80	2.61	-	2.20	2.50	-	2.13	1.71	-
16.0 - 22.4	-	2.03	-	2.20	2.92	-	2.13	1.74	-

Particle sizes of the Ryan's Helley-Smith data were tallied in whole phi-units. This prevented backcalculation of particle number transport rates from weight-based fractional transport rates, since Equation 5 in Section 5.2.2 is based on 0.5 phi size-classes. Fractional weight-based transport rates for 1.0 phi size-classes were plotted for Ryan's (1998) Helley-Smith samples from Site 4a (Fig 7.1). The intercepts of the rating curves with discharge for preset fractional transport rates of 0.1, 0.4, and 1 g/m³s were read off the graphs and listed in Table 7.2.

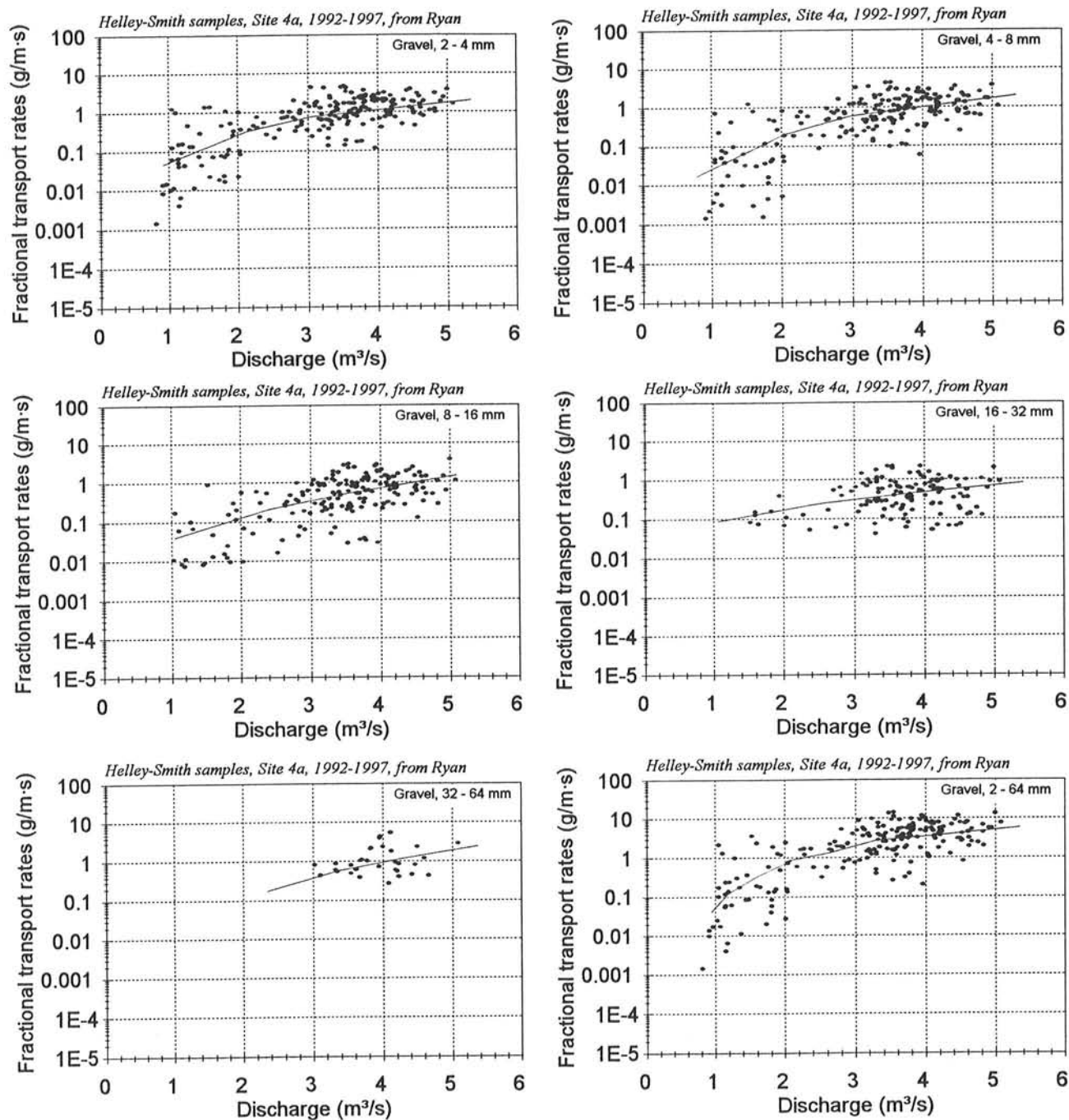


Fig. 7.1: Fractional weight-based transport rates for 1.0 phi size-classes of Ryan's Helley-Smith data.

Table 7.2: Critical discharge (m^3/s) for 1.0 phi-unit particle size classes and various criteria for initial motion based on Ryan's Helley-Smith samples from Site 4a (St. Louis Creek, 1992-1997).

Size class (mm)	Fractional transport rates			Flow competence (D_{max})	Graphical- visual ($\text{g}/\text{m}\cdot\text{s}$)	x-axis intercept ($\text{g}/\text{m}\cdot\text{s}$)
	1	0.1	0.4			
	(g/m·s)					
2.0 - 4.0	3.65	1.38	2.30	1.1	1.00	0.93
4.0 - 8.0	4.00	1.70	2.60	1.4	1.00	1.06
8.0 - 16.0	4.50	1.80	3.19	2.1	1.55	1.31
16.0 - 32.0	5.80	1.25	3.56	3.3	1.95	1.26
32.0 - 64.0	4.05	-	3.17	5.8	3.00	1.73

7.1.2 Flow competence curve

Flow competence usually refers to the largest, or a large, particle size actually transported by a given flow. Thus, flow competence can refer to the D_{max} , or a high percentile value such as the D_{84} , or D_{95} particle size of a bedload sample. The flow competence curve in this study was obtained from a regression analysis of a plot of the largest particle size per bedload sample versus discharge. If the data set is large enough, the outer envelope curve can be used as an indication of the earliest onset of particle motion.

The flow competence curve for the D_{max} particle size collected in the stationary net sampler for various flows at the upper site of St. Louis Creek is shown in Fig. 7.2 (top), and the flow competence curve for Ryan's (1998) Helley-Smith samples from Site 4a in Fig. 7.2 (bottom). The discharges at which the flow competence curve intercepts with each of the particle size classes is read of the graph and listed in Table 7.1 for the net-frame sampler, and Table 7.2 for Ryan's Helley-Smith data, respectively.

7.1.3 Graphical-visual approach

The graphical-visual method visually estimates the flow at which particles begin to have transport rates larger than zero from a scatter plot of fractional bedload transport versus discharge. The advantage of the method is that it does not require to compute a rating curve. If many data points are available within the transition zone between transport, and roughly the same number of measurements fall in each discharge interval, visual determination of critical flow should be unproblematic. However, if the range of zero to beginning transport is poorly represented, user decision plays a role in selecting the exact point of initial motion and this in turn is influenced by the visual appearance of the scatter plot.

Critical flow may be defined as the smallest flow in which *one* measured transport rate is above zero. The presence of "outliers" with above-zero transport rates for very low flows makes this rule inapplicable. Two or three transport rates larger zero, or two transport rates larger zero within the same discharge increment may be appropriate criteria. The user may also find himself compelled to apply various criteria to account for a variable number of data points in scatter plots. For reproducibility, chosen criteria should be discussed.

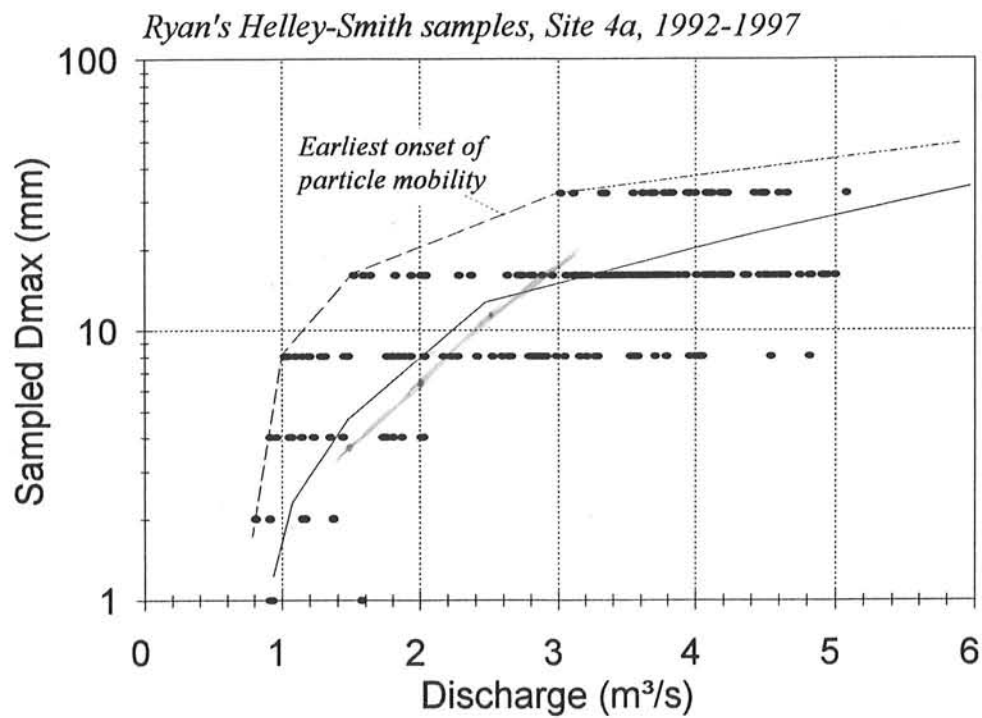
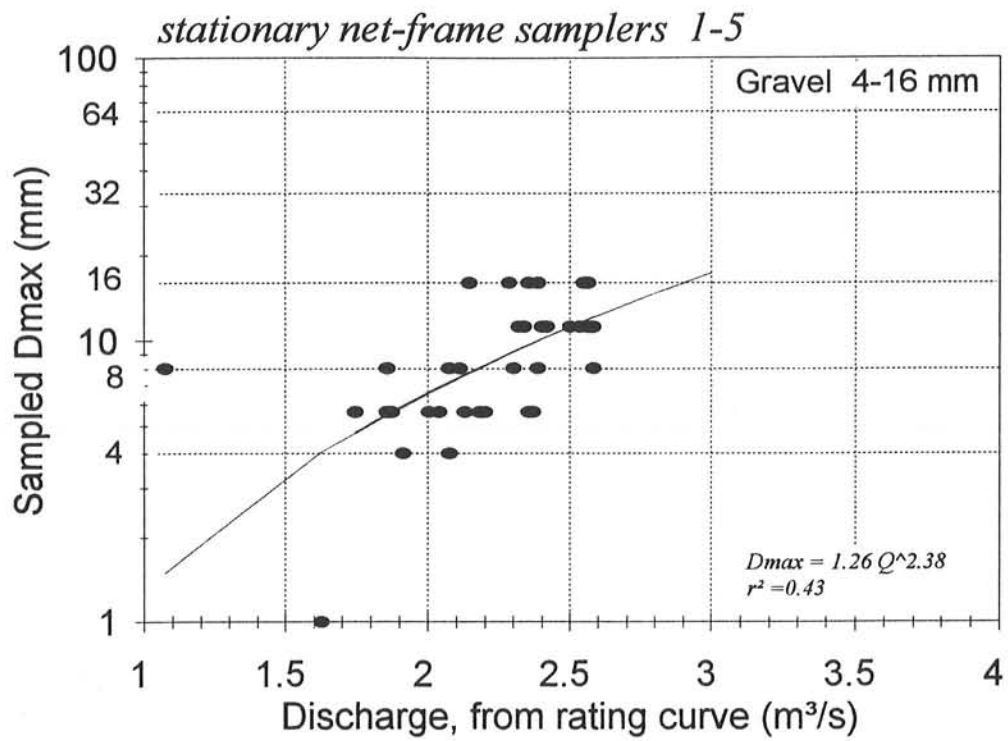


Fig. 7.2: Flow competence curve for the D_{max} particle size collected in the stationary net sampler for various flows at the upper site of St. Louis Creek (top) and collected with the Helley-Smith sampler at Site 4a during 1992-1997 by Ryan (1998) (bottom).

This study selected a minimum of two above-zero transport rates for one discharge increment of $0.05 \text{ m}^3/\text{s}$ for scatter plots with more than three data points per discharge increment, while one transport rate above zero qualified for the onset of motion for the largest particle size class with less than three data points per discharge increment. These criteria were applied to the scatter plots of fractional weight-based transport rates from the net frame sampler in Fig. 5.7, (though results are almost the same when using particle number transport rates in Fig. 5.6), and to Ryan's Helley-Smith data in Fig. 7.1. Critical flows resulting from these selection criteria are listed in Table 7.1 and 7.2, respectively.

7.1.4 x-axis intercept

Another approach to determine critical flow for initial motion is the computation of the x-axis intercept of a regression function through the scatter plot of bedload transport rates versus discharge. The regression model needs to be linear so that the y-value (transport rate) can become zero. $y = 0$ is not defined for logarithmic y-axis scales, and power functions in the form of $y = ax^b$ pass through the origin when plotted in a linear scale.

Linear regressions require less computational effort in spread sheet programs than power function regressions. However, bedload data often have a poor fit only to linear regressions, especially when bedload data extend over a large range of flow and cover a large range of transport rates. Scatter plots of the largest particle size classes usually have a large number of zero transport rates. Inclusion of those data points in the linear regression analysis shift the x-axis intercept towards small flows, while exclusion of zero transport rates results in steeper rating curves with a higher flow at the x-axis intercept. This study included zero values in the regression analysis. x-axis intercepts were computed from the linear regression functions for all size classes for the net-frame sampler (Fig. 7.3 and 7.4) and Ryan's Helley-Smith data (Fig. 7.5). Again, the results of the analysis are the same for weight-based and particle number transport rates. Critical flows obtained from the x-axis intercept are listed in Tables 7.1 and 7.2, respectively.

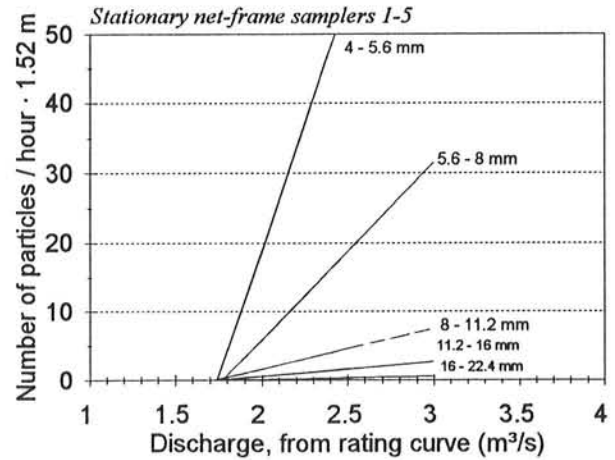
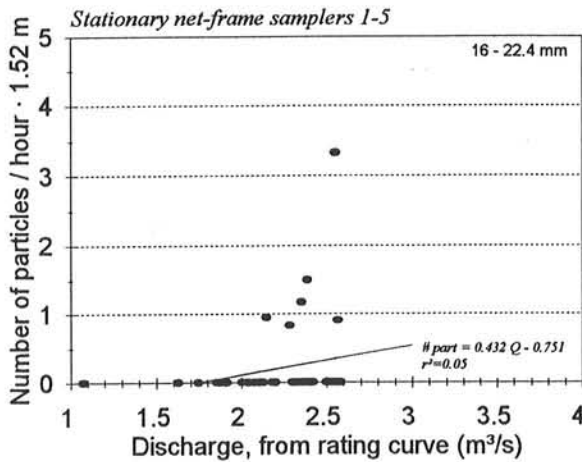
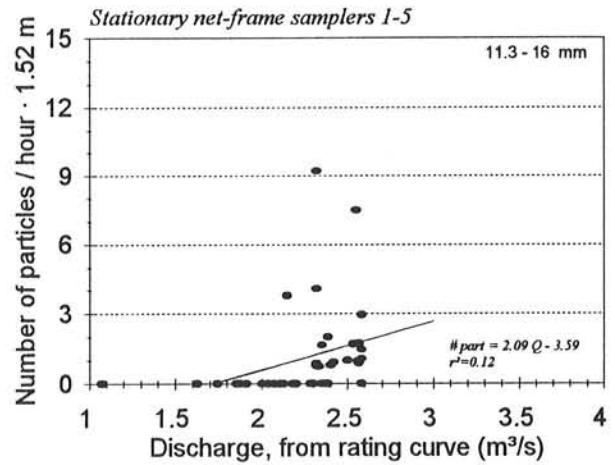
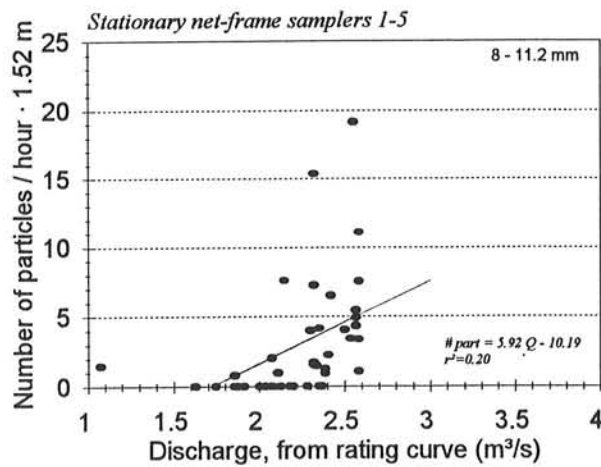
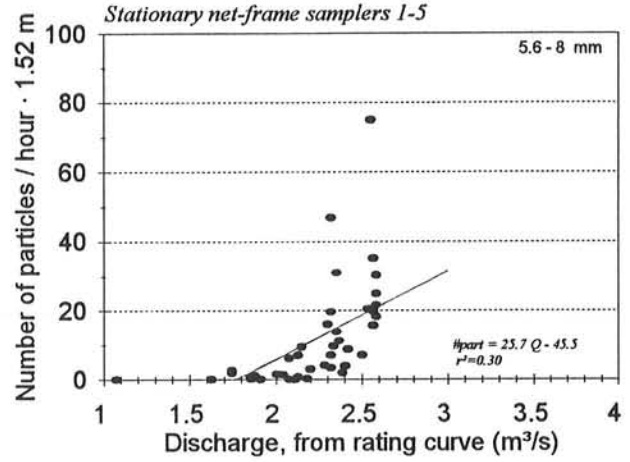
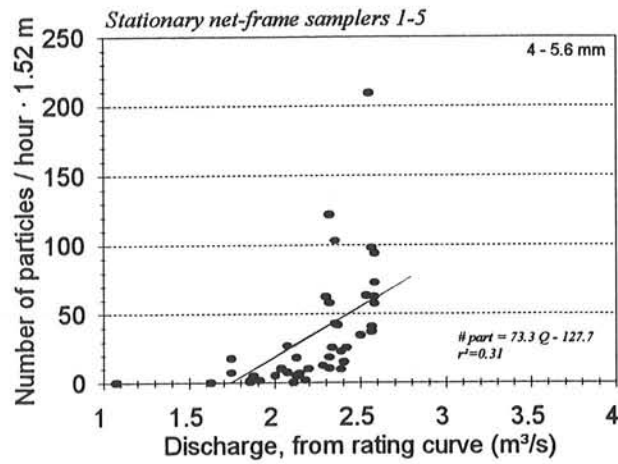


Fig. 7.3: Particle number transport rates per size class for data from the net-frame sampler plotted in linear scale with linear regression functions.

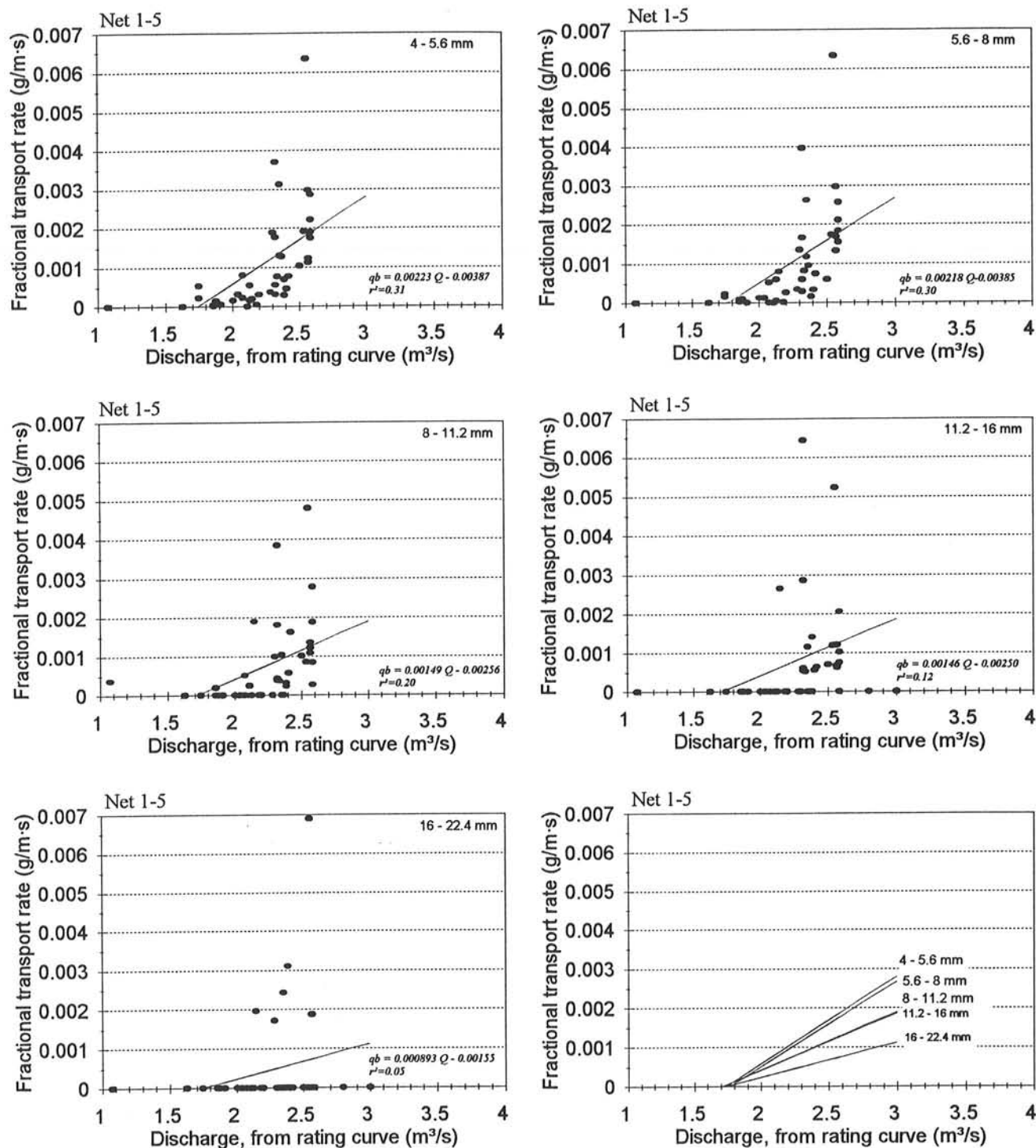


Fig. 7.4: Fractional weight-based transport rates for data from the net-frame sampler plotted in linear scale with linear regression functions.

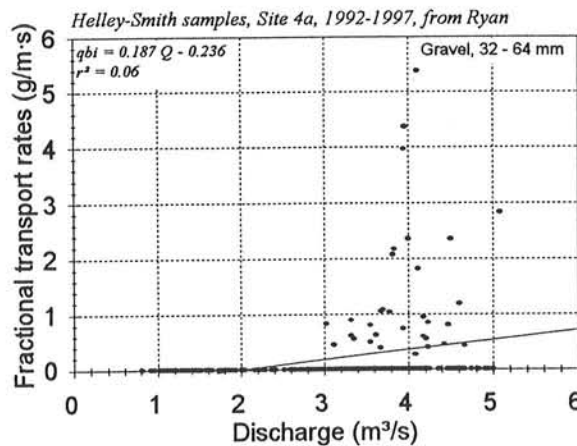
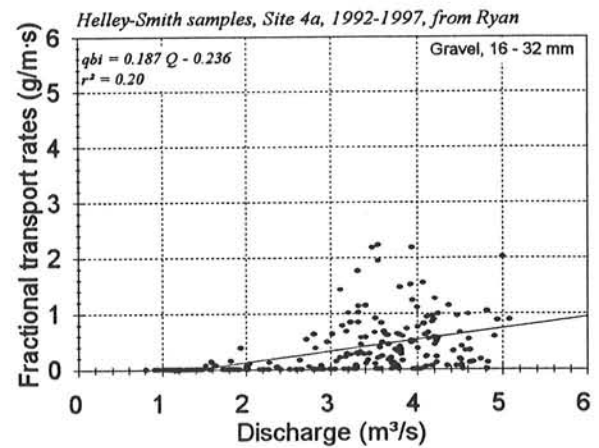
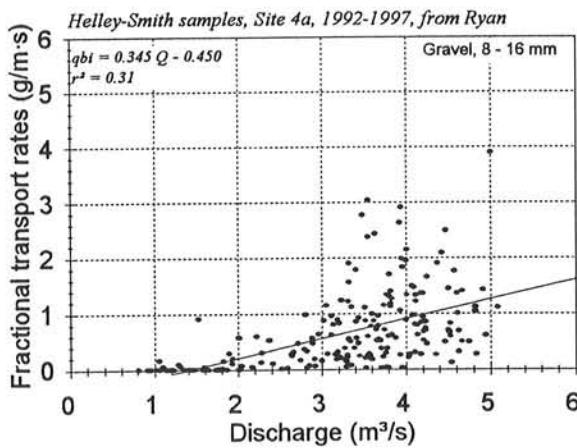
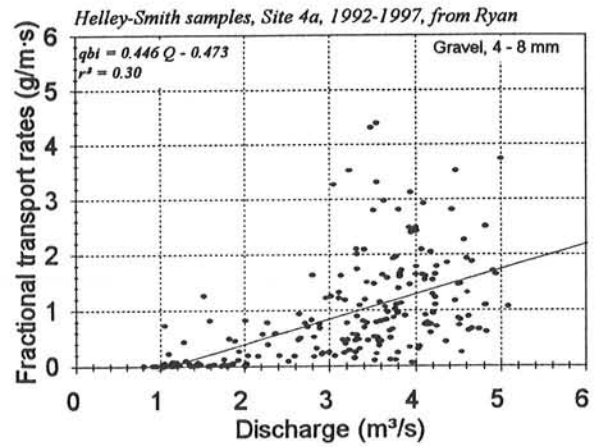
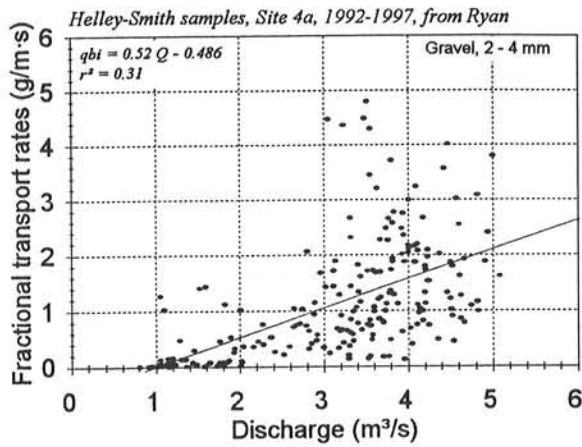


Fig. 7.5: Fractional weight-based transport rates for Ryan's Helley-Smith data plotted in linear scale with linear regression functions.

7.1.5 Reference transport rate $W_i^* = 0.002$

Parker and Klingeman (1982) developed a dimensionless reference transport rate W_i^* in order to standardize the transport rate that must be exceeded at initial motion. Using W_i^* has been recommended by several authors (e.g., Wilcock 1988). W_i^* is and computed from

$$W_i^* = \frac{\left(\frac{\rho_s}{\rho_f} - 1\right) \cdot g \cdot qb_{vol,i}}{f_i \cdot (g \cdot d_m \cdot S)^{3/2}}$$

1997

- $\frac{(\frac{\rho_s}{\rho_f} - 1) \cdot g \cdot qb_{vol,i}}{f_i \cdot \rho_s \cdot (g \cdot d_m \cdot S)^{1.5}} \cdot (g/m.s)$

where ρ_s and ρ_f are sediment and water density, g is acceleration due to gravity and set to 9.81 m/s^2 , $qb_{vol,i}$ is the volumetric transport rate of the i th size fraction, f_i is the percentage frequency of the i th size fraction of the subsurface particle size distribution, d_m is the mean flow depth, and S the water surface gradient, which was substituted by the channel gradient in this study.

To compute W_i^* , mean flow depth d_m is predicted for each discharge increment Q (see Table 7.3, column 1) from a rating curve $d_m = a Q^b$ (column 2). The bedload transport rate in terms of number of particles per width and time is predicted for each discharge increment from a rating curve $N_{part,i} = c Q^d$ (column 3). An adjustment may be necessary to obtain units of $\text{m}^3/\text{m}\cdot\text{s}$ (column 4). The volume of a particle in the i th size class is computed for the logarithmic center of class D_{ic} and a spherical particle shape. Particle volume is $V_{Dic} = 4/3 \pi \cdot D_{ic}/2$ (column 5). The volumetric transport rate is the product of particle volume times particle number transport rate (column 6). W_i^* is computed from the equation above using the input parameters calculated for each discharge increment. When computing W_i^* in a spread sheet, a discharge value for which W_i^* is close to 0.002 is slightly altered until $W_i^* = 0.002$. That discharge value becomes the critical flow for the i th particle size class. The computation is repeated for each particle size class. Critical discharges were computed from the W_i^* approach for the lower three size classes of samples obtained from the net-frame sampler. Results are listed in Table 7.1.

Table 7.3: Example computation of $W_i^* = 0.002$ for the particle size class 5.6-8 mm.

Q (m ³ /s) (1)	d_m (m) (2)	$N_{part,i}$ per (1.52.m·s) (m·s) (3) (4)		V_{Dic} (m ³) (5)	$qb_{vol,i}$ (m ³ /m·s) (6)	W_i^* (-) (7)
1.5	0.28	0.17	0.11	1.57E-07	1.71E-08	0.00060
1.6	0.29	0.29	0.19	1.57E-07	3.01E-08	0.00102
1.736	0.30	0.60	0.39	1.57E-07	6.16E-08	0.00200
1.8	0.30	0.82	0.54	1.57E-07	8.45E-08	0.00270
2	0.31	2.06	1.35	1.57E-07	2.13E-07	0.00648
2.5	0.33	14.5	9.57	1.57E-07	1.50E-06	0.04125

The reference transport rate approach is sensitive to variations in the percent frequency of a size class in the subsurface particle size distribution, and especially to the shape of the rating curve. For representative results, flows and transport rates for all size classes considered need to extend over a large range in order to yield a well defined rating curve. It

is difficult to establish rating curves for transport rates of the largest size classes. Those data sets are small, have scattered transport rates, and remain within a small range of flow. In this study, statistically significant rating curves could only be established for size classes smaller than 11.3 mm.

7.2 Comparison of critical discharge

7.2.1 Bedload samples from the net-frame sampler

Values listed for critical discharge and different size classes in Table 7.1 are plotted for different initial motion criteria in Fig. 7.6. The plots show that different initial motion criteria can lead to different relationships between critical discharge and particle size when applied to bedload transport data from the same stream site. Initial motion curves can either be positive increasing (Fig. 7.6, top), or more or less horizontal (Fig. 7.6, bottom).

Positive initial motion curves indicate that increasing particle sizes require increasing discharge for entrainment and are obtained from the following three initial motion approaches (Fig. 7.6, top):

- ◊ preset particle number transport rate,
- ◊ flow competence curve, corresponds to a transport rate of about 2-5 particles, and
- ◊ graphical-visual analysis, the result of which is quite similar to (1).

Positive initial motion curves indicate the concept of "selective transport" for particle entrainment.

Near horizontal initial motion curves suggesting the same critical discharge for all particle sizes are obtained from (Fig. 7.6, bottom):

- ◊ preset weight-based threshold transport rates,
- ◊ the x-axis intercept approach, and
- ◊ reference transport rate approach.

The latter two approaches yield very similar results for the data used in this study. Horizontal initial motion curves indicate the concept of "equal mobility" for particle entrainment. The fact that both the selective transport and the equal mobility principle can be demonstrated for the same data set shows that the distinction between selective transport and equal mobility is largely based on computational differences, and not on different physical processes governing particle entrainment.

The difference between critical flow from positive increasing and near-horizontal initial motion curves is most pronounced for the largest particle sizes. For the smallest particle size class in this study, 4 - 5.6 mm, critical discharge is within 1.6 to 2.0 m³/s (40-50% Q_{bkt}) for all approaches, except those with large preset critical transport rates of 0.001 and 0.01 g/m·s, and 10 particles/1.52 m · hr. For the particle size class 11.2 - 16 mm, critical discharge is about 1.7 m³/s (43% Q_{bkt}) for the preset weight-based transport rate of 0.0001 g/m·s, the x-axis intercept, and the reference transport rate, but reached 2.1 m³/s (53% Q_{bkt}) for a preset particle number transport rate of 1 particle/1.52 m and hr and the visual approach, and 2.5 m³/s (63% Q_{bkt}) for the flow competence approach.

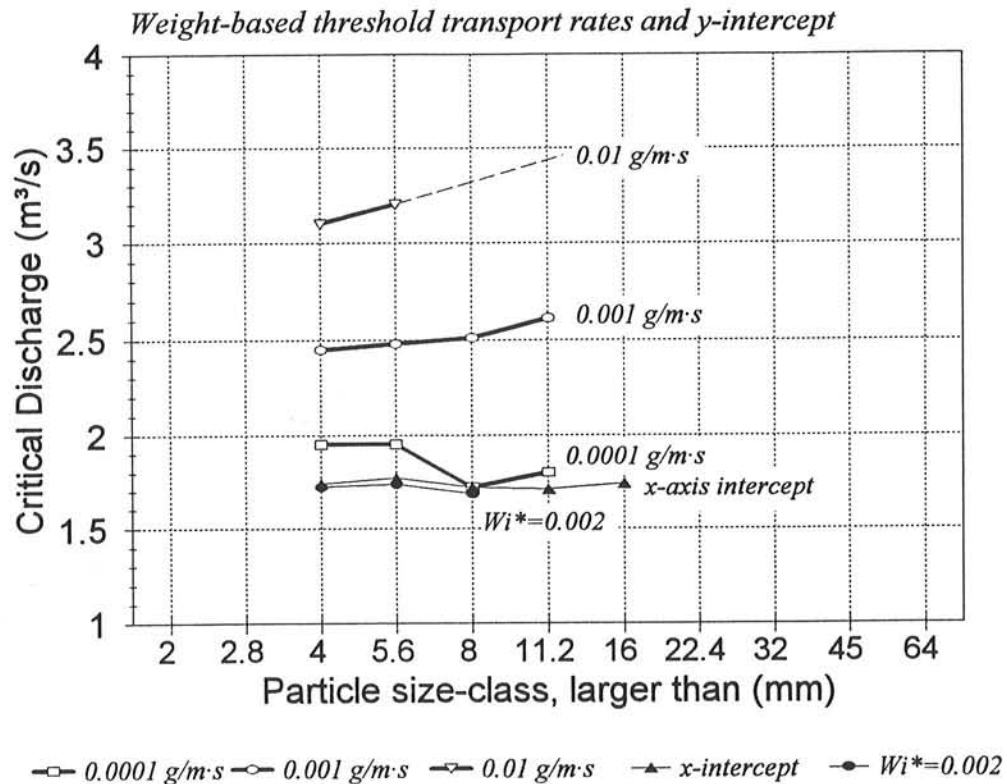
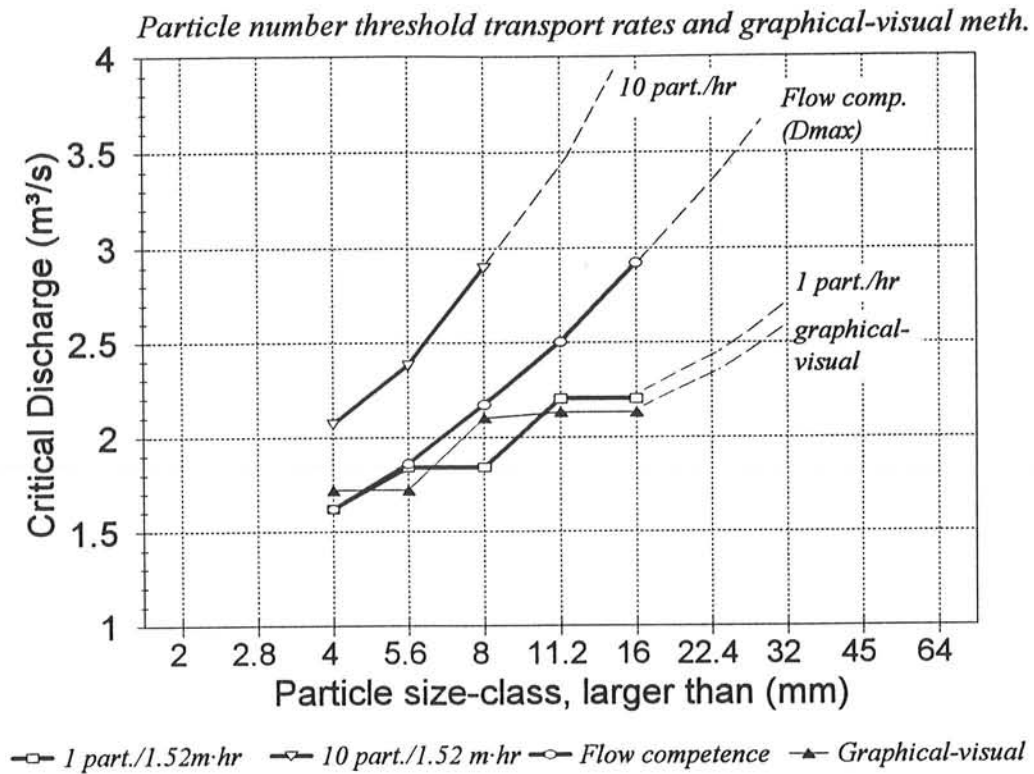


Fig. 7.6: Initial motion curves with critical discharge for different particle size classes for samples from the stationary net-frame sampler at the upper site based on the flow competence curve, particle number transport rates, and the graphical-visual analysis (top), and on fractional weight-based transport rates, x-axis intercept, and the reference transport rate $Wi^*=0.002$ (bottom).

7.2.2 Ryan's bedload samples from the Helley-Smith sampler

Initial motion was also computed for the Helley-Smith data obtained by Ryan (1998) using preset weight-based fractional transport rates, the x-axis intercept, and the graphical-visual approach, as well as the flow competence approach. Particle number transport rates, and the reference transport approach could not be computed with the data available to this study. Critical discharges are listed in Table 7.2 and graphically combined in Fig. 7.7. Note that Fig. 7.7 has a slightly different scale than Fig. 7.6. Again, initial motion curves are more or less horizontal for the lowest preset weight-based transport rate (Fig. 7.7, top) and the x-axis intercept approach (Fig. 7.7, bottom), and positive increasing for high preset weight-based transport rates, the flow competence approach, and the graphical-visual approach.

Critical discharge for the size class 4 - 8 mm computed for the Helley-Smith data with the flow competence, x-axis intercept, and graphical-visual approach is on average $0.5 \text{ m}^3/\text{s}$ lower than determined for the size classes 4-5.6 and 5.6-8 mm with the same approaches for the data from the net frame sampler. The main reason for this discrepancy is that the Helley-Smith data set has more data points for low flows than the data set from the net-frame sampler (compare Fig. 7.1 with 5.7). Thus, initial motion is statistically better defined. The generally larger transport rates obtained from the Helley-Smith sampler might attribute to the lower critical discharge as well.

7.2.3 Critical discharge for gravel beds at about 2/3 of bankfull flow?

The beginning of gravel motion in mountain gravel-bed rivers is sometimes assumed to start at a flow of about 2/3 of bankfull (Carling 1995). Results from the critical discharge analysis show that at the upper site at St. Louis Creek 7 mm particles were definitely present in bedload transport with about 10 particles per 1.52 meter and hour at 2/3 of bankfull ($2.7 \text{ m}^3/\text{s}$), while the competence of flow suffices to transport particles around 13 mm. Extrapolating the initial motion curves for 1 particle per 1.52m-hr and the visual approach suggest that at 2/3 Q_{bkf} an occasional particle up to 32 mm in size should be moving.

An extrapolation to bankfull has a high error potential, but if done nevertheless suggests a bankfull flow competence for particles up to 45 mm, 10 particles in the size class 16-22.4 mm per hour and 1.52 m. Occasionally, a cobble larger 90 mm might move.

The initial motion analysis for Ryan's (1998) Helley-Smith data collected at Site 4a produced similar results with respect to flow competence and the visual approach. For other approaches, Helley-Smith samples predict a lower critical discharge for small gravels, and a higher critical discharge for large gravels and cobbles. Specifically, flows of 50%, 70% and 100% of bankfull have a flow competence for particles in the size classes of 7-14 mm, 11-22 mm, and 19-38 mm, respectively. The fact that the Helley-Smith samples predict a lower critical discharge for small gravels, and a higher critical discharge for large gravels and cobbles could be related to the tendency of Helley-Smith samplers to oversample sand and fine gravels (due to a hydraulic efficiency larger than 100%), while undersampling coarse gravels and cobbles (due to small size of the sampler opening).

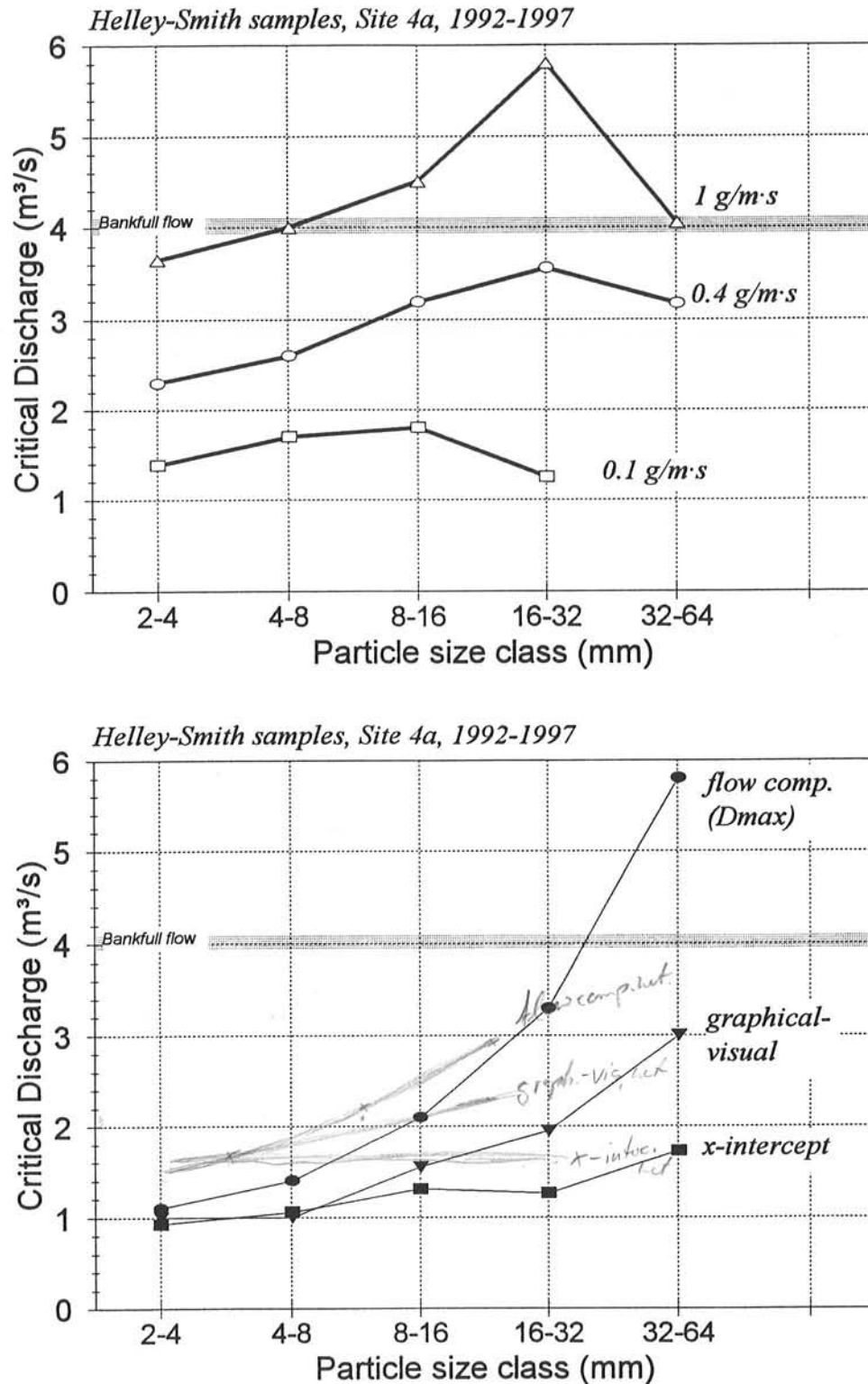


Fig. 7.7: Initial motion curves with critical discharge for different particle size classes for Ryan's (1998) Helley-Smith samples from site 4a based on fractional weight-based transport rates (top), the flow competence curve, the x-axis intercept, and the graphical-visual approach (bottom).

Corresponding to the three to one orders of magnitude difference in weight-based transport rates, flows of 50, 70, and 100% of bankfull produce lower weight-based transport rates for samples from the stationary net-frame sampler in 1998 than for the 6-year set of Helley-Smith samplers from site 4a. Interpolation between initial motion curves in Fig. 7.6 indicates transport rates for the stationary net-frame samplers of 0.0001 - 0.0002 g/m's for all particle size classes between 4 and 16 mm for 50% Q_{bkf} , of 0.004 to 0.002 g/m's for 70% Q_{bkf} , and in the order of 0.1 g/m's at bankfull flow. For the Helley-Smith samples from site 4a, transport rates of 0.1 - 0.2 g/m's, 0.3 - 0.4 g/m's, and 0.5 - 1.0 g/m's can be interpolated for discharges of 50, 70, and 100% of bankfull for all particle size classed between 4 and 64 mm from Fig. 7.7. This comparison suggests that initial motion and critical flow cannot be predicted from the exceedance of a fixed weight-based transport rate, because different samplers and their sampling schemes produce different transport rates, let alone the differences in transport to be expected between different streams.

7.3 Critical dimensionless shear stress τ_c^* for net-frame samples

Particle entrainment is often connected with the exceedance of a critical value for dimensionless shear stress. Critical dimensionless shear stress is computed as

$$\tau^* = \frac{\tau_c}{(\rho_s - \rho_f) \cdot g \cdot D_{50}} = \frac{\rho_f \cdot g \cdot d_m \cdot S}{(\rho_s - \rho_f) \cdot g \cdot D_{50}} \quad (8)$$

where τ_c is critical shear stress at the beginning of motion, ρ_s and ρ_f are sediment and water density and usually taken to be 2,650 and 1,000 kg/m³, respectively; g is acceleration due to gravity and usually taken to be 9.81 m/s², d_m is mean depth of flow, and S is channel gradient¹⁰. The D_{50} particle size can refer to the particle size-distribution of the surface, or the subsurface. In the latter case, the value of τ^* is about twice as high, since the subsurface D_{50} in armored mountain gravel-bed streams tends to be about half the size of the surface D_{50} . For the computations in this study the surface D_{50} size of 76 mm was used. Reported values of critical dimensionless shear stress τ_c^* for gravel bed rivers range from 0.03 to 0.2 and varies over an order of magnitude.

τ^* was computed for each discharge value, and particle number transport rates, flow competence, as well as fractional weight-based transport rates were plotted versus τ^* for all size classes. Regression functions were fitted by eye. The intercepts of the regression function with τ^* for preset fractional particle transport rates of 1, and 10 particles/1.52 m · hour, and preset fractional transport rates of 0.001, and 0.0001 g/m's were read off the graphs, listed in Table 7.4, and plotted for the different initial motion criteria in Fig. 7.8.

At the upper site at St. Louis Creek, gravel particles 8-11.2 mm can be found, albeit rarely as τ^* exceeds 0.043, and are an expectable part of bedload at $\tau_c^* = 0.045$. Particles 4-5.6 mm are beginning to be transported at $\tau_c^* = 0.041$. Those values agree well with values reported by Julien (1995) for experiments by Bagnold. However, a computational procedure for τ_c^* that takes into account the entirety of parameters affecting particle entrainment in mountain gravel bed rivers, and is generally accepted by a wide user community has not become available yet.

¹⁰ Ideally, computations should be based on the water surface slope with its temporal variability and highest values during the steepest increases of flow over time.

Table 7.4: Critical dimensionless shear stress values for different particle size classes and various criteria for initial motion at St. Louis Creek, upper site.

Size class (mm)	Fractional transport rates			Particle transport rates		Flow competence (D_{max})
	0.0001	0.001	0.01	1	10	
	(g/m ² ·s)			(part./1.52m·hr)		
4.0 - 5.6	0.044	0.047	0.052	0.041	0.044	0.041
5.6 - 8.0	0.043	0.040	0.053	0.043	0.047	0.043
8.0 - 11.2	0.042	0.042	-	0.043	0.051	0.045
11.2 - 16.0	-	0.041	-	0.044	0.053	0.048
16.0 - 22.4	-	0.044	-	0.045	-	0.051

It is known, for example, that values of τ_c^* increase with particle size (Julien 1995) and stream gradient (Rosgen 1994, 1996), and with parameters that aid in particle stability such as particle pivot angle, particle shape and angularity (Komar and Li 1986), particle embeddedness and hiding (Fenton and Abbot 1977; Andrews 1983), density of particle packing (Gordon et al. 1992), stream bed roughness (Fisher et al. 1983; Wiberg and Smith 1987; Kirchner et al. 1990), and depth of pocket angles (Andrews and Smith 1992). Values of τ_c^* increase with the amount of sediment to be entrained (Milhous 1989), and values of τ_c^* vary depending on the method used for computations. τ_c^* is higher, often by a factor of about 2, when computations are based on subsurface D_{50} particle size instead of the surface D_{50} size¹¹. Values of τ_c^* based on reference shear stress tend to be higher than those based on visual estimates of particle entrainment or on flow competence (Buffington and Montgomery 1997). Until a generally accepted computational procedure is available predicting particle entrainment seems to make little sense if it is based on a controversially debated approach of computing τ_c^* .

In light of such variability it seems to make little sense to predict particle entrainment in mountain gravel-bed streams from a critical dimensionless shear stress value, unless a methodology for computing τ_c^* has been found that combines the various physical factors affecting particle entrainment and that is based on distinctly qualifiable criterion for initial motion.

7.4 Initial motion criteria for channel maintenance flows

Channel maintenance flows are concerned with the entrainment of river gravels. There seems to be an open discussion as to which particle sizes of the bed material need to be moved. Conceivably, the critical particle size could be set at some medium gravel size (e.g., at 8 - 22 mm).

The analysis of critical discharge above (Fig. 7.6) showed that only initial motions considerations based on particle transport rates and flow competence analysis go along with the intuitively understandable principle that flow needs to increase to entrain consecutively larger particle sizes. Initial motions considerations based on fractional weight-based transport rates lead to the less intuitively understandable phenomenon that flow required for initial motion is basically the same for all particle sizes.

¹¹ This is because the ratio of surface to subsurface D_{50} often assumes a value around 2 in armored gravel-bed streams.

$$d_c = 0.2498 Q_{m^3/s}^{0.3199}$$

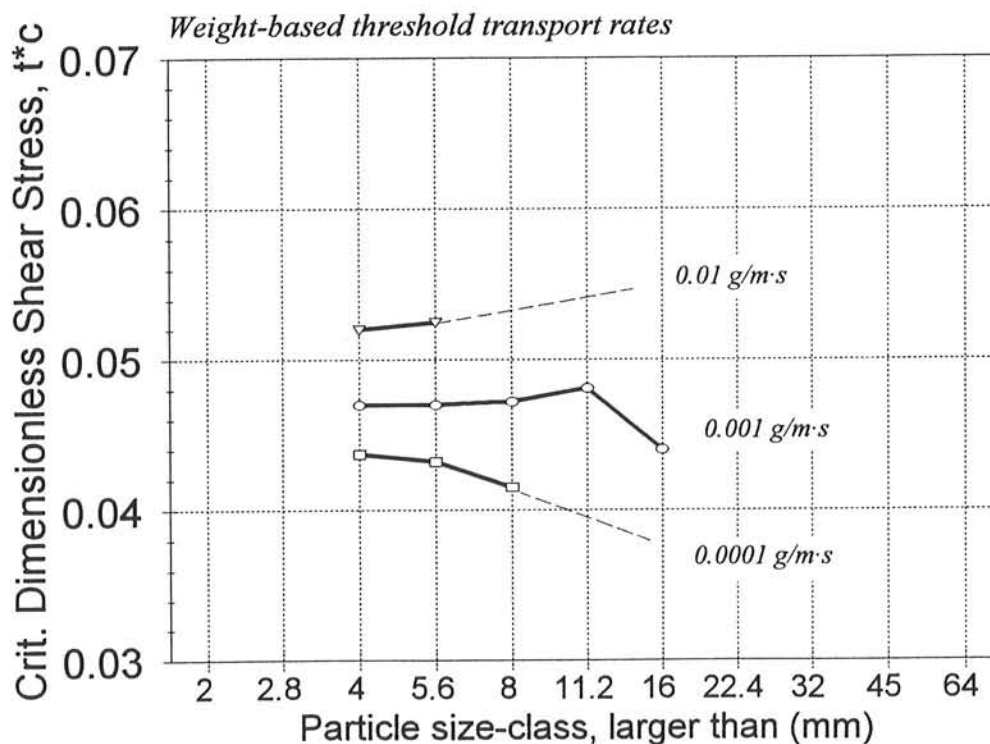
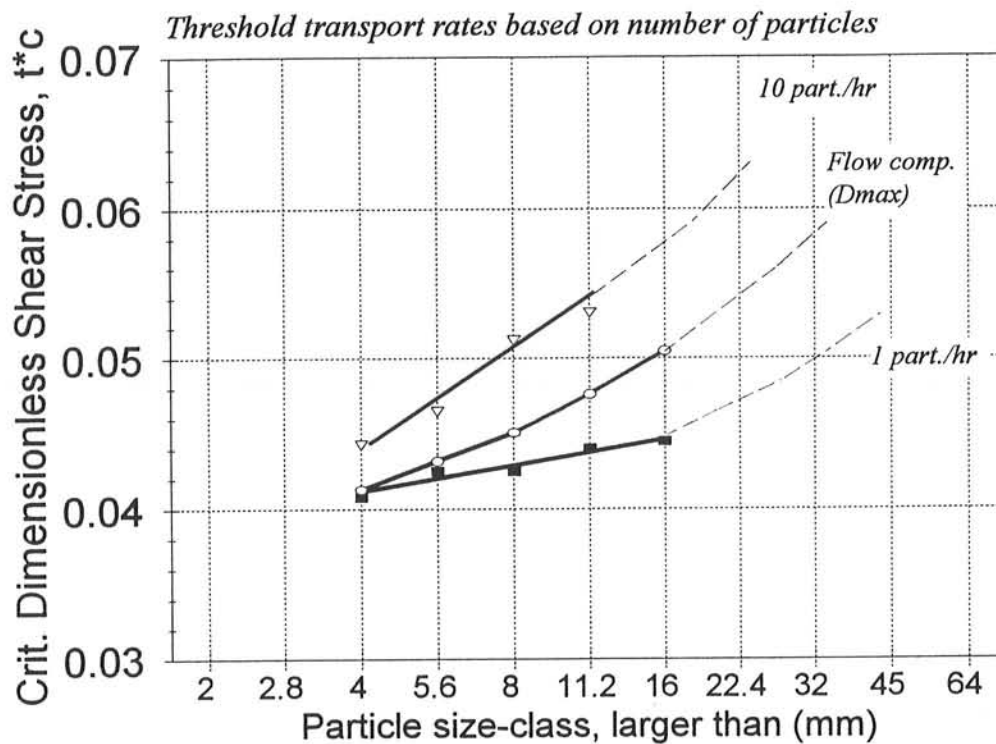


Fig. 7.8: Initial motion curves with critical dimensionless shear stress for different particle size classes for samples from the stationary net-frame sampler at the upper site based on a flow competence curve and particle number transport rates and (top), and on fractional weight-based transport rates (bottom).

Fractional weight-based transport rates for given particle size classes differ by orders of magnitudes between streams, and there is no absolute and standard value of a fractional weight-based transport rate in g/m/s or similar units to indicate initial motion. Thus, critical discharge is strongly influenced by the minimum fractional transport rate selected. A possibility would be to base critical transport rates on a preset small percentage of the bankfull total gravel transport rate, a value of 1-5 %, for example. However, this requires that bankfull transport rates are known.

Initial motion for individual streams can be determined with the least amount of controversy using either a flow competence approach, or measuring low particle number transport rates of, for example, 2 - 5 particles per meter and hour. Both flow competence and particle number transport rates can be measured with reasonable effort and accuracy using stationary net-frame samplers. The computational part of the analysis is straight forward and intuitively understandable.

Besides sampling accuracy, the accuracy of measurement-based initial motion analysis depends on the number of bedload samples taken and on the range of flow sampled. Collecting 30-40 samples stretched over the entire range of flows should be considered a minimum and amounts to 2-3 weeks of field work. Extrapolation of sampling results to near bankfull flow is necessary for years of small high flow and this might involve some inaccuracy. But since none of the computations are based on bankfull conditions of flow or transport, no measurements have been wasted if bankfull flows were not reached.

8. Evaluation of the stationary net-frame sampler and summary

The net-frame sampler has a large opening consisting of an aluminum frame 12 inches wide and 8 inches high. A three foot trailing fishing net serves as sampling bag. The mesh width was 3/16 inch (4.7 mm), but larger mesh widths can be selected. Such a net-frame sampler can be easily constructed in a metal shop, while the net and the webbing loops can be assembled with a little handicraft skill. Sampler installation in the stream bed involves moving some surface particles and pounding in a couple of stakes, an easy procedure although a couple of tries may be necessary in cobble beds to position the samplers at locations where the stakes remain vertical. The stationary net-frame samplers can be operated by one person, but work is easier and safer in a stream during the onset of high flow for a team of two persons. Sampler operation requires that the stream remains wadable at all flows and locations of concern.

The main objective of the stationary net-frame sampler is to representatively sample the transport of gravels and cobbles in order to determine the critical flow needed for gravel and cobbles entrainment. The large sampler opening allows large particles to enter the sampler, while the attached large fishing net allows fine sediment to pass, while large particles accumulate at a low rate, and sample volumes are not likely to become unmanageably large during a sampling period. Yet, even a set of 5 samplers is portable, and easy enough to install and operate by two persons at a remote field site.

The stationary that results from using a set of 5 samplers across the stream at a time, as well as the capacity of the samplers to accumulate large amounts of bedload and debris, permits sampling to extend over a large percentage of the time and width. The ensuing high sampling intensities exceed those from a typical Helley-Smith sampling scheme by a factor of almost 50, or 1.5 orders of magnitude. Even clamping a set of several Helley-Smith samplers to stakes in the stream bed will not necessarily extend the sampling intensity because sampling efficiency of Helley-Smith samplers decreases when the bag fills to about half its capacity.

A high sampling intensity is desirable because it increases sampling accuracy, and averages over highly fluctuating transport rates thus reducing rating curve scatter. The ability to accurately measure low transport rates is desirable for initial motion studies, because sampling infrequently moving particles permits computation of actual low transport rates instead of "zero" transport rates. "Zero" transport rates are of limited utility, because it remains unknown whether the rate was truly zero or only too small to be measured by the sampling scheme employed. "Zero" transport values are also unable to be used for power function rating curves, since power function regression ($y = ax^b$) analysis does not accept zero-values.

The ability of intensive sampling schemes to compute actual low transport values instead of "zero"-values for small flows leads to steep rating curves with rating curve exponents several times larger than those obtained from non-intensive sampling schemes. Thus it is important to bear in mind that rating curve steepness is not only a function of actually occurring transport rates, but is greatly affected by the measurability of transport rates. Consequently, only rating curves obtained by similar samplers and sampling schemes are comparable.

The stationary net-frame sampler was tested at a mountain gravel-bed river. At the measuring site, the cobble-bed stream had a stream gradient of 0.018, stream width 6.5 m, a surface D_{50} of 76mm, and a subsurface D_{50} of 41 mm. High flow reached only about 70 percent of bankfull discharge this year. The largest bedload particle size-class was 16 -

22.4 mm. Samples comprised large amounts of organic debris which is a nuisance for bedload sampling, but can provide useful information for fisheries biologists or stream ecologists.

Rating curves for total gravel bedload transport, fractional transport rates and particle transport rates are well defined. However, transport rates are very low. For small transport rates, the rating curve for 4-16 mm gravel transport rates measured with the stationary net-frame samplers was about 3 order of magnitude smaller than gravel transport rating curve from the Helley-Smith sampler. This difference reduced to 1 order of magnitude for transport rates at flows 70% of bankfull. Rating curves for both samplers approached each other for higher flows, suggesting that both samplers may obtain similar transport rates for flows above bankfull. Much of this discrepancy is attributable to the different sampling schemes and the high sampling intensity that allows the stationary net-frame sampler to measure much lower transport rates than the Helley-Smith sampler.

Other reasons for this discrepancy which remain to be clarified include:

- sediment detention behind a beaver dam upstream from the site of the stationary net-frame sampler,
- diminished supply of small gravels after two consecutive years of above average high flows in 1996 and 1997,
- the stationary net-frame samplers may need to be placed deeper into the armor layer to facilitate entry of bedload into the sampler, and
- Helley-Smith sampler may oversample gravels due to scooping;

On average, both samplers sampled similar particle sizes, but concurrent samples from the two samplers usually have different particle size distributions.

Additional parallel testing of both samplers is necessary for a more detailed sampler evaluation. Field tests should extend to bankfull flows to compare sampling behavior for high transport rates and large particle sizes. Flume testing will allow particle paths near the sampler entrance to be observed and sampling efficiency to be tested. The allegation that the Helley-Smith sampler may scoop gravel particles from the bed needs to be examined as well.

The sampler design can still be refined. A quick-release connection between sampler and net is desirable for an easy exchange of nets with different mesh sizes if transport rates or transported particle sizes change during a high flow event. A velcro closure for the net end would be convenient as well.

There are several ways to compute critical discharge for initial gravel motion based on actual bedload transport measurements: fractional particle number transport rates, flow competence analysis, weight-based fractional transport rates. Initial motion analysis for samples taken with the stationary net-frame samplers at St. Louis Creek showed an increase of critical flow for increasingly larger particle sizes (selective transport) for particle number transport rates and the flow competence approach, while weight-based fractional transport curves produced horizontal initial motion curves in which all particle sizes start to move at about the same flow (equal mobility). Proving both principles with the same data set demonstrates that the distinction is computational, and not based on different processes in particle entrainment.

The initial motion analysis from data of the stationary net-frame sampler confirm the assumption that gravel motion in mountain gravel-bed rivers begins at flows of about 70%

of bankfull. At the upper site at St. Louis Creek, a flow of 70% of bankfull ($2.8 \text{ m}^3/\text{s}$) transported 10 particles in the size class 8-11.2 mm per hour and 1.52 m of width, and had a competence to transport particles of the size class 14-20 mm. Extrapolation to bankfull flow suggests a flow competence of 32-45 mm, transport of 10 particles in the size class 19-27 mm per hour and 1.52 m, and the occasional movement of a cobble.

Initial motion seems to harbor the least controversy potential when based on flow competence or a low particle number transport rate of 2 - 5 particles per meter and hour, both of which can be reliably measured with stationary net-frame samplers. Accuracy of measurement-based initial motion analysis improves with increased sample size and a wide range of sampled flows, and extrapolation to bankfull flow in years of small high flow might involve inaccuracy, but no measurements have been wasted if flows did not reach bankfull that year.

Prediction of particle entrainment in mountain gravel-bed streams using a critical dimensionless shear stress value is contingent upon the availability of a method that (1) combines the various physical factors controlling particle entrainment in the computation of τ^*_c and that (2) is based on distinctly qualifiable criteria for initial motion.

Acknowledgement

Sean McCoy, Dan Armstrong, John Potyondy, Rhett Travis, Kurt Swingle and Brian Smith helped with field and lab work, Chad Lipscomb and Chris Thornton provided organizational support. The shop of the Engineering Research Center constructed the metal parts of the sampler. The U.S. Forest Service and Manuel Martinez made possible the field work and stay at the Fraser Experiment Station. Steve Abt, John Potyondy, Kurt Swingle and Sandra Ryan provided helpful comments. Sandra Ryan kindly supplied the bedload transport data sampled with the Helley-Smith sampler at Site 4a during the years 1992-1997 (Ryan 1998). John Potyondy's constructive review improved the manuscript. This study was funded by the Stream Systems Technology Center, USDA Forest Service, Rocky Mountain Forest and Range Experiment Station, Fort Collins, CO. I would like to thank everybody involved for their support which is greatly appreciated.

9. References

- Andrews, E.D. and J.D. Smith, 1992. A theoretical model for calculating marginal bedload transport rates of gravel. In: *Dynamics of Gravel-Bed Rivers*. P. Billi, R.D. Hey, C.R. Thorne, and P. Tacconi (eds.), John Wiley and Sons, Chichester, p. 41-52.
- Andrews, E.D., 1983. Entrainment of gravel from naturally sorted riverbed material. *Geological Society of America Bulletin* 94: 1225-1231.
- Buffington, J.M. and D.R. Montgomery, 1997. A systematic analysis of eight decades of incipient motion studies, with special reference to gravel-bed rivers. *Water Resources Research* 33 (8): 1993-2029.
- Buffington, J.M., W.E. Dietrich and J.W. Kirchner, 1992. Friction angle measurements on a naturally formed gravel streambed: implications for critical boundary shear stress. *Water Resources Research* 28(2): 411-425.
- Bunte, K., 1996. Analyses of the temporal variation of coarse bedload transport and its grain size distribution (Squaw Creek, Montana, USA). English translation of Bunte (1991). USDA Forest Service, Rocky Mountain Forest and Range Experiment Station, *General Technical Report* RM-GTR-288, 124 pp.
- Bunte, K., 1997a. Development and field testing of a bedload trap for sand and fine gravels in mountain gravel-bed streams (South Fork Cache la Poudre Creek, CO). Report prepared for the Stream Systems Technology Center, USDA Forest Service, Rocky Mountain Forest and Range Experiment Station, Fort Collins, CO, 53 pp.
- Bunte, K., 1997b. Spatial variability of bed material particle-size distribution in consecutive pool-riffle sequences in a mountain gravel-bed stream: Squaw Creek, Montana. Report prepared for the Stream Systems Technology Center, USDA Forest Service, Rocky Mountain Forest and Range Experiment Station, Fort Collins, CO, (in preparation).
- Carling, P., 1995. Implications of sediment transport for instream flow modelling of aquatic habitat. In: *The Ecological Basis for River Management*. D.M Harper and A.J.D. Ferguson (eds.), Wiley and Sons, Chichester, UK, p. 17-31.
- Church, M., J.F. Wolcott, and W.K. Fletcher, 1991. A test of equal mobility in fluvial sediment transport: Behavior of the sand fraction. *Water Resources Research* 27 (11): 2941-2951.
- Fenton, J.D and J.E. Abbott, 1977. Initial movement of grains on a stream bed: the effects of relative protrusion. In: *Proceedings of the Royal Society of London A* 352: 523-537.
- Fisher, J.S., B.L. Sill and D.F. Clark, 1983. Organic detritus particles: initiation of motion criteria on sand and gravels. *Water Resources Research* 19 (6): 1627-1631.
- Gordon, N.D., T.A. McMahon and B.L. Finlayson, 1992. *Stream Hydrology*. Wiley and Sons, Chichester, UK.
- Hayward, J.A., and A.J. Sutherland, 1974. The Torlesse stream vertex-tube sediment trap. *Journal of Hydrology (N.Z.)* 13(1): 41-53.
- Hubbell, D.W., 1987. Bed load sampling and Analysis. In: *Sediment Transport in Gravel-Bed Rivers*. C.R. Thorne, J.C. Bathurst and R.D. Hey (eds.), John Wiley, Chichester, UK, p. 89-118.
- Julien, P., 1995. *Erosion and Sedimentation*. Cambridge University Press, Cambridge, UK.
- Kirchner, J.W., W.E. Dietrich, F. Iseya and H. Ikeda, 1990. The variability of critical shear stress, friction angle, and grain protrusion in water-worked sediments. *Sedimentology* 37: 647-672.
- Kirchner, J.W., W.E. Dietrich, F. Iseya and H. Ikeda, 1990. The variability of critical shear stress, friction angle, and grain protrusion in water-worked sediments. *Sedimentology* 37: 647-672.

- Knott, J.M., S.W. Lipscomb and T.W. Lewis, 1987. Sediment transport characteristics of selected streams in the Susitna River Basin, Alaska: Data for the water year 1985 and trends in bedload discharge, 1981-1985. *U.S. Geological Survey Open File Report 87-229*, 51 pp.
- Komar, P.D. and Z. Li, 1986. Pivoting analysis of the selective entrainment of sediments by shape and size with application to gravel threshold. *Sedimentology* 33: 425-436.
- Lewis, J., 1991. An improved bedload sampler. In: Proceedings of the Fifth Federal Interagency Sedimentation Conference, March 18-21, 1991, Las Vegas, Nev., Subcommittee of the Interagency Advisory Committee on Water Data, p. 6.1- 6.8.
- Milhous, R., 1973. Sediment transport in a gravel-bottomed stream. Ph.D. thesis, Oregon State University, Corvallis, USA.
- Milhous, R.T., 1989. Physical habitat simulation and sedimentation. In: *Sediment and the Environment*, R.F. Hadley and E.D. Ongley (eds.), IAHS Publ. no. 184: 211-218.
- Nankervis, J., 1994. Summary of fluvial study site data collection. Water Division 1 Water Rights Adjudication, Greeley, CO. Report prepared for the Stream Systems Technology Center, USDA Forest Service, Rocky Mountain Forest and Range Experiment Station, Fort Collins, CO, 24 p.
- Petts, G.E. and I. Maddock, 1992. Flow allocation for in-river needs. *The Rivers Handbook: Hydrological and Ecological Principles*. P. Calow and G.E. Petts (eds.), Blackwell Scientific Publication, Oxford, Vol. 1, p. 60-79.
- Powell, D.M., I. Reid, J.B. Laronne and L.E. Frostick, 1995. Cross stream variability of bedload flux in narrow and wider ephemeral channels during desert flash floods. Paper presented at the Gravel-Bed Rivers IV Workshop -- *Gravel-Bed Rivers in the Environment* --, held at Gold Bar, WA, Aug. 20-26, 1995.
- Reid, I. and J.B. Laronne, 1995. Bed load sediment transport in an ephemeral stream and a comparison with seasonal and perennial counterparts. *Water Resources Research* 31(3): 773-781.
- Reid, I. and L.E. Frostick, 1986a. Dynamics of bedload transport in Turkey Brook, a coarse grained alluvial channel. *Earth Surface Processes and Landforms* 11: 143-155.
- Reid, I. and L.E. Frostick, 1986b. Turkey Brook bedload data-base. Birkbeck College, University of London, Malet St., London WC1E 7HX, UK.
- Reid, I., J.T. Layman, and L. Frostick, 1980. The continuous measurements of bedload discharge. *Journal of Hydraulic Research* 18 (3): 243-249.
- Reid, I., L.E. Frostick, J.T. Layman, 1985. The incidence and nature of bedload transport during flood flows in coarse-grained alluvial channels. *Earth Surface Processes and Landforms* 10: 33-44.
- Rosgen, D.L., 1994. A classification of natural rivers. *Catena* 21: 169-199.
- Rosgen, D.L., 1996. *Applied River Morphology*. Wildland Hydrology, Pagosa Springs, Colorado.
- Ryan, S., 1994. Bedload transport patterns in pool-riffle and step-pool stream systems. Proceedings of the American Water Resources Association 1994 Annual Summer Symposium "Effects of Human-Induced Changes in Hydrologic Systems". *American Water Resources Association Technical Publication Series* TPS-94-3: 669-678.
- Ryan, S., 1994. *Effects of Transbasin Diversion on Flow Regime, Bedload Transport, and Channel Morphology in Colorado Mountain Streams*. Ph.D. thesis, Department of Geography, University of Colorado.
- Ryan, S., 1997. Morphologic response of subalpine streams to transbasin flow diversion. *Journal of the American Water Resources Association* 33 (4): 839-854.
- Ryan, S.E. and C.A. Troendle, 1996. Bedload transport patterns in coarse-grained channels under varying conditions of flow. *Proceedings of the Sixth Federal Interagency Sedimentation Conference*, March 10-14, Las Vegas, Nevada. Interagency Advisory on Water Data, Subcommittee on Sedimentation, Vol. 2: VI.22-VI.27b.

- Ryan, S.E. and C.A. Troendle, 1997. Measuring bedload in coarse-grained mountain channels: procedures, problems, and recommendations. In: *Proceedings of the Symposium on Water Resources Education, Training, and Practice: Opportunities for the Next Century*. xx (eds.). American Water Resources Association Technical Publication Series TPS-97-x, p. 949-958.
- Ryan, S.E., 1998. Sampling bedload transport in coarse-grained mountain channels using portable samplers. In: *Proceedings, Federal Interagency Workshop, "Sediment Technology for the 21'st Century"*, St. Petersburg, FL, Febr. 17-19, 1998. <http://wwwrvares.er.usgs/osw/sedtech21/ryan.html>, 4 pp.
- Tacconi, P. and P. Billi, 1987. Bed load transport measurement by a vortex-tube trap on Virginio Creek, Italy. In: *Sediment Transport in Gravel-Bed Rivers*. C.R. Thorne, J.C. Bathurst, and R.D. Hey (eds.), John Wiley, Chichester, p. 583-615.
- Troendle, C.A., J.M. Nankervis and S.E. Ryan, 1996. Sediment transport from small, steep-gradient watersheds in Colorado and Wyoming. *Proceedings of the Sixth Federal Interagency Sedimentation Conference*, March 10-14, Las Vegas, Nevada. Interagency Advisory on Water Data, Subcommittee on Sedimentation, Vol. 2: IX.39-IX.45.
- Whitaker, A.C. and D.F. Potts, 1996. Validation of two threshold models for bedload initiation in an upland gravel-bed stream. In: *Watershed Restoration Management - Physical, Chemical, and Biological Considerations*. American Water Resources Association, Proceedings of the Annual Symposium 1996, p.85-94.
- Wiberg, P.L. and J.D. Smith, 1987a. Initial motion of coarse sediment in streams of high gradient. In: *Erosion and Sedimentation in the Pacific Rim*. IAHS Publ. no. 165: 299-308.
- Wiberg, P.L. and J.D. Smith, 1987b. Calculations of the critical shear stress for motion of uniform and heterogeneous sediments. *Water Resources Research* 23 (8): 1471-1480.
- Wilcock, P.R., 1988. Methods for estimating the critical shear stress of individual fractions in mixed-sized sediment. *Water Resources Research* 24 (7): 1127-1135.

10. Appendix

10.1 Recommendations for using the stationary net-frame sampler

- * Plan for ample field time and have the samplers in the stream before the beginning of high flow because the exact occurrence of high flow is difficult to predict.
- * Use at least two staff gages, one on each bank, to improve the stage-discharge relationship even in relatively straight reaches without pronounced riffle-pool morphology, because flow might alternately bulge up at one of the banks, but not both.
- * Use a current meter that integrates flow measurements over the measuring period to account for large fluctuations in flow velocity.
- * Ensure good contact between the sampler and the stream bottom. Squeeze a rag or other material into any voids between the sampler and the stream bed. Consider omitting the ground plate in order to place the sampler deeper into the armor layer.
- * Use a snoop-scope to verify an unobstructed particle paths at the sampler entrance and adjust sampler installation in the stream bed if necessary.
- * Use at least one sampler per meter stream width in mountain gravel-bed streams because bedload transport is spatially very variable. The samplers are not that expensive.
- * Bedload transport can be focused on a narrow band in mountain gravel-bed streams. Make sure that the sampler array in the stream does not miss the location of highest transport rates. Observe the patterns of flow and microtopography of the bed. Bedload transport rates in mountain gravel-bed streams are not highest at the location of fastest and deepest flow, but at locations of upwelling flow, recognizable as boils on the water surface, as opposed to standing waves. Upwelling flow usually occurs on the bar slope somewhere near the middle between thalweg and high flow water line and has the tendency to form low longitudinal ridges.
- * Examine each sample collected with the stationary net-frame sampler for bedload particles. Even a sample that does not seem to contain any bedload particles at first sight may have particles hidden within the abundant organic debris.
- * Irrespective of whether a weight or number-based initial motion approach is used, or a flow competence approach, bedload samples used for initial motion purposes in snowmelt regimes need to fulfill several criteria in order to be representative: measurements need to extend over many days and cover the entire range of flow in order to include the entire range of variability in transport rates. Consecutive samples vividly show the short-term variability. The total sample size needs to be large enough for meaningful statistical regression analysis. 40 samples evenly distributed over the range of flow should be considered a minimum sample size.

10.2 Field equipment for bedload sampling with stationary net-frame samplers and supporting field measurements

Bedload samples with stationary net sampler

stationary net samplers with ground plates
0.5 inch diameter stakes, smooth surface, 3 feet long
drill hammer (heavy, short-handled hammer)
chest waders
neoprene gloves
assortment of large and small ziplock bags

Discharge measurements

2 rebar stakes, 2-3 feet long
measuring tape (at least 10 m or 30 feet, better longer, both metric and English)
current meter
two meter sticks or plastic rulers, 30 cm or longer

Bedload measurements with Helley-Smith sampler

Helley-Smith sampler
stop watch
ziplock bags of various sizes

Surface and subsurface sampling

gravel template
barrel sampler, small metal bowl, small sturdy trowel
several large buckets
landscaping cloth, black, perforated
sieve set (2, 2.8, 4, 5.6, 8, 11.3, 16, 22.6, 32, 45, 64 mm)
accurate hanging scale (up to ca. 10 kg)

Site survey

tripod and stadia rod
surveying level (or theodolite)

General items

field book or prepared forms and pencils
light-weight camping stools
sunscreen, insect repellent, appropriate clothing, water, food, towel

